SOME PROBLEMS IN THE CRYSTAL CHEMISTRY OF PLATINUM COMPLEXES

By

JAMES FRANCIS BRITTEN, B.Sc.

A Thesis

Submitted to the Faculty of Graduate Studies

in Partial Fulfilment of the Requirements

for the Degree

Doctor of Philosophy

McMaster University

CRYSTAL CHEMISTRY OF PLATINUM COMPLEXES

TO MY FATHER

"Upon the whole this Semi-metal seems a very singular Body that merits an exacter Inquiry into its Nature than hath hitherto been made."

William Brownrigg M.D. F.R.S.
(1711-1800)

upon presentation of platinum samples to the Royal Society, Dec. 5, 1750.

DOCTOR OF PHILOSOPHY (1984) McMASTER UNIVERSITY
Department of Chemistry Hamilton, Ontario

TITLE: Some Problems in the Crystal Chemistry of Platinum Complexes

AUTHOR: James Francis Britten, B. Sc. (St. Francis Xavier University, Antigonish, Nova Scotia)

SUPERVISOR: Professor C. J. L. Lock

NUMBER OF PAGES: xx, 233

ABSTRACT

Molecular and crystal structure studies related to various aspects of the chemistry and biochemistry of platinum are presented. The first terminal Pt(II)-OH_2 bond observed in a single crystal verifies the existence of a stable, four-coordinate aquaplatinum(II) complex. The Pt-OH_2 bond is normal and the cis-$[Pt(OH_2)(NH_3)_3(1\text{-methylcytosine})]^{2+}$ ion models a proposed initial monofunctional Pt-DNA complex. The molecular structure of trans-$[Pt(NO_3)_2(NH_3)_2]$ in the solid state is shown to be similar to the cis isomer in that it has two monodentate nitrato ligands, but it differs in that the non-bonded oxygen atoms of the two nitrato ligands lie above and below the ligand square plane. Evidence is presented for ionic and tetravalent platinum impurities in freshly prepared solutions of trans-$[PtCl_2(NH_3)_2]$. The structure of trans-$[Pt(NH_3)_2(1\text{-methylcytosine})(9\text{-ethylguanine})]^{2+}$ offers a possible model for DNA interstrand crosslinking which can explain the thermal stabilization of DNA (with the preservation of base stacking) observed after exposure to low concentrations of trans-$[PtCl_2(NH_3)_2]$.

Various problems of crystallographic interest are discussed. The geometry of diethylenetriamine complexes in the solid state is examined, and a convention is proposed

for assigning conformations. A survey of dien complexes is used to emphasize the importance of intermolecular hydrogen-bonding, as opposed to intramolecular steric interactions, in the configuration of the dien ligand. Various types of disorder in linear chain halogen-bridged mixed-valence platinum compounds are examined. An unusual example of a Pt(II)...Cl-Pt(IV)-Cl chain compound with three-dimensional ordering at the Pt(II) site is presented. The importance of weak intensity data and careful photographic work in these systems is also demonstrated.

The structural analyses of aqua, nitrato, and ammine nitrate complexes are aided by the use of the bond valence model. Quantitative bond length and qualitative packing predictions are made, and structural anomalies are explained, using empirical bond valence curves.

Abbreviations

A	adenine
A_2L_2	$(amine)_2(ligand)_2$
aq.	aqueous
ave.	average
C	cytosine
d(GpG)	3'-deoxyguanosinemonophosphate-5'-deoxyguanosine
dien	diethylenetriamine
dien·3H	diethylenetriammonium ion
diff.	difference
DNA	deoxyribonucleic acid
E·coli	Escherichia coli
en	ethylenediamine
eq.	equivalent
9-EtG	9-ethylguanine
fac	facial
G	guanine
IR	infrared
iso	isotropic
M	metal
max.	maximum
1-MeC 1-Me-Cyt	1-methylcytosine
mer	meridonal
min.	minimum

Abbreviations (continued)

MO	molecular orbital
M_m	molar mass (relative)
nmr	nuclear magnetic resonance
PES	photoelectron spectroscopy
py	pyridine
refl.	reflection
r(GpC)	3'-guanosinemonophosphate-5'-cytidine
RNA	ribonucleic acid
T	thymine
$tRNA^{phe}$	phenylalanine transfer-RNA
undet.	undetermined
X	halogen
xs	excess

Unit Abbreviations

Å	Ångstrom
°C	degrees Celcius
cm	centimeter
d	day
deg, °	degree
e	electron
g	gram
H	hour
K	Kelvin
kV	kilovolt.
L	litre
M	molar
mA	milliamp
min	minute
mL	millilitre
mM	millimolar
mm	millimeter
mmol	millimole
mol	mole
mW	milliwatt
vu v.u.	valence unit

Compound Abbreviations

Code	Compound
3A	$[PtCl_4] \cdot (dien \cdot 3H)_2 \cdot Cl_4$
3B	fac-$[PtCl_3(dien)] \cdot Cl \cdot H_2O$
3C	$[PtCl(dien)] \cdot Cl$
3D	$[Pt(NO_3)(dien)] \cdot NO_3$
3E	cis-$[Pt(NH_3)_2(OH_2)(1\text{-MeC})] \cdot (NO_3)_2 \cdot H_2O$
4A	trans-$[Pt(NO_3)_2(NH_3)_2] \cdot [Pt(NH_3)_4]_2 \cdot (NO_3)_4$
4B	trans-$[PtCl_2(NH_3)_4] \cdot (NO_3)_2$
5A	trans-$[PtCl_2(NH_3)_4]_{0.87} \cdot [Pt(NH_3)_4]_{4.13} \cdot (ClO_4)_{10}$
5B	$K_2 \cdot [PtBr_3(NH_3)] \cdot [PtBr_5(NH_3)] \cdot (H_2O)_2$
5C	$(NH_4)_2 \cdot [PtBr_3(NH_3)] \cdot [PtBr_5(NH_3)] \cdot (H_2O)_2$
6A	trans-$[PtCl(NH_3)_2(1\text{-MeC})] \cdot Cl \cdot (H_2O)_{1.5}$
6B	trans-$[Pt(NH_3)_2(1\text{-MeC})(9\text{-EtG})] \cdot (ClO_4)_2 \cdot (H_2O)_{1.4}$

ACKNOWLEDGEMENTS

I would like to thank Professor Colin Lock for his guidance and friendship, and for always knowing what was 'good for my soul'.

Thanks are due to my supervisory committee members: Dr. Mike McGlinchey for his resourcefullness and Dr. David Brown for many hours of discussion on crystallography and computer programming.

The past few years have been enjoyable because of the help and cooperation provided by my friends in our research group, Brian Allore, Brenda Brown, Deb Harvey, Lurdes Martins, Pierre Pilon (and his sense of humor), Mary Turner, and Maruta Zvagulis, and by those in the neighbourhood, Ray Batchelor, Ron Myers, Lynne Soderholm, and Zin Tun. Special thanks and a 1984 Olympic Gold Medal go to Deb Harvey for her help in the preparation of this thesis and for an excellent showing in the 200 page speed typing event.

I am also grateful to Romolo Faggiani for his technical help in both crystallography and tennis.

Above all, I would like to thank my family, for their faith and support, and Jen, for showing me the way.

Financial support in the form of a National Research Council Scholarship and Scholarships and Teaching Assistant-

ships from the McMaster University Department of Chemistry is also gratefully acknowledged.

TABLE OF CONTENTS

TABLE OF CONTENTS (continued)

TABLE OF CONTENTS (continued)

TABLE OF CONTENTS (continued)

TABLE OF CONTENTS (continued)

LIST OF TABLES

LIST OF TABLES (continued)

LIST OF TABLES (continued)

LIST OF FIGURES

LIST OF FIGURES (continued)

CHAPTER 1

GENERAL INTRODUCTION

1.1 Introduction

The work presented in this thesis is a part of a series of structural studies of possible platinum complexes involved in the biological interactions of various amino-platinum compounds, some of which are antineoplastic. It includes examination of simple inorganic complexes, nucleo-base complexes, and various related compounds of mainly chemical and crystallographic interest. In this chapter the chemical and biochemical properties of platinum which prompted these experiments are outlined. More introductory details are given in the relevant chapters.

1.2 Biochemical Activity of Platinum Complexes

Since it was discovered by Rosenberg (1971) that cis-diamminedichloroplatinum complexes were active against certain tumors, a great deal of effort has been directed toward determining the molecular mechanism of the drug activity. It is hoped that this information will allow the design of more active, less toxic drugs. There are several recent symposia proceedings which detail these studies (Martell (ed.)(1980); Lippard (ed.)(1983); Hacker, Douple, Krakoff (eds.)(1984)).

The process by which cis-$PtCl_2(NH_3)_2$ kills cells and inhibits the growth of tumors is very complex, and may involve the disruption of normal enzyme and protein activity, and of the reproductive process. The fact that the cis isomer is active and the trans isomer is inactive (Cleare (1974)) (see Figure 1.1), however, indicates that there is a basic structural requirement for effective interaction. Furthermore, it has been found that the amine ligand must be either primary or secondary, thus having at least one hydrogen atom bound to the coordinated nitrogen (Cleare, Hoeschele (1973)). These simple geometric restrictions justify the study of simple model systems.

1.2.1 The Hydrolysis of Pt Complexes

It has long been known that when neutral, square planar $PtCl_2(NH_3)_2$ complexes are dissolved in water, the Pt-Cl bonds are slowly hydrolysed to give mono- and diaqua ions (Werner, Miolati (1893)). This process can be hastened by the addition of silver salts, such as $AgNO_3$, which quantitatively remove the chloride from solution. An anion (eg. NO_3^-) is chosen which is a poor ligand for platinum. Jensen (1939) has found that the $[Pt(NH_3)_2(OH_2)_2]^{2+}$ species can form mono- and dihydroxo species, with $pK_1 = 5.56$ and $pK_2 = 7.32$ for the cis isomer and $pK_1 = 4.32$ and $pK_2 = 7.38$ for the trans isomer. Recently various hydroxo-bridged oligomers have been isolated (Lock (1980)) from the cis-diammine systems.

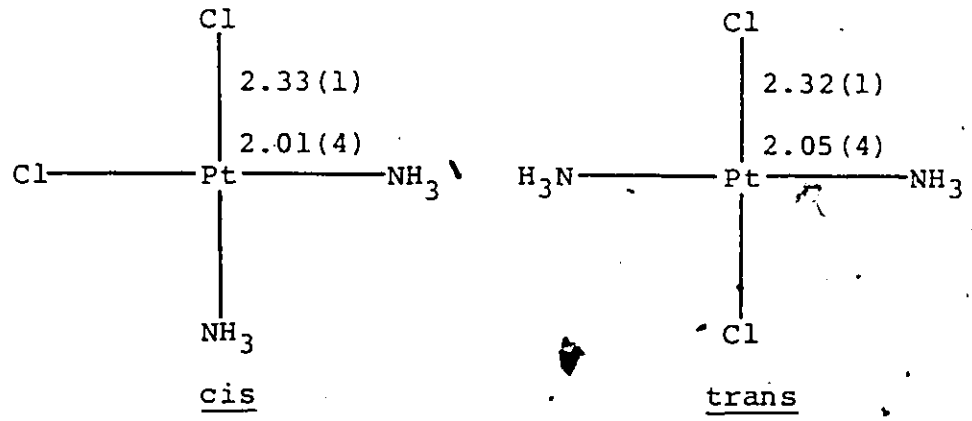

Figure 1.1. The isomers of $PtCl_2(NH_3)_2$ with average bond lengths (Å) (Milburn, Truter (1966))

No analogues are known for the trans compounds, for which cyclic di- and trinuclear complexes are geometrically impossible. King (1938) has isolated some diammine complexes which he claims are monomeric $[Pt(NH_3)(H_2O)(OH)]OH$, $[Pt(NH_3)_2(OH)_2]$, $[Pt(NH_3)_2(OH)(NO_3)]$, and $[Pt(NH_3)_2(H_2O)(SO_4)]\cdot H_2O$, based on elemental analyses, conductivity measurements, and molecular weight determinations. Unfortunately, in the cryoscopic molecular weight determinations water was used as a solvent, therefore monomers were actually observed in solution. Thus the solid samples may not have been monomers, but oligomers which were hydrolysed. No single crystal X-ray analyses were done. A recent ^{15}N, ^{195}Pt nmr study of cis-$[Pt(^{15}NH_3)_2(H_2O)_2]^{2+}$ with various weakly-coordinating oxygen-donor anions, X^{n-}, demonstrated an equilibrium between the diaquo complex and cis-$[Pt(^{15}NH_3)_2X(H_2O)]^{(2-n)+}$ (X = nitrate, sulfate, phosphate, or acetate). For X = phosphate or acetate, dimeric and oligomeric species were also observed, including highly coloured mixed-oxidation state compounds (Appleton, Bowie, Hall, Ralph (1984)). The oxidative-addition of two ligands to square planar, 16e$^-$, platinum(II) to give octahedral, 18e$^-$ platinum(IV) complexes is common in the aqueous chemistry of the divalent compounds.

In the blood, where chloride concentration is approximately 103 mM, the dichloroplatinum species predominates (95%, Lim, Martin (1976)). After the neutral complex enters the cell ($[Cl^-]$ = 4 mM) hydrolysis occurs, giving mainly

$[Pt(OH)(H_2O)(NH_3)_2]^+$, as well as the chloroaqua, chlorohydroxo, diaqua, dihydroxo, and possibly some oligomeric complexes. The labile aqua ligand can then be replaced by more stable electron donors, such as N and S atoms of the cell constituents. Because the deoxyribonucleic acid (DNA) molecule is by far the largest in the cell ($M_m \simeq 2,500,000,000$ $g \cdot mol^{-1}$ in E. coli, whereas the next largest molecule (RNA) has $M_m \simeq 1,000,000$ $g \cdot mol^{-1}$) and makes up most of the organic nuclear mass it is the main target of platinum coordination.

1.2.2 The Interaction with DNA

The primary structure of DNA (see Figure 1.2) is that of a polymeric chain of alternating, covalently linked phosphate and deoxyribose moieties, with a purine or pyrimidine base covalently attached to each sugar (deoxyribose) molecule. The sequence of bases along the sugar-phosphate backbone is responsible for preserving and transmitting the genetic information of the cell.

The secondary structure of DNA is the union of two matched single strands via hydrogen-bonds between complementary base pairs (G:::C and A:::T; Watson, Crick (1953)). The resulting dimer forms a helix, with the base pairs almost perpendicular to the helix axis. In A-DNA, the helix is right-handed, with two large grooves and 10.9 base pairs per 31.6Å turn. In B-DNA, also right-handed, there are 10.0 base pairs per 34.0Å turn, with a major and a minor groove

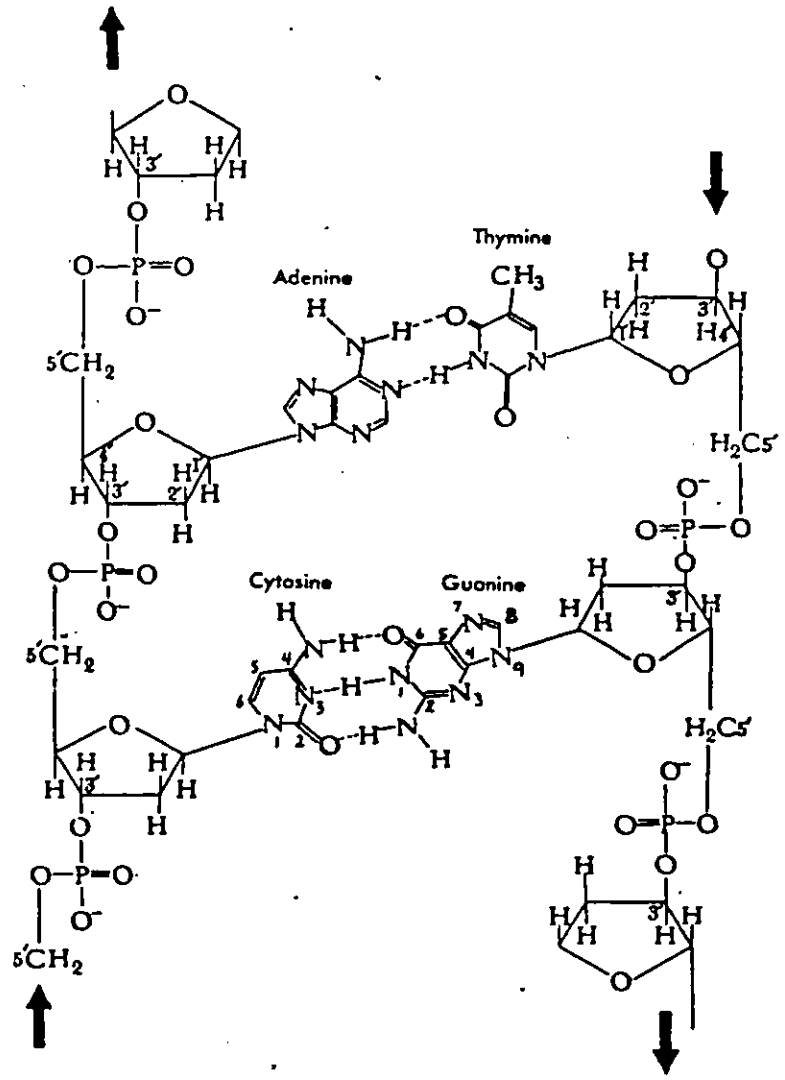

Figure 1.2. A segment of a DNA molecule showing the sugar-phosphate backbone, base pairing, and standard labelling (from Levine (1969))

along the helix. In Z-DNA the helix is left-handed, with six sets of two base pairs per turn. This odd structure is adopted because the guanine sugars are flipped (syn) relative to the bases. In each type of DNA there are local modifications to the twist angle between bases along the chain (16°-44° for A-DNA) which depend on the local base sequence. These modifications are responsible for the tertiary, or superhelical structure of DNA, and are important for the protein and enzyme recognition of instructions (eg. where the genetic code starts and stops). An excellent review of these and more subtle structural features of DNA has been presented by Dickerson (1983).

The current description of the major lesion of cis-$PtCl_2(NH_3)_2$ which results in the antitumoral activity is a bidentate intrastrand chelation of two neighbouring G's (either d(GpG) or d(GpNpG) where N is another nucleobase) (Lippard (1984)). A clip such as this would disrupt the local structure of the DNA and possibly interfere with cell reproduction. This disturbance of base stacking is also consistent with circular dichroism measurements (Macquet, Butour (1978)), which in turn are dependent on guanine content in the DNA. Furthermore, this stacking disorder can explain the decrease in melting point (thermal unwinding) of DNA after treatment with cis-$PtCl_2(NH_3)_2$ (Macquet, Butour, Johnson (1983)).

Trans-$PtCl_2(NH_3)_2$, when administered in high enough doses, can cause many of the phenomena observed with the cis

analogue. The cis and trans-$Pt(NH_3)_2^{2+}$ hydrolysis products both favour coordination to N7 of G when reacted with DNA (Macquet, Butour, Johnson, Razaka, Salles, Vieussens, Wright (1984)), and both were bound to two G's after digestion of the DNA. Both can cause inhibition of DNA, RNA, and protein synthesis (Macquet et al. (1984)); they can kill cells (Macquet et al. (1983)); they can unwind supercoiled DNA and interfere with restriction endonucleases (Scovell, Kroos, Capponi (1983)). For both the initial binding to DNA is monofunctional becoming bifunctional with time (Zwelling (1983)). They can form interstrand crosslinks (Zwelling (1983)), and they prevent the B→Z transition in poly(dG·dC)·poly(dG·dC) (Ushey, Santella, Caradonna, Grunberger, Lippard (1982)). These experiments imply that none of these processes are directly involved in antitumor activity, since the trans isomer is inactive.

The trans isomer differs from the cis in that it forms DNA-protein crosslinks (Zwelling (1983)), it is non-mutagenic (Johnson, Hoeschele, Rahn, O'Neill, Hsie (1980); Zwelling (1983)), it does not enhance the rate of nuclease digestion (Scovell et al. (1983)), it stabilizes DNA at low Pt/base ratios (Macquet et al. (1983)) without disrupting the stacking. These differences can be explained by the inability of trans-$Pt(NH_3)_2^{2+}$ to form an intrastrand crosslink between two adjacent guanines. What is not explained is the nature of the DNA-DNA crosslink (likely interstrand) of

the trans-species which stabilizes the polymer. The trans-G_2 species proposed by Macquet et al. (1984), whether intra- or interstrand, would cause disruptions to the base stacking.

1.3 Objectives

At the outset of this work three structural problems were chosen for examination. Firstly, what is the nature of the Pt(II)-OH_2 bond? Can it be stabilized in the solid state? Are cis-$[Pt(OH)(NH_3)_2(nucleobase)]^+$ or cis-$[Pt(OH_2)(NH_3)_2(nucleobase)]^{2+}$ plausible intermediates in the initial interaction with DNA (Reedijk, denHartog, Fichtinger-Schepman, Marcelis (1984))? These questions have been answered in Chapter 3.

Secondly, what is the nature of trans-$Pt(NO_3)_2(NH_3)_2$ and its hydrolysis products? Are oligomers possible? A partial answer is given in Chapter 4.

Thirdly, is there a model for trans-$Pt(NH_3)_2^{2+}$ binding which can account for the observed thermal stabilization of DNA? One is presented in Chapter 6.

In the course of these studies, several other interesting crystallographic problems arose, such as the conformation possibilities for the diethylenetriamine ligand (Chapter 3) and disorder phenomena in halogen-bridged mixed-valence compounds (Chapter 5). They are introduced and discussed in their respective chapters. The theory and methods of heavy-metal X-ray crystallography (the procedure

used throughout this work) are first outlined in Chapter 2.

CHAPTER 2

CRYSTALLOGRAPHIC METHODS

2.1 Introduction

A good measure of the importance and usefulness of any physical technique is its rate of change in terms of theoretical basis and technical methods. As the precision and accuracy of the physical measurement are improved, and as the 'blind' faith in the results becomes acceptable, more demands are made on the technique, and stricter experimental criteria must be imposed. X-ray crystallography is fast becoming one of the most important techniques for the characterization and study of various compounds, and as a result the methods of acquisition and treatment of X-ray diffraction data are constantly improving, especially in the study of macromolecules. Although basic diffraction theories still apply, there have been many advances in the practice and theory of data collection (area detectors, synchrotron radiation, triple-beam experiments, computer controlled diffractometers, etc.), of data analysis (more efficient computers and algorithms, new direct methods of phasing, etc.), and of interpretation of results (graphics, information storage and retrieval, correlation studies, etc.).

In our laboratories, X-ray crystallography procedures

are continuously being upgraded as a result of new computer software and hardware, stricter requirements imposed by crystallographic journals, and knowledge gained from tackling difficult problems. The material presented in this chapter focuses on the procedures and computations used for the most recent structure solutions, and any significant differences from earlier methods (i.e. those used for certain structures presented in this thesis) are mentioned. Where problems are incurred in solving crystal structures, methods of handling or avoiding them are suggested. Before discussing procedures, however, a brief outline of the basic points of single crystal diffraction theory is presented in Section 2.2. Full introductory treatments can be found in such texts as those of Buerger (1942), Stout and Jensen (1968), Woolfson (1979), or Luger (1980).

2.2 Single Crystal Diffraction Theory

In order to appreciate some of the methods and results presented in this thesis, an understanding of the interaction of X-rays with a crystal lattice is necessary. In this section the diffraction process and the relationship between scattered X-ray intensities and model electron density (i.e. crystal structure) are examined.

2.2.1 The X-ray Scattering Process

The X-rays used in these experiments are chosen because their wavelengths (~1Å) are of the same order of

magnitude as interatomic distances, the quantities sought. Furthermore, the radiation energies involved are suitable for interaction with core electrons, which have density distributions centered about the atomic positions.

This interaction is mainly an absorption of the radiation and an elastic, spherical scattering of coherent radiation phase-shifted by π radians relative to the incident beam. This process, known as Thompson scattering, is possible because each electron is in a fixed energy state. For an atom in a monochromatic X-ray beam an atomic scattering factor, f_a, can be calculated from the known radial distribution of electrons around the atom, using theoretical electronic wave functions, Ψ_n. f_a is the ratio of the total amplitude of the coherent scattered radiation from the n electrons to that of one free electron positioned at the atomic center. Its magnitude decreases radially as the angle 2θ (between the direction of the incident beam and the direction of the scattered radiation) increases to π radians (see Figure 2.1). The atomic scattering factors for X-rays are tabulated in the "International Tables for X-ray Crystallography" (Cromer, Waber (1974)).

For an atom shifted from an arbitrary origin O by a vector $\mathbf{r}$, the scattering amplitude is given by $f_{a,2\theta}\exp(2\pi i\mathbf{r}\cdot\mathbf{s})$, where the scattering vector $\mathbf{s}$ is defined in Figure 2.2. The exponential term accounts for the phase difference of $2\pi\mathbf{r}\cdot\mathbf{s}$ in the wave scattered from the atom relative to the

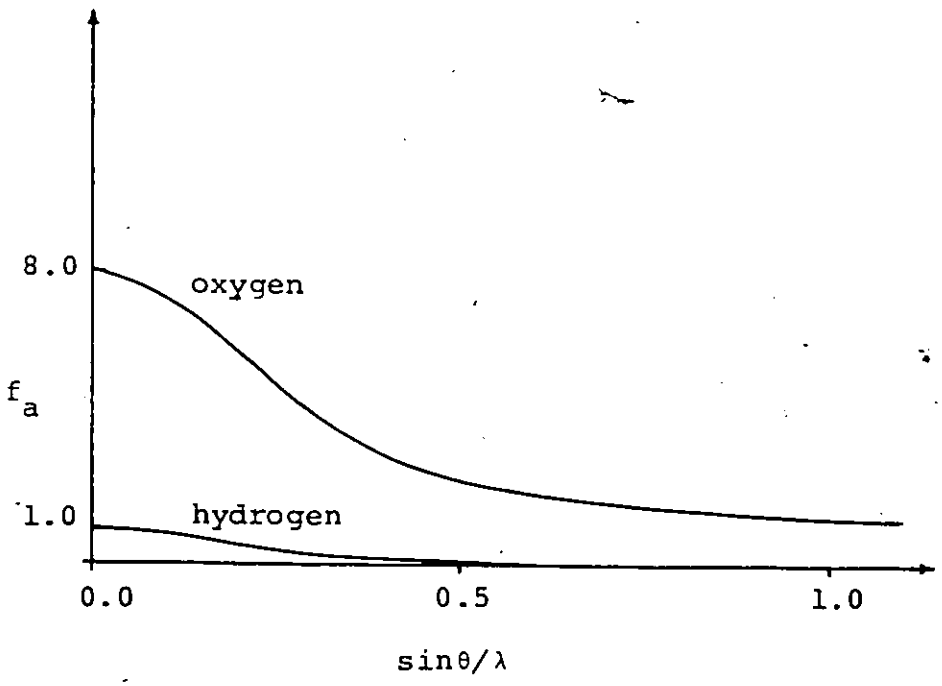

Figure 2.1. Typical atomic scattering factor curves

$$S_s = S_i = 1/\lambda$$

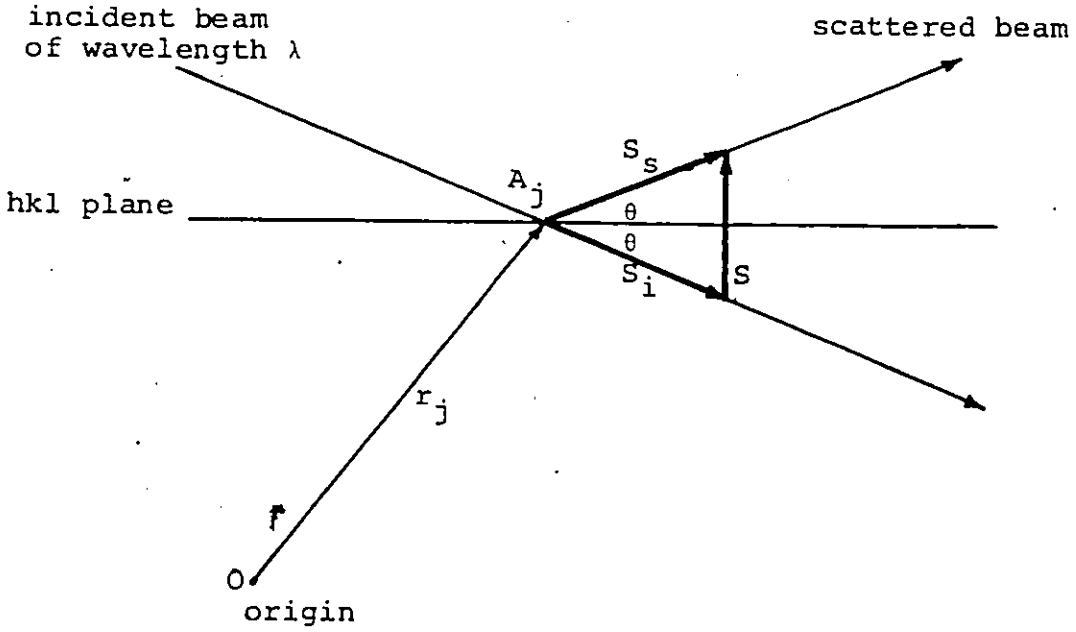

Figure 2.2. The scattering vector

phase of a scatterer at the origin. Thus for a macroscopic solid sample of n atoms, each atom exposed to X-irradiation of the same intensity, the total amplitude of the scattered radiation at angle 2θ, relative to that of all atoms scattering from the origin, is given by

$$F_{2\theta} = \sum_{j=1}^{n} f_{j,2\theta} \exp(2\pi i \mathbf{r}_j \cdot \mathbf{s}) \qquad (2.1)$$

or

$$F_{2\theta} = \sum_{j=1}^{n} f_{j,2\theta} \cos(2\pi \mathbf{r}_j \cdot \mathbf{s}) + i \sum_{j=1}^{n} f_{j,2\theta} \sin(2\pi \mathbf{r}_j \cdot \mathbf{s}) \qquad (2.2)$$

The intensity of the scattered radiation is directly proportional to the square of the wave amplitude:

$$I_{2\theta} = k F_{2\theta} F^*_{2\theta} \qquad (2.3)$$

2.2.2 Single Crystal Scattering

The X-ray scattering experiment described thus far can yield no information on the molecular structure of the compound unless the sample is a single crystal. In a single crystal, the atoms or molecules are packed in such a way that a pattern is repeated in three dimensions. The building block, or unit cell, is defined in terms of a basis set of non-coplanar vectors **a**, **b**, and **c**, or the scalars and angles: α opposite a, β opposite b, and γ opposite c.

A unit cell can belong to one of seven crystal systems, defined by symmetry-imposed restrictions on the cell parameters (see Woolfson (1979), p.9). The cell symmetry

is a result of symmetry relationships among the atoms of the cell (rotation axes, mirror planes, inversion centers). Different combinations of symmetry elements allow thirty-two possible crystal classes. With the addition of translational symmetry elements (screw axes, glide planes, centering), which generate the fourteen Bravais lattices from the seven crystal systems, a total of 230 three-dimensional space groups are possible.

The periodic arrangement of atoms in a single crystal gives rise to sets of parallel planes of identical electron distribution. Each plane is separated from its parallel neighbour by a constant vector $\mathbf{d}$ along the normal to the plane (the ψ-axis). The set of planes which cut the a, b and c axes at 1/h, 1/k, and 1/l, respectively, are indexed hkl. The repeating nature of the cell in the lattice restricts h, k, and l to integer values. Bragg (1913) has shown that in order for constructive interference of Thompson scattered X-rays to occur, these planes must be aligned at an angle θ from the incident beam such that

$$2d_{hkl}\sin\theta = n\lambda \qquad (2.4)$$

The direction of the 'reflected' beam is 2θ from that of the incident beam or θ from the set of planes (as in Figure 2.2 with the hkl plane bisecting and perpendicular to $\mathbf{s}$, i.e., $\mathbf{s} \parallel \mathbf{d}$). The integer n is simply the factor which relates the Miller indices of the external-face of a crystal to the hkl

indices of an internal set of planes (eg. the 422 set is parallel to the (211) face, with n = 2). Bragg's equation thus explains why, for a crystal with at least several hundred planes per set, the scattering is discrete and not continuous, similar to a reflection of the incident beam from the set of planes.

It can be seen from Figure 2.2 that the magnitude of **s** is given by

$$s_{hkl} = 2\sin\theta/\lambda \qquad (2.5)$$

From Bragg's law, with n = 1,

$$s_{hkl} = 1/d_{hkl} \qquad (2.6)$$

or

$$\mathbf{s}_{hkl} = \mathbf{d}_{hkl}/d^2_{hkl} \qquad (2.7)$$

since **s** and **d** are parallel. Laue (1912) defined conditions for diffraction by a single crystal in terms of the vector **s**. He stated that discrete diffracted beams would arise only when

$$\mathbf{a}\cdot\mathbf{s} = h,\ \mathbf{b}\cdot\mathbf{s} = k, \text{ and } \mathbf{c}\cdot\mathbf{s} = l \qquad (2.8)$$

simultaneously. Again, for a set of integers h, k, and l, a particular incident beam angle, θ, is required for an observable 'reflection'.

To simplify this discussion, it is convenient to

define a cell in 'reciprocal space', with basis vectors $\mathbf{a}^*$, $\mathbf{b}^*$ and $\mathbf{c}^*$ related to $\mathbf{a}$, $\mathbf{b}$ and $\mathbf{c}$ such that

$$\begin{array}{lll} \mathbf{a}\cdot\mathbf{a}^* = 1 & \mathbf{a}\cdot\mathbf{b}^* = 0 & \mathbf{a}\cdot\mathbf{c}^* = 0 \\ \mathbf{b}\cdot\mathbf{a}^* = 0 & \mathbf{b}\cdot\mathbf{b}^* = 1 & \mathbf{b}\cdot\mathbf{c}^* = 0 \\ \mathbf{c}\cdot\mathbf{a}^* = 0 & \mathbf{c}\cdot\mathbf{b}^* = 0 & \mathbf{c}\cdot\mathbf{c}^* = 1 \end{array} \qquad (2.9)$$

This gives a reciprocal cell, fixed relative to the real cell, with the basis vectors perpendicular to the real cell faces (eg. $\mathbf{a}^* \perp \mathbf{b}$ and $\mathbf{a}^* \perp \mathbf{c}$) and with inverse length for unit dimensions. The complete set of relationships among the scalar constants of the two cells is presented by Stout and Jensen (1968), page 31.

$\mathbf{s}$ can be written as a vector of reciprocal space:

$$\mathbf{s}_{hkl} = h\mathbf{a}^* + k\mathbf{b}^* + l\mathbf{c}^* \qquad (2.10)$$

Therefore, the planes hkl in real space each have a corresponding lattice point hkl in reciprocal space, at a distance s_{hkl} or $1/d_{hkl}$ from the origin along the normal to the plane (parallel to $\mathbf{d}$). Equation (2.10) has the integers h, k, and l as scalars since they give a solution for the Laue diffraction conditions (2.8).

From equation (2.1), the 'structure factor' or amplitude now becomes

$$F_{hkl} = \sum_{j=1}^{n} f_{j,2\theta} \exp(2\pi i \mathbf{r}\cdot(h\mathbf{a}^* + k\mathbf{b}^* + l\mathbf{c}^*)) \qquad (2.11)$$

and is zero when the diffraction conditions are not met. The

summation is now over the n atoms of the unit cell, each at position

$$\mathbf{r}_j = x_j\mathbf{a}+y_j\mathbf{b}+z_j\mathbf{c} \qquad (2.12)$$

in the cell. F_{hkl} is now relative to the potential scattering amplitude of the total cell contents situated at the cell origin. Equations (2.11) and (2.12) can be combined to give

$$F_{hkl} = \sum_{j=1}^{n} f_{j,2\theta}\exp(2\pi i(x_j\mathbf{a}+y_j\mathbf{b}+z_j\mathbf{c})\cdot(h\mathbf{a}^*+k\mathbf{b}^*+l\mathbf{c}^*))$$

or

$$F_{hkl} = \sum_{j=1}^{n} f_{j,2\theta}\exp(2\pi i(hx_j+ky_j+lz_j))$$

or

$$F_{hkl} = \sum_{j=1}^{n} f_{j,2\theta}\exp(i\phi_j) \qquad (2.13a)$$

where ϕ_j ~~is~~ the phase shift of the j^{th} atom,

$$\phi_j = 2\pi(hx_j+ky_j+lz_j). \qquad (2.13b)$$

In section 2.2.1 it was stated that stationary atoms were scattering X-rays phase-shifted by π radians relative to the uniform intensity incident beam. Three assumptions in this model are not generally valid, and corrections must be made to the calculation of the structure factor, F_{hkl}. Firstly, atoms are not stationary, but have thermal motion which, in general, is anisotropic. This results in the spreading out of the electron cloud for each atom, thereby adjus-

ting the radial scattering power. To account for this, the atomic scattering factors are modified:

$$f'_{j,2\theta} = f_{j,2\theta}\exp(-T_j) \qquad (2.14)$$

where

$$T_j = 2\pi^2(U_{11}h^2a^{*2}+U_{22}k^2b^{*2}+U_{33}l^2c^{*2}+2U_{12}hka^*b^*\cos\gamma^* + 2U_{13}hla^*c^*\cos\beta^*+2U_{23}klb^*c^*\cos\alpha^*) \qquad (2.15)$$

and the tensor U_{ij} represents both the mean square amplitudes of vibration along the principal axes of an ellipsoid ($i = j$) and the orientation of the ellipsoid ($i \neq j$).

The second assumption is that the X-rays are elastically scattered with a scattering phase angle of π radians. This is not true for the tightly held core electrons, especially when the energy of the X-ray is near an absorption edge of the scattering atom. $f_{a,2\theta}$ must therefore be modified by an amplitude factor, $\Delta f'$, and a phase factor, $i\Delta f''$, the so-called "anomalous dispersion" corrections:

$$f_j = (f'_{j,2\theta}+\Delta f'+i\Delta f'') \qquad (2.16)$$

These extra terms are, of course, functions of the wavelength, but do not vary with $\sin\theta$ because of their core electron origins. The magnitude of the effect generally increases with increasing atomic weight. The correction factors are tabulated in the "International Tables" (Cromer (1974)).

The third assumption is that the whole of the crystal

interacts with X-irradiation of a constant intensity. This is true for weaker reflections, but for strong, low angle reflections the incident beam is significantly weakened by upper planes of scatterers. Thus the lower planes cannot contribute fully to the 'reflected' beam, and the intensity of the affected reflection is weakened relative to the rest of the data set. Zachariasen (1963) has formulated a correction for this 'secondary extinction' which was applied to the calculated structure factors by Larson (1967) ($F_c = F_{hkl} \cdot (1 + g\beta F_{hkl}^2)^{-\frac{1}{2}}$ with g variable and β a function of 2θ). This was later modified by Sheldrick (1976) to give

$$F_c = F_{hkl}(1-0.0001gF_{hkl}^2/\sin\theta) \qquad (2.17a)$$

where g is a variable parameter of the order of 10^{-3}. F_{hkl} is now given by

$$F_{hkl} = \sum_{j=1}^{n} (f_{j,2\theta}+\Delta f'+i\Delta f'')\exp(i\phi_j)\exp(-T_j) \qquad (2.17b)$$

In order to make use of equation (2.17), the intensity data, I_{hkl}, must be expressed as a set of structure factors, F_o. In general, the intensity of a beam of light is proportional to the square of the modulus of the amplitude. For single crystal diffraction the proportionality constant must account for several factors. Corrections are made for absorption (A^*), polarization (p), and the Lorentz effect (L):

$$I_{hkl} = Lp|F_{hkl}|^2/A^*t^2 \qquad (2.18)$$

1/t is a proportionality constant. Rearranging (2.18) gives

$$F_o = |F_{hkl}| = +t(I_{hkl}A^*/Lp)^{\frac{1}{2}} \qquad (2.19)$$

where the plus sign indicates that the positive root is taken. For the remainder of the text $|F_o|$, although sometimes redundant, will be used for clarity. The transmission factor A^* is used to correct for the X-ray absorption by the atoms of the crystal, and has the general form

$$A^* = V(\int \exp(\mu x)\, dV)^{-1} \qquad (2.20a)$$

where μ is the linear absorption coefficient, V is the crystal volume, and x is the length of the X-ray path through the crystal.

$$\mu = \sum_{j=1}^{n} \mu_{a_j} \qquad (2.20b)$$

where the summation is over the n atoms of the unit cell. The atomic μ_a, in units of cm^{-1}, are tabulated in the "International Tables" (Cromer (1974)).

The integration can be approximated numerically if the crystal dimensions and orientation are known accurately. In practice, a transmission factor composed of an analytical term, A^*_θ, and an empirical term, A^*_ψ, are satisfactory (Flack (1974)). Thus

$$A^* = A^*_\theta A^*_\psi \qquad (2.21)$$

A^*_ψ is calculated and applied at the time of data

collection. An intensity measurement for a reflection of reasonable intensity is taken at several ψ settings (by rotating the crystal around the diffraction vector **s**), and an empirical correction curve for the shape of the crystal in that 2θ region is obtained. This process is repeated using reflections representing 2θ values which span those of the data set. A value for A^*_ψ can then be interpolated for each reflection in the data set. The data is thus modified to represent a crystal with a C_∞ axis. Therefore the crystal can be approximated as a cylinder or sphere of radius R, which can be calculated from the volume of the crystal, and an analytical correction for 2θ dependence of absorption can be applied when μR is known. The values of A^*_θ can be obtained by interpolation of the values given by Bond (1974).

The Lorentz correction, L, is necessary because the intensity of the diffracted beam is a function of the time it takes for the reflecting planes to pass through the Bragg angle. This in turn depends on the geometry of the data collection method, and for the procedures used for this work (c.f. § 2.4)

$$L = 1/\sin 2\theta \qquad (2.22)$$

The polarization factor, p, accounts for the loss of intensity of both the incident and reflected beams because of polarization by the monochrometer (m) and the crystal (c), respectively:

$$p = f\,\frac{1+\cos^2 2\theta_m \cos^2 2\theta_c}{1+\cos^2 2\theta_m} + (1-f)\,\frac{1+\cos 2\theta_m \cos^2 2\theta_c}{1+\cos 2\theta_m} \qquad (2.23)$$

where f represents the fraction of mosaic spread in the monochromator. When no monochromator is used, (2.23) reduces to

$$p = (1+\cos^2 2\theta_c)/2. \qquad (2.24)$$

The scale factor t in equation (2.19) can be estimated from a Wilson plot (Wilson (1942)) when the cell contents are known. This is not often the case, however, so a 'relative' structure factor and its estimated standard deviation are defined:

$$F_{rel} = |F_o|/t = +(I_{hkl}A^*/Lp)^{\frac{1}{2}} \qquad (2.25a)$$

$$\sigma(F) = \sigma(I)\cdot(A^*/2F_{rel}Lp) \qquad (2.25b)$$

2.2.3 The Phase Problem

In section 2.2.2 an expression relating the coordinates of the atoms in the unit cell of a single crystal to a reflection (hkl) structure factor, F_c, was derived (equation (2.17)). By substituting F_c for F_{hkl} in (2.18) the intensity, I_{hkl}, for a reflection from the set of planes hkl, can be obtained. In the X-ray experiment, however, it is the intensities which are measured, from which are derived the structure factors (the $|F_o|$'s or F_{rel}'s). Equation (2.19)

shows that $|F_o|$ is the modulus of F_{hkl}, $+(F_c F_c^*)^{\frac{1}{2}}$, and the phase angle δ is not available. Therefore the F_c's cannot be obtained analytically from the I_{hkl}'s, and the atomic parameters cannot be calculated.

Fortunately, there are two general methods which can be used to determine the phases. The first of these, known as 'direct methods', solves the structure by directly assigning phases to the $|F_o|$'s. Direct methods are divided into two cases: centrosymmetric and non-centrosymmetric.

In a centrosymmetric packing of atoms in a cell the inversion center at the standard origin relates the position x,y,z to -x,-y,-z such that the electron density distribution at each of the two points is identical. From (2.13b), $-\phi_j = -2\pi(hx_j+ky_j+lz_j) = 2\pi(h(-x_j)+k(-y_j)+l(-z_j))$: Using (2.13a) and (2.14) and separating the center-related atoms in the cell:

$$F_{cent} = \sum_{j=1}^{n/2} f'_{j,2\theta}(\exp(i\phi_j)+\exp(-i\phi_j))$$

and by Euler's formula

$$F_{cent} = \sum_{j=1}^{n/2} f'_{j,2\theta}(2\cos\phi_j) \qquad (2.26)$$

Since the cosine is an even function,

$$F_{cent}(h,k,l) = F_{cent}(-h,-k,-l) \qquad (2.27)$$

Equation (2.27) is Friedel's law, and holds for centrosym-

metric structures whether or not there are anomalous dispersion effects. Equation (2.26) illustrates that for centrosymmetric structures with negligable anomalous dispersion, the total structure factor is a real (not complex) number with a total phase of either 0 or π. Thus the centrosymmetric direct methods involves only the determination of the signs of the $|F_o|$'s. This is accomplished by examining strong reflections, assigning a few starting phases based on origin shift parity considerations, and then using the Sayre Equation (Sayre (1952)) and probability statistics for phase extension to other reflections. Full treatments of the method are presented by Luger (1980) and Sayre (1982). For the non-centrosymmetric case a modification of the Sayre Equation due to Karle and Hauptman (1956), known as the 'tangent formula', must be used. This case is also discussed by Luger and by Sayre. Direct methods were not required for any of the structures presented in this work, and therefore will not be discussed further.

The alternative approach to solving the phase problem involves finding a model structure, calculating the structure factors with their phases (centrosymmetric or non-centrosymmetric), and then refining the model so that the moduli of the F_c's approach the $|F_o|$'s. This process is carried out in three separate steps:

1) Rough or partial model is found and F_c's are obtained.
2) The $|F_c|$'s are compared to the $|F_o|$'s and an agreement

(R) factor is determined. An electron density difference map is calculated from which modifications to the model are obtained.

3) The model is refined by least-squares calculations minimizing $\sum_{hkl}\omega(|F_o|-|F_c|)^2$. Steps 2 and 3 are repeated until a satisfactory model is obtained.

Although most of these calculations are automated, intervention by the crystallographer is necessary in steps one and two, and often required in step three. Therefore these procedures will be examined briefly.

Several methods exist to find a starting model, including trial-and-error, heavy-atom, anomalous dispersion, and Patterson methods (see Stout and Jensen (1968), chapters 11, 12 and 14). In any structure solution, the symmetry of the cell contents is the first consideration. Examination of the cell parameters and the intensity weighted reciprocal lattice gives indications of mirror planes, rotation axes, and possible inversion centers. This is normally done by photographing layers of the reciprocal lattice and indexing the spots. Translational symmetry operations are indicated by one-(screw axes), two-(glide planes) or three-dimensional (face or body centering) extinction patterns in the lattice. A two-fold screw axis along **b**, for example, is a result of an interleaving layer of electron density between and identical to the faces perpendicular to the axis, but rotated by π radians around the axis. This layer diffracts exactly out

of phase with the 0k0, k odd, layers and the resultant intensities are identically zero.

The determination of the space group possibilities from the known symmetry operators can greatly reduce the volume of the cell for which an atomic model must be found, and consequently reduce the number of calculations involved. In this work, further simplifications arose because the compounds studied all contained the heavy atom platinum. This allowed all unknown starting models to be found using the Patterson method.

Since the measured intensity of a reflection is proportional to the product of the structure factor and its complex conjugate, we get from (2.1) (simplifying subscripts)

$$I \sim FF^* = \left(\sum_j f_j \exp(2\pi i \mathbf{r}_j \cdot \mathbf{s}) \right) \left(\sum_j f_j^* \exp(-2\pi i \mathbf{r}_j \cdot \mathbf{s}) \right)$$

or

$$I \sim \sum_i \sum_j (f_j f_i^*) \exp(2\pi i (\mathbf{r}_j - \mathbf{r}_i) \cdot \mathbf{s}) \qquad (2.28)$$

where the f's are the corrected scattering factors. Equation (2.28) illustrates that the measured intensities are related to the interatomic vectors, $\mathbf{r}_j - \mathbf{r}_i$, weighted by the product of the scattering powers of the atom pairs ($f_j f_i^*$) at that particular $\sin\theta/\lambda$ value. Patterson (1935) used a Fourier transformation to map the intensities, or $|F_o|^2$'s, in reciprocal space into interatomic vectors in real space. Thus,

$$P(\mathbf{u}) = \left(\sum_i F_{oi}^2 \cos 2\pi \mathbf{u}\cdot\mathbf{s}_i \right)/V \qquad (2.29)$$

where V is the cell volume and $P(\mathbf{u})$ is the value (or height) of the Patterson function at $\mathbf{u} = u\mathbf{a}+v\mathbf{b}+w\mathbf{c}$. A three dimensional map of $P(\mathbf{u})$ within the Patterson asymmetric unit of the cell gives peaks corresponding to the interatomic vectors for all atom pairs. (A more rigorous derivation using the convolution theorem is given by Luger (1980)). Because the peaks are proportional to $f_j f_i^*$, vectors between heavy atom centers will be much higher than those between heavy-light or light-light atom pairs. Therefore in heavy-atom structures the position (x,y,z) of the heavy atom can be derived from the positions of the strongest Patterson peaks with knowledge of the symmetry relationships among the atoms. For example, in a centrosymmetric structure with Pt atoms at (x,y,z) and (-x,-y,-z), a Patterson peak will appear with u = 2x, v = 2y, and w = 2z. The situation becomes more complicated when several independent heavy atoms are in the cell, but the same procedures (with more variables) will give a solution. With a partial model available a trial set of F_c's can be obtained.

The second step in solving the structure (after any method of phase determination, including direct methods) requires a comparison of the F_c's to the $|F_o|$'s. The R-factor is used as a figure of merit:

$$R = \frac{\sum ||F_o| - |F_c||}{\sum |F_o|} \qquad (2.30)$$

or

$$R_\omega = \frac{(\sum \omega(|F_o|-|F_c|)^2)^{\frac{1}{2}}}{(\sum \omega |F_o|^2)^{\frac{1}{2}}} \qquad (2.31)$$

where

$$\omega = (\sigma_c^2 + G|F_o|^2)^{-1} \qquad (2.32)$$

and the summations are over all $|F_o|$'s greater than zero. σ_c is the estimated standard deviation in $|F_o|$ from counting statistics. G is of the order of 10^{-3} and allows $||F_o|-|F_c||$ to be independent of $|F_o|$. The $|F_o|$'s are scaled to approximately absolute values by equating $\sum |F_o|$ to $\sum |F_c|$. If the R-factor indicates that the model is reasonable (i.e. R<0.4) then a Fourier synthesis of a three dimensional electron density difference map is produced.

Electron density in a single crystal is a periodic function and can be represented by the Fourier series

$$\rho(\mathbf{r}) = (\sum_j F_j \exp(-2\pi i \mathbf{r}\cdot\mathbf{s}_j))/V \qquad (2.33)$$

where the F_j are structure factors with phases and $\rho(\mathbf{r})$ is the density at position $\mathbf{r}$, and it is mapped in three-dimensions over the asymmetric unit on a grid of $\mathbf{r}$ values. To relate the F_c density model (which is not actually calculated) to the $|F_o|$ generated density, the $|F_o|$'s are given the phases, δ's, from the corresponding F_c's:

$$F_c = |F_c|\exp(i\delta) = A+iB \qquad (2.34)$$

where

$$\tan\delta = B/A \qquad (2.35)$$

and

$$|F_c| = (A^2+B^2)^{\frac{1}{2}} \qquad (2.36)$$

A difference map is obtained when the F_j in equation (2.33) are replaced by

$$\Delta F_j = (|F_o|-|F_c|)_j \exp(i\delta_j) \qquad (2.37)$$

The finite number of terms, ΔF_j, in the Fourier synthesis and the uncertainty in the δ_j's result in spurious peaks and valleys in the map, but in general the larger peaks correspond to missing atoms and the deeper valleys indicate incorrect atom positions. For an adequate model, the peaks and valleys may indicate that slight position adjustments are required, or temperature factors need modification. Absorption and extinction problems also increase the 'noise' on a difference map. The noisy difference map for heavy atom structures often makes it difficult to locate hydrogen atoms, although when low angle reflections are given increased weight, they often appear (Sheldrick (1976)).

Following construction of the model, several cycles of least-squares refinement of the model parameters are performed. The technique is standard and automated. For X-ray data, the quantity minimized is $M = \sum_r w(|F_{or}|-|F_{cr}|)^2$, where

the summation is over all observed ($|F_o|>0$) data and the variable parameters are the positional and thermal atomic parameters which define the F_c's. Other parameters such as scale factors and secondary extinction parameters are often refined. The basic process involves differentiating M with respect to each of the parameters, and setting the sum of the partial differentials equal to zero. $|F_c|$ must be expressed as a truncated Taylor series in order to make it linear. After differentiation, a set of NP linear equations with NP unknowns is set up in matrix form:

$$\mathbf{Ax} = \mathbf{v} \tag{2.38}$$

where NP is the number of parameters, **A** is a square matrix of a_{ij} representing sums of weighted products of partial derivatives of F_c's for pairs of parameters p:

$$a_{ij} = \sum_r \omega_r \frac{\partial|F_{cr}|}{\partial p_i} \frac{\partial|F_{cr}|}{\partial p_j} \tag{2.39}$$

x is a column matrix of the approximate correction to the parameters, Δp_j, and **v** is a column matrix with elements v_i representing the sums of weighted differences, $||F_o|-|F_c|| = \Delta F$, times the partial derivatives:

$$v_i = \sum_r \omega_r(\Delta F_r) \frac{\partial|F_{cr}|}{\partial p_i} \tag{2.40}$$

The corrections contained in the **x** matrix are found by

inverting **A**, with $\mathbf{B} = \mathbf{A}^{-1}$, and multiplying through (2.38):

$$\mathbf{x} = \mathbf{B}\mathbf{v} \qquad (2.41)$$

The Δp_j's are then added to the p_j's to obtain a new set of p_j's, and the F_c's and R-factors are recalculated to check for improvement in the model. Estimated standard deviations in the parameters are obtained from the diagonal elements of the **B** matrix, the b_{ii}'s:

$$\sigma_{p_i} = ((b_{ii} \sum_r \omega_r \Delta F_r^2)/(N_{used}-NP))^{\frac{1}{2}} \qquad (2.42)$$

where N_{used} is the number of reflections used for refinement.

The **B** matrix also contains information about the correlation of parameters in the refinement. A correlation coefficient is given by $c_{ij} = b_{ij}(b_{ii})^{-\frac{1}{2}}(b_{jj})^{-\frac{1}{2}}$ and can range from -1 to +1. Simply put, when $|c_{ij}|$ is much greater than 0.5, it is approximately an average of p_i and p_j which is refined, and convergance may be slow or impossible. This problem is averted in cases where correlation is not a necessity (for example when atoms are related by pseudo-symmetry) by using a block-diagonal matrix instead of the full matrix **A**, and refining different parameter blocks in different refinement cycles. An even number of consecutive cycles for each block is required to prevent divergence of the correlated parameters. The final cycle of refinement requires use of the full matrix in order to give a proper estimate of the σ_p's. The refinement is considered complete when the $|\Delta p/\sigma_p|$ ratios

become very small (<0.1), and the R -factor is reasonable (<0.07).

From the final set of atomic parameters a set of interatomic distances (bonds and contacts) and the angles between the interatomic vectors can be obtained, with their estimated standard deviations. Torsion angles and least-squares planes can also be calculated. The equations used are given by Stout and Jensen (1968) and by Pippy and Ahmed (1968). Knowledge of the structure also allows an accurate crystal density calculation to be made.

2.3 Preliminary Experiments

In this section the discussion will focus on the procedures used to obtain information on the cell contents before the collection of intensity data. It will begin with the selection and handling of single crystals. The actual sources of the crystals and any spectroscopic studies not directly related to the X-ray work are outlined in the appropriate section for each compound studied. In general, however, each type of crystal was obtained from the slow evaporation of an aqueous solution of the compound and was at least temporarily air stable.

2.3.1 Crystal Preparation

The crystals were first examined under the stereomicroscope, and were considered acceptable if they were clear and were at least 0.05 mm across the smallest

dimension. They were then rotated under the polarizing microscope, where uniform extinction indicated single crystals. Following this, stability in air was tested by observing the response to cutting or pressure. Often hydrated crystals will lose lattice water to the air, and this process is hastened when the crystal is fractured. Crystals which were found to slowly decompose were handled carefully in a petri dish which was sitting on crushed ice. Specimens of appropriate size and shape were quickly sealed in 0.2 mm (inner diameter) glass capillary tubes containing water droplets.

Hard, irregular crystals were ground to spheres in order to simplify the correction for absorption. Needle-shaped crystals were mounted with the needle axes collinear with the glass fiber axes. This simplified crystal alignment on the camera, since the needle axes are often parallel to cell axes. It also makes analytical absorption corrections easier. The maximum crystal dimension allowed was 0.5 mm, to guarantee that the crystal remained fully immersed in the X-ray beam. Some crystals were cut to the desired size and shape if they were too soft to be ground. The size was chosen to minimize the absorption problem and maximize the intensity, with the average dimension approximately $3/\mu$, when the linear absorption coefficient, μ, was known. In some cases, crystals with well defined faces were mounted as found, with the glass fiber axes parallel to as many faces

as possible (i.e. along possible zone axes). Each crystal was glued to the fiber (or capillary when necessary) with epoxy glue. The fiber was stabilized in a brass pin with plasticine and a coating of type correction fluid ("Liquid Paper") was applied around the base to assure rigidity. After securing the pin in a goniometer head, the crystal was optically centered on a Buerger precession camera for initial X-ray examination.

2.3.2 X-ray Photographs

The Buerger precession camera was used to determine the cell constants and the space group possibilities by photographically mapping out the necessary regions of the reciprocal lattice for each crystal. The sample was aligned on the precession camera (using standard methods, Buerger (1964)) so that a real cell axis (eg. **a**) was parallel to the primary X-ray beam and one of the perpendicular reciprocal cell axes was in the horizontal plane (eg. $\mathbf{c}^*$), parallel to the spindle, or ϕ-axis of the camera. The radiation used was Zr-filtered MoKα at a 50 kV, 12 mA power setting (λ = 0.71069 Å). A film-holder, perpendicular to the primary beam, was mechanically coupled to the crystal at a distance of 60 mm. An annular screen was positioned between the crystal and the film in such a way as to allow only one layer (or cone) of reciprocal lattice points to appear on the film. By adjusting the crystal, screen, and film to an angle of 30° from the primary beam, and allowing the system

to precess at this angle around the beam axis, the hkl planes of the crystal could each repeatedly come into reflecting position and produce a reciprocal lattice point on the film. The resulting photograph (after approximately 24 h exposure) showed an undistorted representation of a zero layer of reciprocal space (eg. 0kl) scaled by 60λ mm·Å. Rotation about the spindle axis (eg. by γ) to place a second axis (eg. **b**) parallel to the beam was sufficient to align the crystal for a different zero layer photograph (eg. h0l). At each spindle setting film positions, screen sizes, and screen positions were calculated (International Tables; Vol. II, page 194) and set to obtain photographs of upper layers (eg. h1l, 1kl), which were required to determine the space group possibilities.

The reciprocal cell axes were chosen to coincide with any symmetry elements observed in the reciprocal lattice (eg. diad axes, tetrad axes, mirror planes) and right angles between axes were noted. Patterns of extinguished reflections, when observed, helped identify the axes and were used to decide on space group possibilities (International Tables; Vol. I)

Another type of photograph used was the rotation photograph, obtained on a Weissenberg camera. On this camera the crystal is aligned and rotated about a real axis, which is perpendicular to the primary beam and coincides with the axis of the cylindrical film holder. The resulting

photograph shows the reciprocal lattice planes perpendicular to the rotation axis as parallel lines of unevenly spaced reflections. The spacing between the lines is directly related to the lattice constant of the rotation axis (see Luger (1980) pp. 52-56). When a third zero layer was required (to check intensity symmetry, for example) the aligned crystal was transferred from the Buerger camera to the Weissenberg camera and a full zero layer was photographed (eg. hk0). The camera was fitted with a slotted screen to allow only the zero layer line to be recorded, and a translational motion of the film in the direction of the crystal's rotation axis, coupled to the rotation (2°/mm in the 2θ direction), mapped the zero layer onto the film in two dimensions. Thus the spots could be indexed (and compared).

2.3.3 The Cell Contents

Any physical or chemical evidence suggesting possible molecular species or functional groups in the crystal is often useful in structure solution, but the crystallographer must not be too biased as to what the answer should be. The most trustworthy experiments are done with isomorphous crystals from the same batch, and the two most useful are elemental analyses and density measurements.

The elemental analyses of crystals prepared in our laboratory were done by either A. B. Gygli, Microanalyses Laboratory, Toronto or by Guelph Chemical Laboratories,

Guelph.

Densities were measured, when possible, by the flotation method, using a mixture of two liquids, one more dense and one less dense than the crystal under study. The density of the liquid mixture was measured by the standard pycnometer technique.

The results of these tests were useful in determining the exact atomic contents of the unit cell, and in checking the density calculated from the model structure.

2.4 Data Collection

2.4.1 The Diffractometer

The X-ray diffraction intensity data for this study were collected using either a Syntex $P2_1$ or a Nicolet P3 diffractometer. The following discussion applies to both instruments, since the hardware and software required were essentially identical. All data measurements were made at room temperature, using Mo Kα radiation and a graphite monochromator (the 200 reflection, $2\theta_m = 12.06°$).

The diffractometer consists of a four-circle goniometer, an X-ray tube, and a scintillation counter resting on an X-ray generator, and a separate computerized control module with a keyboard, printer, and magnetic tape mount. The four concentric circles (see Figure 2.3) 2θ, ω, ϕ, and χ can be used independently to adjust the position of the scintillation counter and the orientation of the crystal,

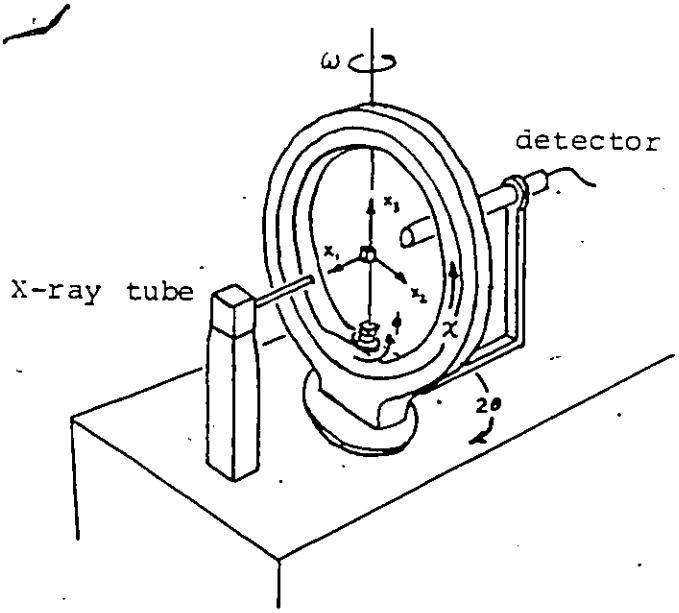

Figure 2.3. The four-circle goniometer

which is optically positioned at the intersection of the circle centers. The 2θ-circle moves the detector relative to the fixed incident beam such that all measurements are made in a plane parallel to the base of the goniometer. The ω-axis coincides with the 2θ-axis and is used to orient the χ-circle, the plane of which is always perpendicular to the base plane. In the normal data collection mode (2θ-θ) the ω-circle is coupled to the 2θ-circle such that $\omega = \theta$. The φ and χ-circles are then required to adjust the orientation of the crystal so that the diffraction vector **s** for the reflection being measured is in the χ-circle and parallel to the base of the plane, bisecting the 2θ angle. There are no restrictions on the φ or χ settings in the room temperature 2θ-θ mode, but 2θ is restricted (physically) to the 0-120° range.

2.4.2 Orientation

The first step was the optical centering of the crystal, which was aided by the telescope attached to the χ-circle. The orientation of the crystal was not crucial because of the four circle design, but attempts were made to align cylindrical crystals with the cylinder axes along the 2θ, ω-axis (with $\chi = 0^\circ$) in order to minimize errors in the absorption corrections. The crystal shape and dimensions were then recorded.

The second step was the determination of the

orientation matrix, which relates the cell axes to the crystal axes (x_i, Figure 2.3), which in turn are related to the diffractometer angles. The process involved first setting all diffractometer angles to zero and then taking a full ϕ-rotation flat polaroid photograph of the crystal. The full rotation generated a vertical 2-fold axis on the film (each refection hkl appeared twice) and a horizontal 2-fold axis relating the Friedel pairs. Examination of the spot shape and intensity range was used to indicate whether or not the crystal and the power setting (normally 50 kV, 15 mA) were appropriate.

Up to fifteen sets of distances between the symmetry related spots on the film were entered into the diffractometer computer, and the χ and 2θ values for each reflection were calculated. A centering routine was used to determine the precise location of each reflection: with the calculated χ and 2θ angles fixed, ϕ was rotated until a reflection was detected. The homing process began with a slow ω-scan through the peak to find its maximum. This was followed by a 2θ-scan, another ω pass, and finally a scan using χ rotation. The process was automatically repeated until the changes in ω, 2θ, and χ were less than 0.001, 0.02, and 0.04°, respectively.

The set of centered reflections was then used to generate a set of 30 indexed vectors in an arbitrary cell. Each vector length and the cosines of the angles to all other

vectors were printed out, and from this list the basis vectors of the true cell, previously determined on the precession camera, were used to reindex the chosen reflections. These properly indexed reflections with refined angles were used in a least-squares calculation to determine the orientation matrix and the cell parameters with their estimated standard deviations. The matrix was stored in computer memory for use in calculating the orientation of the crystal for diffraction from any given set of hkl planes. Later, when reflections with 2θ values between 20° and 40° had been measured, the centering and least-squares procedures were repeated using fifteen of the stronger high-angle reflections. Choosing all fifteen reflections from the same hkl octant gives better unit cell parameters, but when seven or eight of them are from the opposite octant, the orientation matrix is better for data collection. The algorithms used in the Syntex-Nicolet software are outlined by Sparks (1982).

2.4.3 Intensity Measurement

The ranges of h, k, and l values, which were collected, were determined by the space group possibilities, the lengths of the cell edges, and the time available for data collection. The space group symmetry dictated how many octants of reciprocal space were required to make up a full unique set of $|F_o|$ data. When a non-centrosymmetric space group was a possibility, data were collected to include

the Friedel pairs, or their symmetry equivalents. A minimum of two octants was collected in all cases. When time allowed, symmetry related octants were examined to study absorption effects and to reduce errors by averaging equivalent reflections. The upper limit for the modulus of each index was limited to the integer nearest to the ratio of the corresponding cell axis divided by λ. A further restriction limited 2θ to a maximum of 55°. However, when the polaroid rotation photograph indicated that fairly intense reflections could be measured at higher angle, a larger volume of reciprocal space was examined. The philosophy, then, for deciding which reflections to collect was to assume a primitive cell with no systematic absences, and to collect everything that could possibly be needed —— the first time. A trustworthy space group determination could then be made by careful examination of the diffractometer data.

Periodically during data collection two or three standards were measured (eg. after every 48 or 47 reflections). The intensities and peak profiles (printed out on the console) were regularily examined for any signs of crystal decay or movement. If a crystal moved slightly, the fifteen reflections used for orientation were recentered and a new orientation matrix was calculated. The data collection was restarted at a point which would allow replacement of any bad data. The order of data collection was l varying fastest, then k, then h, each incremented in ascending order.

For all crystals the 2θ-θ mode of reflection scanning and the variable scan rate option were used. The maximum scan rate was 29.30°/min and the minimum (R_{scan}^{min}) was normally about 5°/min. R_{scan}^{min} was set to 2.93°/min when more accurate measurements of weak reflections were required. The intensity measurement was preceded by a fast scan across the peak which was used to determine the scan rate for that reflection. The rate was automatically chosen such that the relative experimental standard deviation was roughly the same for all reflections. The peak was then scanned with the detector (2θ movement) from 1.0° below $K\alpha_1$ (λ_1 = 0.70926Å) to 1.0° above $K\alpha_2$ (λ_2 = 0.71354Å), with simultaneous movement of the crystal (in ω) at half the 2θ scan rate. The total background measurement time was set equal to the peak scanning time, and the counts were made at the 2θ limits for each scan.

The reflection intensity and estimated standard deviation are given by

$$I = (N_T - N_{BG1} - N_{BG2})(R_{scan})/\Delta\omega \qquad (2.43)$$

$$\sigma(I) = (N_T + N_{BG1} + N_{BG2})^{\frac{1}{2}}(R_{scan})/\Delta\omega \qquad (2.44)$$

where N_T is the total peak count, N_{BG1} and N_{BG2} are the background counts, and $\Delta\omega$ is the scan range in the ω-circle ($\Delta\omega \simeq 1°$).

For every intensity measurement the reflection

number (negative for a standard), h, k, l, 2θ, ω, φ, χ, 2θ scan range, R_{scan}, a (16 step) peak profile, N_{BG1}, N_T, N_{BG2}, I, σ(I), and the cumulative exposure hours were printed on the console and written on magnetic tape. The local program PRELIM, written by Zin Tun, was used to store all but the profile information as a file on the CYBER 170/730 or 170/815 computers. Earlier programs did not store angle data, which are required for calculating empirical absorption corrections based on ψ-scan data.

The ψ-scan collection was the final procedure using the diffractometer. 36 intensity measurements at 10° intervals around the diffraction vector (ψ-axis) were made for each particular reflection chosen to represent a 2θ range. 16 to 20 reflections were chosen, with $\chi = 270 \pm 20^\circ$ or $\chi = 90 \pm 20^\circ$. The ψ scan data were stored in a separate file and used by the program PSI (Calabrese, Burnett (1980)) to apply the empirical absorption correction to the full data set.

2.5 Procedures and Programs

2.5.1 Data Reduction

The data reduction process was used to generate a unique set of F_{rel}'s from the raw data. After a ψ-scan correction, the program XRAY76 (Stewart (1976)) was used to apply group scale factors based on the fluctuations of the standards. For each standard, a plot of intensity vs. sequence number (i.e. time) was generated before and after the

scaling, so that any systematic errors in the data could be revealed. The estimated standard deviations for the standards were also calculated (before the scaling). A listing of the reflections was generated, and standards, negative intensities, weak reflections ($I<3\sigma(I)$), and uneven profile reflections were flagged. Identical reflections (i.e. standards) were then averaged.

The A^*_θ, L, and p corrections (equation 2.25) were then applied to the I's and $\sigma(I)$'s (with $I < 0$ reflections set to $I = 0$) to give a set of F_{rel}'s and $\sigma(F)$'s. When the A^*_θ values were unavailable because the cell contents were not known, A^*_θ was set to 1.0, and after the structure solution $(A^*_\theta)^{\frac{1}{2}}$ was applied to each F and $\sigma(F)$.

The resulting set of unaveraged F's and $\sigma(F)$'s along with the corresponding h, k, and l indices and a flag (observed, weak, or systematically absent), were stored as a file on the CYBER computer for subsequent use in other programs.

The averaging of symmetry equivalent F's to give a 'unique' set of data for the chosen space group was done by XRAY76 for the first two structures (3A, 3B; chapter 3). Because this program supplied only an arithmetic average, the averaging for the later structures was done with programs allowing σ^{-2} weighted averaging. When enough symmetry related data were collected (e.g. 4 or 8 equivalent reflections) the local program ABSCHK was used (3C, 3D, 3E; chapter 3), which

set $\sigma = \sigma_c(F)+GF^2$ and $\omega = \sigma^{-2}$ in the weighted average. The value of G was determined by fitting (by trial and error) a curve of SDEV vs. FMEAN to a curve of ESD vs. FMEAN, where

$$\text{FMEAN} = \sum_i \omega_i F_i / \sum_i \omega_i \qquad (2.45)$$

$$\text{SDEV} = \left(\sum_i \omega_i \right)^{-\frac{1}{2}} \qquad (2.46)$$

$$\text{ESD} = \left[\frac{\sum_i \omega_i (F_i - \text{FMEAN})^2}{(N-1) \sum_i \omega_i} \right]^{\frac{1}{2}} \qquad (2.47)$$

with sums over the N symmetry equivalent F_i's in each set. After averaging, the FMEAN's and SDEV's replaced the F's and σ_c's in the reduced data set. Thus later structure refinement using $\omega = \sigma^{-2}$ was equivalent to using equation (2.32) for the weights in equation (2.38), that is the σ's were 'F-weighted'. Also, the tables of $|F_o|$, $|F_c|$, σ data (Britten (1984)) for data sets processed by ABSCHK have 'F-weighted' σ's.

Unfortunately, the use of ABSCHK was very time consuming, both on the diffractometer and the computer, especially for low symmetry structures. The SHELX (Sheldrick (1976)) averaging with σ_c^{-2} weights was used for all other structures.

2.5.2 Structure Solution

The reduced data were processed by the structure solving programs, as outlined in Section 2.2.3. For the first two structures (3A, 3B; Chapter 3), the programs CUDLS (Stephens (1973)) and SYMFOU (Rutherford (1965)) were used

for the full-matrix least-squares and Fourier calculations, respectively. N_{used} was defined as the number of reflections with $I \geq 3\sigma(I)$ plus those with $3\sigma(I) > I > 0$ and $|F_c| > |F_o|$. The secondary extinction correction was due to Larson (1967).

The remaining structures were solved using the program SHELX (Sheldrick (1976)), which was chosen because of its great efficiency. SHELX offered full- or blocked-matrix least-squares, Fourier map peak search with a plot of possible molecules (made up of atoms and Fourier difference map peaks), condensed data decks, and 'tied' variables. The subroutine MOLGEOM from CUDLS was retained for geometry calculations (bond lengths and angles) and NRC-22 (Pippy, Ahmed (1968)) was used for the calculation of least-squares planes and torsion angles.

The SHELX calculations (outlined in this chapter) were adopted from Cruickshank's (1970) text. N_{used} was defined as the number of measurements with $I > 0$. The secondary extinction correction is given by equation (2.17a).

For all structures, the final refinement cycles used full-matrix (occasionally without hydrogen atom parameters) least-squares methods.

2.5.3 Data Presentation

For each compound studied, the source of the crystal is first presented, followed by the elemental analyses. A crystal data summary is then given in abbreviated form:

structural formula, ionic formula; M_m = relative molar mass; space group; diffractometer used; reflection 2θ range for cell parameter least-squares refinement; the cell parameters not defined by symmetry; V = cell volume, Z = the number of formula units in the cell; D_x = calculated density, D_m = measured density, 'solvents' used for D_m; 2θ limit for data, N_{meas} = total number of reflections measured (including all standards), minimum R_{scan}; temperature at which data were collected; h k l (estimated standard deviation from XRAY76) for standards; the type of absorption correction used, μ, crystal dimensions, A^*_θ limits; N_{unique} = number of reflections in the reduced data set, including those with I = 0, N_{used}; NP = number of parameters in final cycle; F(000) not including $\Delta f'$ or $\Delta f''$; the weighting factor ω, $S = (\Sigma\omega(|F_o|-|F_c|)^2/(N_{used}-NP))^{\frac{1}{2}}$ (when available from programs used), the secondary extinction factor g; the maximum shift per error $|\Delta p/\sigma_p|$ (and the average in brackets), R and R_ω (equations (2.30) and (2.31)); the highest peak and lowest valley on the final difference map; the programs used.

The list is followed by the details of the phase solution, and tables of the atomic parameters x, y, z and U where U is either U_{iso} or U_{eq}.

$$U_{eq} = (U_{11}+U_{22}+U_{33}+2U_{12}\cos\gamma+2U_{13}\cos\beta+2U_{23}\cos\alpha) \qquad (2.48)$$

Selected bond lengths and angles are tabulated, and the molecular geometry and packing is discussed, with the aid of

ORTEPII (Johnson (1976)) diagrams. σ values used for comparison of bond lengths or angles are given by

$$\sigma = (\sigma_1^2 + \sigma_2^2)^{\frac{1}{2}} \qquad (2.49)$$

Tables of hydrogen atom parameters and anisotropic temperature factors are found in the appendices. The moduli of F_o and F_c (with σ) are given in a separate volume (Britten (1984)).

CHAPTER 3

DIETHYLENETRIAMINE AND AQUA COMPLEXES OF Pt

3.1 Introduction

The mechanism of action of the anticancer drug cis-$Pt(NH_3)_2Cl_2$ is thought to involve the hydrolysis of the Pt-Cl bonds in the cell, where the chloride ion is in low concentration. The resulting aqua and hydroxo complexes (monomers, dimers, trimers, etc.) can then attack the bases of the DNA, and prevent proper cell replication (Lock, Bradford, Faggiani, Speranzini, Turner, Zvagulis (1977); Lock (1980); Cleare (1974); Thomson (1974); Cleare (1977)). In the study of the hydrolysis products, compounds having bridging hydroxo groups have been isolated in the solid state, such as $[(NH_3)_2Pt(OH)_2Pt(NH_3)_2](NO_3)_2$, $[(NH_3)_2Pt(OH)]_3(NO_3)_3$, $[\{(NH_3)_2Pt(OH)\}_3]_2(SO_4)_3 \cdot 6H_2O$, $[\{(NH_3)_2Pt(OH)_2Pt(NH_3)_2\}_2](CO_3) \cdot 3H_2O$ (Lock (1980) and references therein). However, complexes of Pt(II) having terminal hydroxo or aqua ligands, which are known to exist in solution (Basolo, Gray, Pearson (1960); Reishus, Martin (1961)), could not be crystallized, even from solutions at low pH (Lippert, Lock, Rosenberg, Zvagulis (1977)). The measurement of the Pt(II)-OH_2 or Pt(II)-OH bond distance would be of interest in relating the thermodynamic strength of the bond to its obvious kinetic lability. For example, is the Pt(II)-O bond stronger in a nitrato complex

than in an aqua-complex, since only cis-$Pt(NH_3)_2(ONO_2)_2$, and not an aqua-complex, crystallizes from solution?

At the suggestion of Harry B. Gray, complexes of the type $[Pt(dien)X]X$, where $X=I^-,Cl^-,NO_3^-$, or F^-, and dien= diethylenetriamine, $NH_2(CH_2)_2NH(CH_2)NH_2$, were prepared. The tridentate dien ligand would leave only one coordination site remaining on Pt(II), minimizing the possibility of OH^- bridges forming in solution (although mono-bridged species are known (Lippert (1983))). The crystal structures of $[Pt(dien)Cl]Cl$, 3C, and $[Pt(dien)ONO_2]^+\cdot NO_3^-$, 3D, were determined, and are presented here. Two other compounds, $[PtCl_4]^{2-}\cdot 2[NH_3(CH_2)_2NH_2(CH_2)_2NH_3]^{3+}\cdot 4Cl^-$, 3A, and fac-$[Pt(dien)Cl_3]^+\cdot Cl^-\cdot H_2O$, 3B, were also prepared (unexpectedly) in an attempt to make $C_8H_{30}Cl_8N_6OPt_3$ (for details see discussion below). A comparison of the configuration of the dien ligand in 3B to similar fac-M(dien) complexes prompted a more precise definition of the geometry of such compounds, and a revision of the prediction of configuration as found in the literature (Schmidtke, Garthoff (1968)).

After failing to obtain $[Pt(dien)(OH_2)]^{2+}\cdot(NO_3)_2^-$ in the solid state, the fluorine analogue was prepared. This compound was very hygroscopic, and yielded a glassy, yellow-brown solid when dried under N_2 at room temperature. No crystals were obtained. The infrared spectrum could not unambiguously distinguish between $[Pt(dien)F]^+\cdot F^-\cdot nH_2O$ and $[Pt(dien)(OH_2)]^{2+}(F)_2^-\cdot(n-1)H_2O$ since the $Pt-OH_2$ and Pt-F

vibrations absorb in the same region, and lattice bound water molecules would be strongly hydrogen-bonded. At present, proton and ^{19}F solid state NMR are not readily available.

Using Brown's (1981) bond valence method, it was possible to explain why terminal OH_2 and OH^- moieties on Pt(II) were difficult to crystallize, and why the nitrato complexes were stable (cf. §3.3.4). Predictions on the type of environment which would stabilize such bonds were also possible (Lock (1980); Britten, Lock, Pratt (1982)). Lippert did succeed in preparing crystals containing terminal aqua and hydroxo ligands, and the structure of $[Pt(NH_3)_2(OH_2)(C_5H_7N_3O)]^{2+}\cdot(NO_3)_2^-\cdot H_2O$, 3E, is presented here. The environment of the coordinated water molecule is as predicted, and nicely illustrates Brown's bond valence rules. The hydroxo complex also crystallized as expected. Its structure is presented elsewhere (Britten, Lippert, Lock, Pilon (1982), Pilon (1984)).

In this chapter, the chemistry and structures of 3A, 3B, 3C, 3D, and 3E are discussed in detail, and the bond valence model is outlined and used where required.

3.2 Bis(diethylenetriammonium) Tetrachloroplatinate(II) Tetrachloride (3A) and fac-Trichloro(diethylenetriamine-N^1,N^2,N^3)platinum(IV) Chloride Monohydrate (3B), with a Proposed Convention for the Description of Tridentate Dien Configurations.

The synthesis of [Pt(dien)X]X, where X=Cl, I, is presented by Watt and Cude (1968). In their paper, they also discuss the synthesis, chemistry, and IR spectrum of $C_8H_{30}Cl_8N_6OPt_3$, which they postulate as

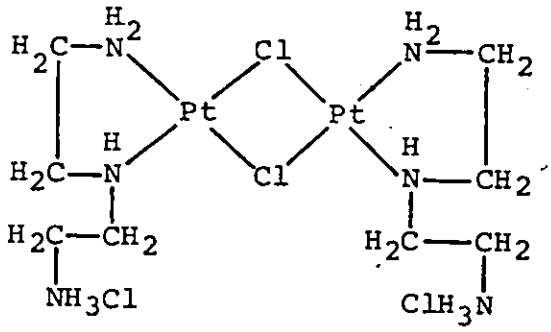

$\cdot [PtCl_4]^{2-} \cdot H_2O.$

The evidence used to justify the proposed structure was

1) $C_8H_{30}Cl_8N_6OPt_3$ + xs 6M aqueous ammonia →

$[Pt(dien)NH_3]^{2+}[PtCl_4]^{2-}$ (pink, 87% yield) +

$[Pt(dien)NH_3]^{2+} + 2Cl^- + 2HCl + H_2O$

$[Pt(dien)NH_3]^{2+}[PtCl_4]^{2-}$ + xs 6M aqueous ammonia

$[Pt(NH_3)_4]^{2+}[PtCl_4]^{2-}$ (green) $(+[Pt(NH_3)_4]^{2+}+2Cl^-)$

2) maintenance of coordination number 4 for Pt(II)

3) the known bidentate role for dien in relatively strong acidic solutions (no references)

4) the preference for a five-membered ring over the alternative eight-membered ring

5) similarity in the "NH_3Cl" stretching bands (3100-3200 cm^{-1} in the IR) to those of $ClCH_2CH_2NH_3Cl$

6) strong IR absorption at 1510 cm^{-1}, assigned as δNH_3Cl: "the influence of the added mass of the HCl unit should lower the frequency (from 1611 cm^{-1} presumably) owing to

inertial effects"

7) elemental analyses: Found: Pt, 53.36; C, 8.85; H, 2.80; Cl, 25.60%. Calculated: Pt, 53.44; C, 8.77; H, 2.76; Cl, 25.90%.

Watt and Cude prepared this compound by reducing K_2PtCl_6(aq) with $N_2H_4 \cdot HCl$ (2:1) and using 20% KOH to neutralize the resulting K_2PtCl_4, HCl solution. Two equivalents of dien·3HCl were then added (ie. 2dien:1Pt), and the solution was refluxed for 8 hours. Orange crystals of $C_8H_{30}Cl_8N_6OPt_3$ were obtained by cooling the solution to 5C. Recrystallization from 1M HCl gave the same compound as dark red crystals.

It was decided that single-crystal X-ray analysis of this compound was needed to determine the structure, as the proposed structure seemed doubtful.

Firstly, the "$-NH_3Cl$ unit" is certainly not a unit, but an ion pair, $-NH_3^+ + Cl^-$, and the mass of Cl^- should have little or no effect on the "$-NH_3^+$" vibration. Secondly, if the dimer $[(Pt(dien \cdot H)Cl)_2]^{4+}$ was formed, it would very likely be unstable in excess Cl^- and a threefold excess of dien, since for Cl-bridged Pt dimers, equilibria generally lie towards the mononuclear complexes (Cotton, Wilkinson (1980), p. 952). Thirdly, recrystallization from 1M HCl would likely cause decomposition, yet none was observed. Fourthly, no evidence of a Cl-bridge was observed in the IR spectrum. A more likely formulation for $C_8H_{30}Cl_8N_6OPt_3$ would

be $2[Pt(dien\cdot H)Cl_2]^+\cdot[PtCl_4]^{2-}\cdot H_2O$.

Two attempts were made to prepare $C_8H_{30}Cl_8N_6OPt_3$. In the first preparation, the procedure was modified because of the availability of K_2PtCl_4. 0.26g K_2PtCl_4 (.626mmol) was refluxed with 0.13g dien (1.26 mmol) in 50 mL 1M HCl for 5h. The high acidity of the solution caused complete protonation of the dien, and the resulting compound, 3A, contained diethylenetriammonium and tetrachloroplatinate(II) in a 2:1 ratio, with four Cl^- ions balancing the charge. Large red-orange crystals were obtained. (Analysis: Found: C, 14.0; H, 4.8; Cl, 41.2; N, 12.1%. Calculated for $2(dien\cdot 3H)^{3+}\cdot[PtCl_4]^{2-}\cdot Cl_4^-$: C, 13.9; H, 4.7; Cl. 41.0; N, 12.2%.)

For the second synthesis, the Watt and Cude procedure was followed carefully. K_2PtCl_6 was prepared by the method of Kauffman and Teter (1963). To a suspension 2.306 g of the K_2PtCl_6 (4.745 mmol) in 20 mL H_2O was added 0.249 g of oven-dried $N_2H_4\cdot 2HCl$ (2.372 mmol) and the mixture was stirred for 20 h, giving the expected deep-red solution. The solution was filtered at room temperature (no solid observed) and the pH was adjusted to 7.0 with 20% KOH(aq). At this point, however, a black precipitate formed, which was not found in the original procedure. It was suspected that the Pt(II) had disproportionated to give Pt^0 and Pt^{IV}, so the solution was refiltered, and an excess of dien·3HCl (2.0167 g, 9.488 mmol) was added to the supernatant to test for Pt(II) or Pt(IV). Large yellow crystals of fac-$[Pt^{IV}(dien)Cl_3]\cdot Cl$ [illegible]O, 3B,

formed when the water was allowed to evaporate, and were used directly for crystallographic study. (Analysis: Found: C, 10.8; H, 3.6; Cl, 31.2; N, 9.4%. Calculated: C, 10.5; H, 3.3; Cl, 31.0; N, 9.2%.)

No further attempts were made to synthesize $C_8H_{30}Cl_8N_6OPt_3$.

3.2.1 Crystal Data for 3A

$2[NH_3(CH_2)_2NH_2(CH_2)_2NH_3]\cdot[PtCl_4]\cdot Cl_4$, $2C_4H_{16}N_3^{3+}\cdot 4Cl^-\cdot Cl_4Pt^{2-}$; 691.09 $g\cdot mol^{-1}$; C2/c; Syntex $P2_1$ diffractometer; 15 refl. ($17° < 2\theta < 25°$) for cell; a=21.496(3), b=6.841(1), c=15.820(4)Å, β=104.14(2)°; V=2256.0(7)Å^3, Z=4; D_x=2.03, D_m=2.02 $g\cdot cm^{-3}$ in CH_2I_2/CCl_4; $2\theta_{max}$=55°, +h, +k, ±l; N_{meas}=2985, min R_{scan}=8.37 $deg\cdot min^{-1}$; 23°C; standards: -5 1 -2 (1.9%), -11 1 2 (2.3%); Bond abs. corr., μ=74.9cm^{-1}, cyl.: r=0.157mm, l=0.506mm, $4.61 < A_\theta^* < 6.77$; N_{unique}=2585, N_{used}=2472; NP=71; F(000)=1344; $\omega=(\sigma_F^2 + 0.00090F_o^2)^{-1}$, S=undetermined, g(CUDLS)=1.353×10^{-7}; max. shift/error, (ave.)=0.020(0.003), R=0.034, R_ω=0.050; Diff. map: -1.5, 2.8 $e^-\cdot Å^{-3}$, both near Pt; XRAY76, CUDLS, SYMFOU, PALS, ORTEPII.

The Pt atom was located on special position 4e (y = .07410) with the use of the Patterson method. Difference Fourier syntheses revealed all of the non-hydrogen atoms (in general positions). The hydrogen atoms were not detected. The final positional parameters and isotropic temperature factors are given in Table 3.1.

Table 3.1. Positional parameters ($x10^4$) and isotropic temperature factors ($Å^2$) ($x10^3$) for 3A.

	x	y	z	U_{iso} or Ueq*
Pt	0	.741.0(4)	2500	23.5(2)*
Cl(1)	200.7(7)	3095(2)	3575.6(9)	33.1(7)*
Cl(2)	156.2(7)	-1613(2)	3562.8(9)	33.5(7)*
Cl(3)	1946.7(8)	-642(2)	2704(1)	36.3(7)*
Cl(4)	1979.7(7)	5254(2)	4556.6(9)	35.8(7)*
N(1)	3935(2)	775(6)	2382(3)	32(1)
C(1)	3601(3)	-954(7)	2627(3)	28(1)
C(2)	3514(3)	-642(7)	3548(4)	30(1)
N(2)	3295(2)	-2553(7)	3866(3)	30(1)
C(3)	3846(3)	-3795(9)	4321(4)	35(1)
C(4)	3644(3)	-5729(8)	4621(4)	37(1)
N(3)	3429(3)	-5602(7)	5452(4)	36(1)

A crystallographically good model composed of $2K^+ \cdot 2Cl^- \cdot [PtCl_4]^{2-} \cdot 2[dienH]^+$ was rejected for chemical reasons (a plus 1 dien molecule would have been coordinated to Pt). The correct structure, verified by elemental analyses, comprises discrete diethylenetriammonium [N(1)C(1)C(2)N(2)C(3)C(4)N(3)], chloride [Cl(3),Cl(4)] and tetrachloroplatinate(II) [PtCl(1)-Cl(2)] ions. Bond distances and angles (see Table 3.2) within the tetrachloroplatinate(II) ion are normal (Purnell, Hodgson (1976)). Distances and angles within the diethylenetriammonium ion, $[dien \cdot 3H]^{3+}$, are similar to those observed in $[dien \cdot 3H][Cu(II)Cl_4]Cl$ (Greenhough, Ladd (1977)), but there are some differences in the two halves of the cation in 3A and between cations in the two compounds. Equivalent bond distances do not differ significantly except that C(2)-N(2) is 3.7σ longer than the equivalent distance in the Cu complex. Differences in angles are much more marked. In the copper complex, the angles N(terminal)-C-C [112.0(2)°] differed by 15.2σ from C-C-N(middle) [107.7(2)°]. In 3A there are insignificant differences in these angles in a given half [113.6(5) 113.4(5) and 108.5(4), 108.4(4)°], but clearly the two halves differ markedly (7.89σ).

The normal configurations of a non-coordinated N-C-C-N system are trans where the dihedral angle between the two N-C-C planes is close to 180° and cis where the dihedral angle is about 70° (N—◎—N or N—◎, N). The former arrangement is observed for 3A in the half where the N-C-C angles

Table 3.2. Selected interatomic distances (Å) and angles (deg) for 3A.

(a) Bonded		(b) Non-bonded or hydrogen bonded	
Pt-Cl(1)	2.306(1)	N(1)-Cl(3)^{i}	3.080(5)
Pt-Cl(2)	2.293(1)	N(1)-Cl(4)^{ii}	3.233(5)
N(1)-C(1)	1.482(7)	N(1)-Cl(1)^{ii}	3.239(6)
C(1)-C(2)	1.529(8)	N(1)-Cl(2)^{i}	3.267(6)
C(2)-N(2)	1.516(7)	N(1)-Cl(2)^{iv}	3.344(5)
N(2)-C(3)	1.492(7)	N(1)-Cl(1)^{iii}	3.438(5)
C(3)-C(4)	1.505(9)	N(2)-Cl(4)^{v}	3.127(5)
C(4)-N(3)	1.50(1)	N(2)-Cl(3)^{ii}	3.205(5)
Cl(1)-Pt-Cl(1)	91.39(5)	N(2)-Cl(3)	3.300(4)
Cl(1)-Pt-Cl(2)	88.97(5)	N(2)-Cl(4)^{vi}	3.599(5)
Cl(1)-Pt-Cl(2)	177.71(5)	N(3)-Cl(4)^{vi}	3.147(5)
Cl(2)-Pt-Cl(2)	90.76(5)	N(3)-Cl(4)^{vii}	3.300(5)
N(1)-C(1)-C(2)	108.5(4)	N(3)-Cl(3)^{vii}	3.323(6)
C(1)-C(2)-N(2)	108.4(4)	N(3)-Cl(2)^{vii}	3.414(5)
C(2)-N(2)-C(3)	112.2(4)	N(3)-Cl(1)^{vii}	3.426(5)
N(2)-C(3)-C(4)	113.4(5)		
C(3)-C(4)-N(3)	113.6(5)		

Atoms with superscripts are related to the atoms in Table 3.1 by the transformations:
(i) ½-x, ½+y, ½-z; (ii) ½-x, -y+½, ½-z; (iii) ½+x, y-½, z; (iv) ½+x, ½+y, z; (v) ½-x, ½-y, 1-z; (vi) x, y-1, z; (vii) ½-x, -y+½, 1-z.

are close to the tetrahedral angle (dihedral angle 169.0°), but larger N-C-C angles are found in the half with the cis arrangement (dihedral angle 79.9°). This geometry brings N(3) and N(2) fairly close together [3.22(1)Å] and apparently induces sufficient strain to enlarge the N-C-C angles. In the Cu structure, both halves have the trans arrangement. The central C-N-C angle in 3A is 6.93σ smaller than that of the Cu compound. In both cases, the conformation is dictated by hydrogen-bonding and packing requirements in the crystal.

Although hydrogen-bonding is clearly important in holding the crystal together, there are ambiguities as to which atoms are hydrogen-bonded and these cannot be resolved by considering interatomic distances and angles (see Table 3.2). The arrangement of the three N atoms about Cl(1) and Cl(2) is interesting because it is essentially the same for both atoms. The three N atoms form the apices of a T with the junction at Cl, the T being oriented such that the Pt-Cl-N angles are all close to 90°.

The packing within the unit cell is shown in Figure 3.1. It is interesting that, although the Pt and Cu complexes are made up of similarly shaped and charged ions, the different stoichiometries result in completely different crystal structures. The structure of 3A is essentially a series of layers parallel to the **bc** plane. Core layers of $PtCl_4^{2-}$ ions lie at x = 0 and 0.5 and these are sandwiched between and hydrogen-bonded to layers of dien·3H ions displaced roughly

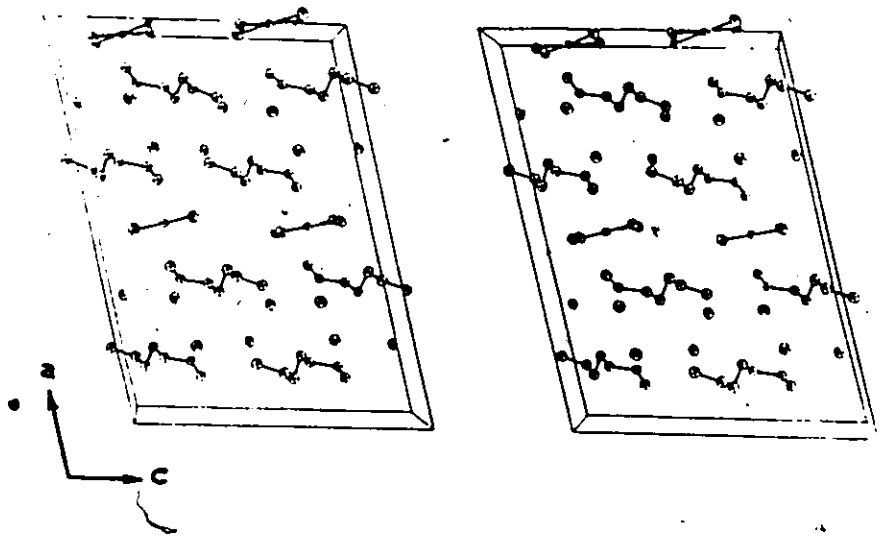

Figure 3.1. The unit cell contents of 3A

± 0.15 along **a**. These cation layers are in turn separated and cross hydrogen-bonded to irregular layers of Cl(3) and Cl(4) ions centered at x = 0.25 and 0.75. Packing within the **bc** planes shows no peculiarities and is determined by the hydrogen-bonding requirements. The $[PtCl_4]^{2-}$ ions do not form the asymmetrically Cl-bridged chains seen in the Cu compound.

The IR spectrum of 3A (Figure 3.2) is quite different from that of $C_8H_{30}Cl_8N_6OPt_3$, although the 1510 cm^{-1} absorbance (δ-NH_3) is seen at approximately 1495 cm^{-1} for 3A.

3.2.2 The Crystal Structure of 3B

$[Pt(NH_2(CH_2)_2NH(CH_2)_2NH_2)Cl_3]\cdot Cl\cdot H_2O$, $C_4H_{13}Cl_3N_3Pt^+\cdot Cl^-\cdot H_2O$; 458.08 $g\cdot mol^{-1}$, Pbca; Syntex $P2_1$ diffractometer; 15 refl. ($22.5<2\theta<34.4°$) for cell; a=16.606(8), b=12.490(4), c=11.293(2)Å; V=2342(1)$Å^3$, Z=8; D_x=2.60, D_m=2.60 $g\cdot cm^{-3}$ in CH_2I_2/CCl_4; $2\theta_{max}$=55°, +h, +k +l; N_{meas}=2297, min. R_{scan}= 8.37 $deg\cdot min^{-1}$; 23°C; standards: 1 0 6 (1.7%), 2 1 4 (1.4%); Bond abs. corr., μ=135cm^{-1}, approx. sphere: r=0.101mm, $4.67<A^*_\theta<6.90$; N_{unique}=2207, N_{used}=1722; NP=79; F(000)=1712; $w=(\sigma_F^2 + .00123F_o^2)^{-1}$, S=undet., g(CUDLS)=$6.973\times10^{-7}$, max. shift/error,(ave.)=0.033(0.007), R=0.058, R_w=0.059; Diff. map: -3.8, 2.1 $e\cdot Å^{-3}$, both near Pt; XRAY76, CUDLS, SYMFOU, PALS, ORTEPII.

The platinum atom was located from a three-dimensional Patterson map and all other non-hydrogen atoms were found from electron density difference syntheses. The hydrogen atoms were not found. The final positional parameters and

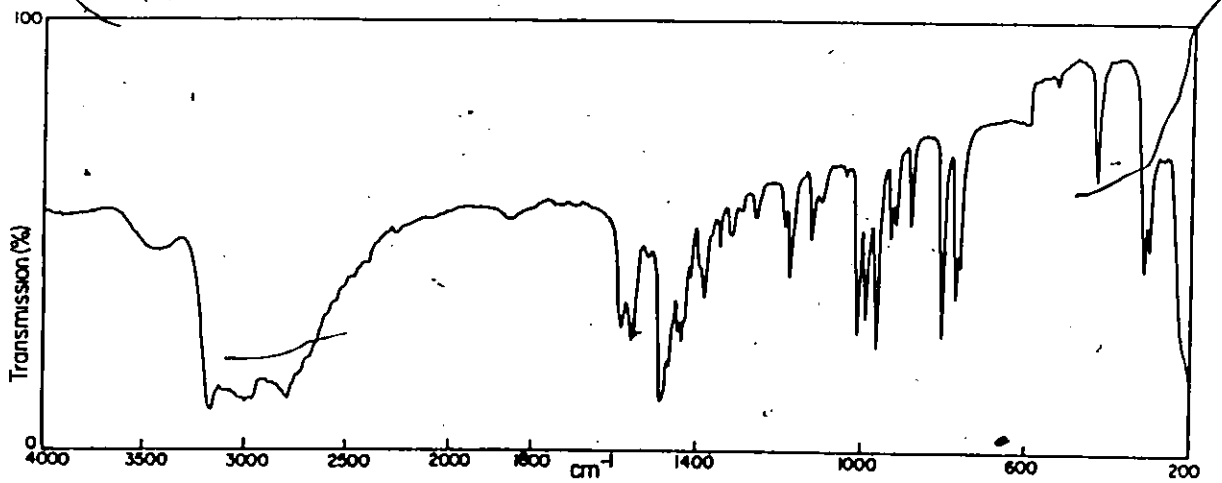

Figure 3.2. Infrared spectrum (KBr disc) of 3A. The drop in absorption at 600 cm^{-1} is caused by a grating change. (Recorded on a Perkin-Elmer 283.)

isotropic temperature factors are given in Table 3.3. The temperature factor for C(1) is large and the possibility of disorder was considered, particularly since in the structural packing of the crystal C(1) in one molecule is close to C(1) of another. Attempts to refine C(1) in two different positions using partial occupancies led to the occupancy at the present position tending to 1.0.

The structure comprises discrete fac-trichloro(dien)-platinum(IV) and chloride ions and water molecules. The molecular cation is illustrated in Figure 3.3. Bond distances and angles are given in Table 3.4. The Pt-Cl(1) distance is significantly shorter than the Pt-Cl(3) distance [2.315(3) vs. 2.332(4)Å], the reason being obscure. All Pt-Cl distances are within the range previously observed (Lock, Speranzini, Zvagulis (1980), and references therein), as are the Cl-Pt-Cl, N-Pt-N, and N-Pt-Cl angles. Bond distances and angles within the dien group agree well with those found previously (see references given in Table 3.5).

The packing within the crystal is shown in Figure 3.4. The molecular ion is arranged such that N(1)...Cl(3), N(2)...Cl(2), and N(3)...Cl(1) are almost parallel to **a**, **b**, and **c** respectively. As a consequence, the PtN(1)C(2)N(2) and PtN(2)N(3) planes are almost parallel to the **ab** and **bc** planes respectively. Thus there are weak dipole-dipole interactions in the **a**, **b**, and **c** directions between molecules related by the a, b, and c glides, respectively. These forces are not

Table 3.3. Atomic positional parameters and isotropic temperature factors ($Å^2$) ($x10^3$) for 3B.

	x	y	z	U_{iso} or U_{eq}*
Pt	151.05(3)	135.10(3)	230.23(4)	20.4(4)*
Cl(1)	154.8(2)	121.2(2)	25.9(3)	34(2)*
Cl(2)	152.7(2)	321.2(2)	223.5(3)	30(2)*
Cl(3)	291.2(3)	125.8(3)	236.2(3)	37(2)*
N(1)	27.9(7)	137.9(8)	220.2(8)	25(2)
C(1)	-2(1)	31(1)	182(2)	59(5)
C(2)	46(1)	-55(1)	238(1)	42(3)
N(2)	137.0(7)	-28.7(9)	248.3(9)	28(2)
C(3)	171.9(8)	-60(1)	363(1)	28(3)
C(4)	142.3(8)	20(1)	456(1)	28(3)
N(3)	153.7(6)	133.0(8)	414(1)	26(2)
Cl(4)	474.6(2)	215.5(3)	16.3(3)	34(2)*
O	307.2(6)	167.0(7)	552.3(8)	36(2)

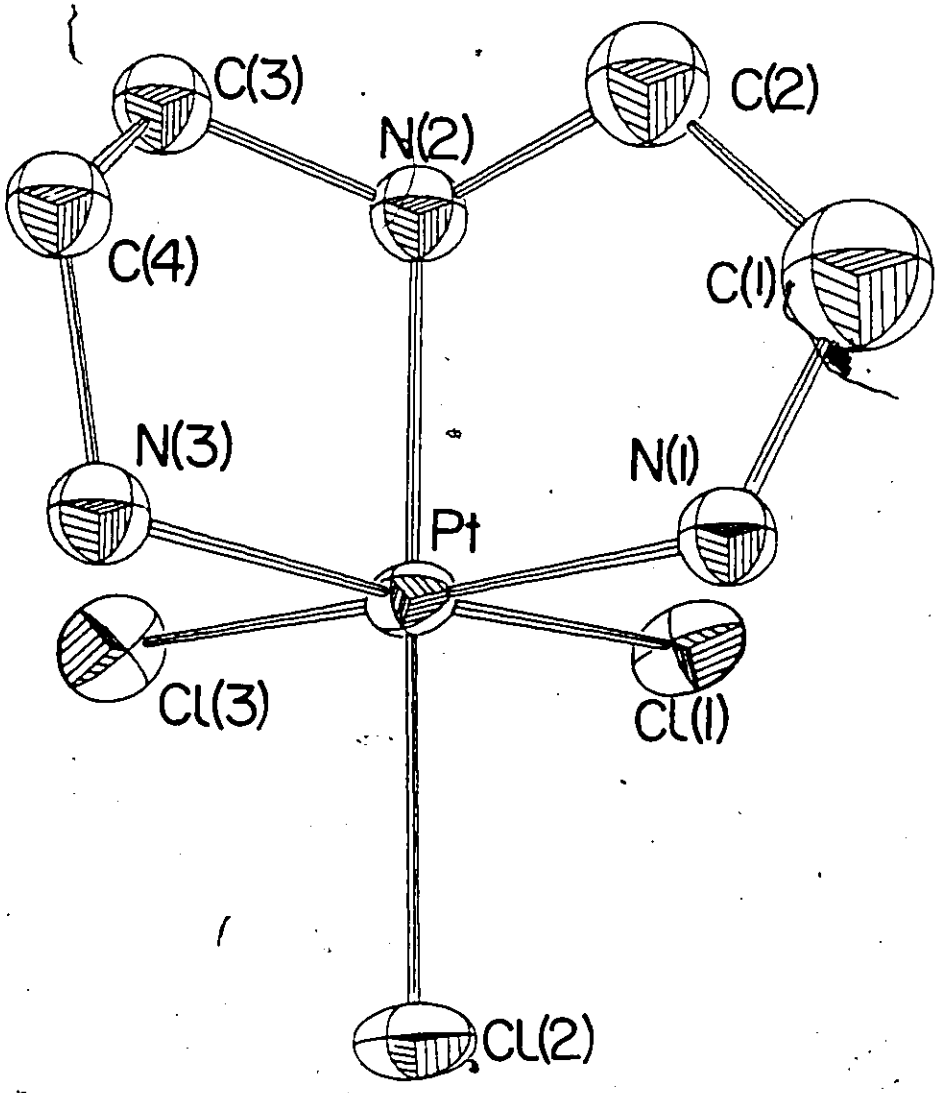

Figure 3.3. The molecular cation in 3B

Table 3.4. Selected interatomic distances (Å) and angles (deg) for 3B.

Pt-Cl(1)	2.315(3)	Pt-N(1)	2.05(1)
Pt-Cl(2)	2.326(3)	Pt-N(2)	2.07(1)
Pt-Cl(3)	2.332(4)	Pt-N(3)	2.08(1)
N(1)-C(1)	1.50(2)	C(1)-C(2)	1.48(2)
N(3)-C(4)	1.50(2)	C(4)-C(3)	1.53(2)
C(2)-N(2)	1.54(2)	C(3)-N(2)	1.48(2)

Possible hydrogen bonds

$N(3)-Cl(1)^{v}$	3.32(1)	$Cl(2)-O^{i}$	3.22(1)
$Cl(3)-O^{i}$	3.33(1)	$N(1)-Cl(4)^{ii}$	3.36(1)
$N(1)-Cl(4)^{iii}$	3.25(1)	$N(2)-O^{iv}$	2.96(1)
$N(3)-Cl(4)^{iii}$	3.24(1)	N(3)-O	3.02(1)
$Cl(4)-O^{i}$	3.17(1)		

Cl(1)-Pt-Cl(2)	92.4(1)	Cl(1)-Pt-Cl(3)	89.9(1)
Cl(1)-Pt-N(1)	88.5(3)	Cl(1)-Pt-N(2)	91.6(3)
Cl(1)-Pt-N(3)	174.3(3)	Cl(2)-Pt-Cl(3)	92.2(1)
Cl(2)-Pt-N(1)	89.6(3)	Cl(2)-Pt-N(2)	173.1(3)
Cl(2)-Pt-N(3)	92.6(3)	Cl(3)-Pt-N(1)	177.6(3)
Cl(3)-Pt-N(2)	93.5(3)	Cl(3)-Pt-N(3)	87.1(3)
N(1)-Pt-N(2)	84.8(4)	N(1)-Pt-N(3)	94.4(4)
N(2)-Pt-N(3)	83.8(4)	Pt-N(1)-C(1)	109.5(9)
N(1)-C(1)-C(2)	110(1)	C(1)-C(2)-N(2)	114(1)
C(2)-N(2)-C(3)	113(1)	N(2)-C(3)-C(4)	108(1)
C(3)-C(4)-N(3)	111(1)	C(4)-N(3)-Pt	108.8(7)
Pt-N(2)-C(2)	108.2(8)	Pt-N(2)-C(3)	107.7(8)

Atoms are related to those in Table 3.3 by (i) x, 1/2-y, z-1/2; (ii) x-1/2, 1/2-y, -z; (iii) x-1/2, y, 1/2-z; (iv) 1/2-x, -y, z-1/2; (v) x, -1/2-y, 1/2+z.

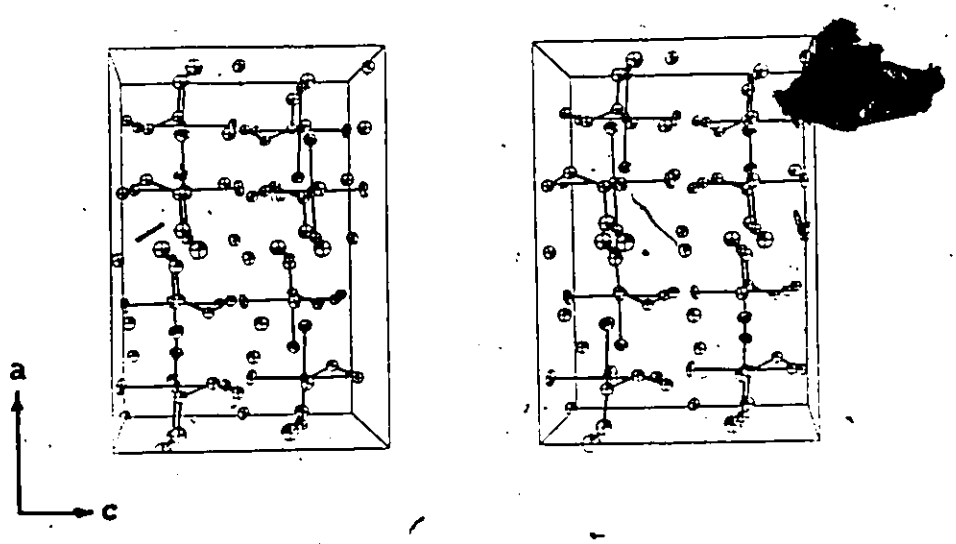

Figure 3.4. The packing of 3B within the unit cell

as important in holding the crystal together, however, as are the the hydrogen-bonds. The molecular cations can be considered as packing in double layers about planes centered at x = 0.25 and 0.75 with molecules in the double layer being related by the a- and c-glide operations. Thus the hydrocarbon fragments are parallel to the double layer, or point out of it, providing hydrocarbon-hydrocarbon contacts between double layers at x = 0 and 0.5. Within the layer, important hydrogen-bonding is between Cl(1) and N(3) of adjacent molecules related by the c-glide and also between the water molecule and Cl(2) and Cl(3) of one molecule, N(3) of a cation related to the first by the c-glide, and N(2) of a cation related to the first by the b-glide. In addition, the water molecule provides cross-linking between double layers since it is hydrogen-bonded to Cl(4) which is in turn hydrogen-bonded to N(1) and N(3) of a molecule in the next double layer and to N(1) of its c-glide related neighbour.

The infrared spectrum of 3B, (Figure 3.5), differs significantly from those of the complexes prepared by Watt and Cude (1968), but is very similar to those reported for fac-M(dien)L_3 complexes by Schmidtke and Garthoff (1968), with minor variations. In particular, the band at 1250 cm-1 is stronger than would be expected for a pure fac-dien complex. It was considered that this undue strength might have arisen from a mer-dien contaminant, which normally has a strong band at 1250 cm^{-1} (Schmidtke, Garthoff (1968)).

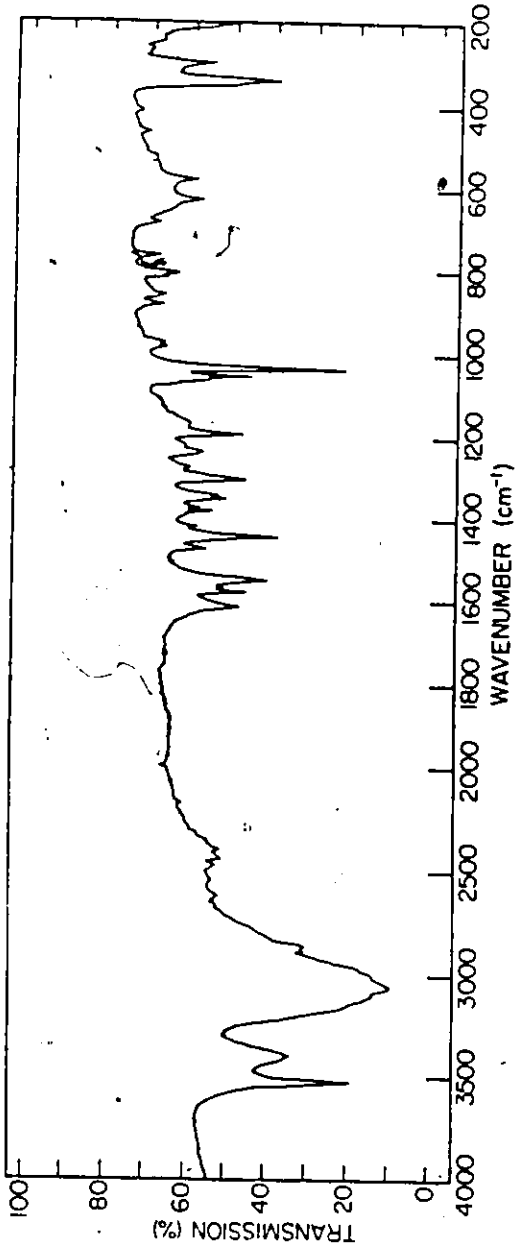

Figure 3.5. The infrared spectrum of 3B (KBr disc, Perkin-Elmer 283)

However, the spectrum is reproducible when using selected single crystals to prepare the sample for vibrational spectroscopy. In addition, the X-ray powder diffraction pattern of the same sample matched one generated from the single-crystal parameters. Therefore, the observed spectrum is that of a pure compound.

The paper of Schmidtke and Garthoff (1968) made some predictions about unstable ring conformations in fac-(dien)M complexes which were at variance with results found in a literature search. In addition, the conformation of fac-MoO_3-(dien) was incorrectly assigned. Therefore, a detailed study of the ring conformations in fac-dien complexes was made.

There are various possible combinations of conformations for the two rings of diethylenetriamine and these have been extensively studied and discussed (see references in Table 3.5). Two methods of discussing the conformation are (1) in terms of the torsional angles about the C-C bonds, in other words the dihedral angle between the N(A)C(A)C(B) and C(A)C(B)N(B) planes, and (2) in terms of the distances of the carbon atoms from the MN(A)N(B) plane. Here three types of distortion can be seen. The carbon atoms can be symmetrically distributed about the plane(I), asymetrically distributed about the plane(II) or both asymetrically distributed on the same side of the plane(III).

I 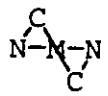 II 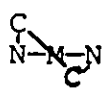 III 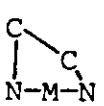

These distortions have generally been explained in terms of non-bonding hydrogen interactions on adjacent CH_2 or NH_2 groups, following the discussions of Corey and Bailar (1959) concerning ethylenediamine (en) complexes. There is an alternative, and hopefully better, way of looking at these structures which shows more clearly that they represent a continuum. By working in terms of the plane N(A)<C>N(B), where <C> is the midpoint between C(A) and C(B), there is an advantage in that C(A) and C(B) are symetrically displaced about the plane and the distance of C(A) or C(B) out of the plane correlates well with the torsion angle (Tables 3.5,3.9). The most important feature is that one now measures the distance of M out of the N(A)<C>N(B) plane, and I, II, and III represent points on a continuum as the metal moves out of the plane. Considering the problem in this way raises the question of why the metal atom moves out of the plane. The most important reason is that it is caused by the rotation of the NH_2 and NH groups in order to maximize hydrogen-bonding interactions in the crystal.

The same effect is probably important in determining ring conformations. Keene and Searle (1972,1974) have shown that this is an important factor in determining the geometry of the bis(dien)cobalt(III) cation. The other factor determining ring conformation is intramolecular non-bonded hydrogen interactions on the CH_2 and NH_2 groups. Based on the arguments of Corey and Bailar (1959), it has been suggested (Schmidtke,

Table 3.5. Comparison of the conformations of fac-M(dien) octahedral complexes

Compound	Distance of C atoms from MN3 plane (Å) M(1)M		M(2)M		Distance of C and M atoms from MN3 plane (Å)* N(1)N(2)*C(1)C(2)*		N(2)N(3)*C(3)C(4)*		Torsional Angles MCCN ** N(1)C(1)C(2)N(2)	N(2)C(3)C(4)N(3)	Conformation I	II	Reference
fac-Mo(dien)$_3$	C(1)	0.04	C(3)	0.54	Mo	-0.36	Mo	0.36	45.1°	-45.1°	(i)	(ii)	A
	C(2)	-0.54	C(4)	-0.04	C(1)	0.30	C(3)	0.30					
					C(2)	-0.30	C(4)	-0.30					
fac-Mo(dien)(CO)$_3$	C(1)	-0.11	C(3)	-0.09	Mo	-0.58	Mo	0.55	48.6°	46.7°	(i)	(ii)	B
	C(2)	0.30	C(4)	-0.65	C(1)	0.30	C(3)	-0.30					
					C(2)	-0.30	C(4)	0.30					
fac-Cr(dien)(CO)$_3$	C(1)	-0.08	C(3)	0.17	Cr	-0.49	Cr	0.54	45.8°	40.3°	(i)	(ii)	C
	C(2)	-0.67	C(4)	0.65	C(1)	0.33	C(3)	-0.25					
					C(2)	-0.33	C(4)	0.25					
fac-Cr(dien)Cl$_3$	C(1)	0.28	C(3)	0.53	Cr	-0.01	Cr	0.28	44.6°	-47.8°	(i)	(ii)	D
	C(2)	-0.50	C(4)	-0.07	C(1)	0.29	C(3)	0.33					
					C(2)	-0.29	C(4)	-0.33					
[u-Co(en)(dien)Cl]$^{2+}$	C(1)	0.04	C(3)	0.23	Co	-0.28	Co	-0.08	50.3°	-41.8°	(i)	(ii)	E
	C(2)	-0.58	C(4)	-0.38	C(1)	0.32	C(3)	0.30					
					C(2)	-0.32	C(4)	-0.30					
[s-fac-Co(dien)$_2$]$^{3+}$	C(1)	0.11	C(3)	0.41	Co	-0.21	Co	0.12	47.1°	-34.3°	(i)	(ii)	F
	C(2)	-0.48	C(4)	-0.18	C(1)	0.30	C(3)	0.30					
					C(2)	-0.30	C(4)	-0.30					
[u-fac-Co(dien)$_2$]$^{3+}$ (A)	C(1)	0.35	C(3)	0.55	Co	0.06	Co	0.28	43.5°	-44.8°	(i)	(ii)	G
	C(2)	-0.24	C(4)	-0.05	C(1)	0.29	C(3)	0.31					
					C(2)	-0.29	C(4)	-0.31					
[u-fac-Co(dien)$_2$]$^{3+}$ (B)	C(1)	-0.53	C(3)	0.68	Co	-0.27	Co	0.45	-42.7°	-41.4°	(ii)	(ii)	G
	C(2)	0.04	C(4)	0.14	C(1)	-0.29	C(3)	0.28					
					C(2)	0.29	C(4)	-0.28					
[u-Co(en)(dien)Cl]$^{2+}$	C(1)	0.21	C(3)	0.43	Co	-0.12	Co	0.16	48.7°	-45.1°	(i)	(ii)	H
	C(2)	-0.42	C(4)	-0.10	C(1)	0.32	C(3)	0.26					
					C(2)	-0.32	C(4)	-0.26					
[fac-Co(dien)(NO$_2$)-(NH$_3$)(H$_2$O)]$^{2+}$	C(1)	0.16	C(3)	0.08	Co	-0.46	Co	0.53	38.6°	37.9°	(i)	(ii)	I
	C(2)	0.66	C(4)	0.54	C(1)	0.26	C(3)	-0.25					
					C(2)	-0.26	C(4)	0.25					
[fac-Pt(dien)Cl$_3$]$^-$	C(1)	-0.54	C(3)	0.59	Pt	-0.35	Pt	0.34	-38.1°	-48.8°	(ii)	(ii)	J
	C(2)	-0.07	C(4)	-0.01	C(1)	-0.25	C(3)	0.32					
					C(2)	0.25	C(4)	-0.32					

References: A. Cotton and Elder, 1964, B. Cotton and King, 1965, C. Cotton and Richardson, 1966, D. Fowlie et al., 1970, E. Colnsford et al., 1971, F. Kobayashi et al., 1972, G. Senno et al., 1973, H. Johnston and Freeman, 1975, I. Pope et al., 1977, J. This work.

* <C> or <C(A)C(B)> represents the midpoint of the line joining the atoms C(A) and C(B).

** The torsional angle represented by M(A)C(A)C(B)N(B) is the dihedral angle between the planes M(A)C(A)C(B) and C(A)C(B)N(B).

Garthoff (1968)) that λδ should be the stable conformation for mer-complexes, while λλ or δδ should be the stable conformation for fac-complexes. In particular, it is argued that the δλ conformation will be "ruled out because of the steric hindrance" due to hydrogen atoms which approach each other appreciably in this ring structure". As can be seen from Table 3.5, the δλ conformation is found for fac-complexes.

For Table 3.5, all atoms in the original papers were relabelled to correspond to the geometry shown in Figure 3.3. The convention for conformation adopted here (column I in Table 3.5) is based on the IUPAC (1970) rules which use δ and λ to designate ring conformations. The dien ligand has been numbered so that if the three nitrogen atoms are placed in the plane of the paper and numbered as shown,

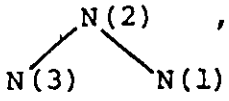

the metal atom is behind the plane of the paper. This is the same convention as that used by Konno, Marumo and Saito (1973). In considering the least-squares planes, the NH_2 group is placed to the left, as in $NH_2CH_2CH_2NH$-, and the metal is placed behind the N and C atoms. Therefore, for both rings, a positive dihedral angle corresponds to a δ configuration and a negative angle to a λ configuration. The convention used by Schmidtke and Garthoff (1968) is based on the k, k' convention of Corey and Bailar (1959) for ethylenediamine rings. The correspondence is k≡λ and k'≡δ. Note, however, that Schmidtke and Garthoff number their rings in the opposite

sense and therefore the ring conformation symbols have to be reversed before conversion. Thus δδλkk' and δδλk'k'. Column II in Table 3.5 shows how Schmidtke and Garthoff would have labelled the rings.

Since the δλ ring conformation is observed for fac metal complexes of dien, despite the predictions, based on calculations of intramolecular CH_2 and NH_2 repulsions, that it should not occur, it can be concluded that this interaction is not the most important factor in determining ring conformation. The more important factor is the directionality requirements of intermolecular hydrogen-bonds.

3.3 Chloro(diethylenetriamine-N^1,N^2,N^3)platinum(II) Chloride, 3C, and (Diethylenetriamine-N^1,N^2,N^3)nitratoplatinum(II) Nitrate, 3D, and Some Comments on the Existence of Pt(II)-OH_2 and Pt(II)-OH Bonds in the Solid State.

[Pt(dien)I]I, was prepared by the method of Watt and Cude (1968). 3.0000 g K_2PtCl_4 (7.227 mmole) was dissolved in the minimum amount of boiling water, and a hot aqueous solution of 3.5992 g KI (21.681 mmole) was added. 2.7976 g $PtI_2 \cdot H_2O$ (5.992 mmole) precipitated from the solution, was filtered and was slurried in a petri dish with 0.58 mL dien (5.4 mmole) and 0.5 mL H_2O over a steam bath for 24 h, with intermittent stirring. [Pt(dien)I]I was extracted with 175 mL hot (90°C) water and the excess $PtI_2 \cdot H_2O$ was removed by filtration. Clumps of fine yellow crystals separated upon evaporation of

the solvent. The [Pt(dien)I]I from this and several other batches was used to prepare the chloride, fluoride, and nitrate analogues by the addition of 2 equivalents of the appropriate silver salt in water. AgI was removed by filtration. The reaction was carried out under N_2 in the dark. Pale yellow crystals of [Pt(dien)Cl]Cl, 3C, were prepared and characterized for use in other studies. The structural information presented here differs from the published data (Britten, Lock, Pratt (1982)) in that further refinement was carried out with the inclusion of the hydrogen atoms. Analyses for 3C: Found: C, 12.7; H, 3.7; N, 12.8%. Calculated: C, 13.0; H, 3.6; N, 11.4%.

$[Pt(dien)ONO_2]NO_3$, 3D, and the fluoride analogue, were synthesized with the hope of obtaining the $[Pt(dien)OH_2]^{2+}$ ion in the solid state. Analyses for colourless crystals of 3D: Found: C, 11.0; H, 3.3; N, 15.8%. Calculated: C, 10.9; H, 3.4; N, 15.9%. The fluoride compound formed a yellow hygroscopic glass, and did not crystallize (see introduction to this chapter).

3.3.1 Crystal Structure of 3C

$[Pt(NH_2(CH_2)_2NH(CH_2)_2NH_2)Cl]\cdot Cl$, $C_4H_{13}ClN_3Pt^+\cdot Cl^-$; 369.17 $g\cdot mol^{-1}$; $Pca2_1$; Syntex $P2_1$ diffractometer; 15 refl. ($19^\circ<2\theta<36^\circ$) for cell; a=13.954(3), b=4.828(1), c=13.272(4)Å; V=894.2(4)Å^3, Z=4; D_x=2.74, D_m=2.74 $g\cdot cm^{-3}$ in $C_6H_6/CHBr_3$; $2\theta_{max}=50^\circ$, h, k, $\pm$l, N_{meas}=1957, min. R_{scan}=3.91; 23°C; standards: 2 0 3 (1.6%), 3 1 1 (1.3%); Bond abs. corr.,

μ=156 cm^{-1}, approx. sphere, r=0.09 mm; $5.96<A^*_\theta<6.68$; N_{unique}=1593, N_{used}=1561; NP=110; F(000)=680; $\omega=(\sigma_F^2 + 0.00070F_o^2)^{-1}$, S=undet, g(SHELX)=0.00076; max. non-H shift/error=.524; R=0.029, R_ω=0.036; Diff. map: -2.22, 2.30 $e\cdot Å^{-3}$, both near Pt; XRAY76, SHELX, NRC-22, ORTEPII.

Melanson, Hubert, and Rochon (1975) have determined the X-ray crystal structure of [Pt(dien)Br]Br ($Pca2_1$, a=14.211(7), b=4.940(3), c=13.450(8)). The Pt position from this compound was used for the initial phasing of the chloro complex, because of the cell and space group similarities. The remaining atoms of 3C were found by difference Fourier syntheses. The final positional parameters and isotropic temperature factors are given in Table 3.6. The parameters for [Pt(dien)Br]Br are related by x, y, z = x', y', ½-z' (ie. the molecules pack in the opposite sense for these particular crystals). The possibility of a centrosymmetric space group (Pcam, non-standard for Pbcm) was ruled out by the successful solution in $Pca2_1$. Only the Pt atoms pack with a center of symmetry.

The structure of 3C will be discussed in conjunction with the nitrate analogue, 3D (cf. §3.3.3).

3.3.2 The Crystal Structure of 3D

$[Pt(NH_2(CH_2)_2NH(CH_2)_2NH_2)ONO_2]\cdot NO_3$, $C_4H_{13}N_4O_3Pt^+\cdot NO_3^-$; 422.27 $g\cdot mol^{-1}$; Pbca; Syntex $P2_1$ diffractometer; 15 refl. ($19°<2\theta<31°$) for cell; a=12.777(4), b=9.749(3), c=17.145(4)Å; V=2135.6(1)$Å^3$, Z=8; D_x=2.63, D_m=2.63 $g\cdot cm^{-3}$ in CH_2I_2/CCl_4;

$2\theta_{max}=55^{\circ}$, +h, +k, ±l; $N_{meas}=5476$, min. $R_{scan}=3.91$ deg·min^{-1}; 23°C; standards: 2 1 3 (1.4%), 1 2 6 (1.3%); Bond abs. corr., $\mu=139$ cm^{-1}, cyl.: r=0.082 mm, l=0.328 mm, $5.527<A_{\theta}^{*}<6.266$; $N_{unique}=2481$, $N_{used}=2314$; NP=141; F(000)=1584; $\omega=(\sigma_F^2 + 0.00070F_o^2)^{-1}$, S=undet, g(SHELX)=0.00019; max. non-H shift/error=0.22; R=0.065, $R_{\omega}=0.050$; diff. map: -1.9, 2.0 e·Å^{-3}, both near Pt; XRAY76, SHELX, NRC-22, ORTEPII.

For 3D, the coordinates of the Pt atom were found from a three-dimensional Patterson synthesis, and a series of least-squares refinements, followed by three-dimensional electron difference syntheses, revealed all the non-hydrogen atoms. At this stage the temperature factors of the Pt, Cl, N, and O atoms were made sequentially anisotropic. Tests were made to show that the use of extra parameters was justified (Hamilton (1965)). Ten of the thirteen H atoms were found from the difference map. Attempts to find the remaining H atoms from a difference map using the SHELX weighting scheme giving increased weight to the low-angle reflections (s = 0.3) were unsuccessful. The atom parameters for 3D are given in Table 3.7.

3.3.3 Comparison of the Structures of [Pt(dien)Cl]Cl and [Pt(dien)ONO_2]NO_3

The molecular cations of 3C and 3D are illustrated in Figure 3.6 and selected interatomic distances and angles are given in Table 3.8. These results will be compared with previous structural determinations of the $[Pt(dien)X]^{n+}$ unit

Table 3.6. Atomic positional parameters ($x10^4$) and temperature factors ($Å^2$)($x10^3$) for 3C.

	x	y	z	U_{iso} or Ueq*
Pt	1813.3(2)	2009.0(6)	2500(0)	23.9(2)*
Cl(1)	2934(2)	4710(6)	1674(2)	41(1)*
N(1)	2609(6)	1470(18)	3790(7)	31(5)*
C(1)	1957(6)	321(26)	4578(8)	37(2)
C(2)	1257(7)	-1675(20)	4082(8)	30(2)
N(2)	799(5)	-76(18)	3256(6)	27(4)*
C(3)	181(6)	-1546(17)	2518(14)	35(2)
C(4)	-29(7)	494(24)	1680(8)	36(2)
N(3)	873(6)	1625(19)	1309(7)	33(5)*
Cl(2)	818(2)	6607(5)	-473(2)	35(1)*

Table 3.7. Atomic positional parameters ($x10^4$) and temperature factors ($Å^2$) ($x10^3$) for 3D.

	x	y	z	U_{iso} or U_{eq} *
Pt	1263(0)	4421(0)	1234(0)	32.0(2)*
N91)	1538(8)	4521(9)	65(6)	48(5)*
C(1)	2636(10)	4906(13)	-63(7)	48(3)
C(2)	3005(9)	5800(12)	607(6)	40(2)
N(2)	2737(7)	5035(9)	1333(4)	34(2)
C(3)	2836(9)	5834(11)	2090(6)	35(2)
C(4)	2256(10)	4994(13)	2681(6)	46(3)
N(3)	1192(8)	4669(10)	2417(5)	47(5)*
O(1)	-282(6)	4004(8)	1091(5)	51(4)*
O(2)	-68(7)	1927(8)	1566(5)	61(5)*
O(3)	-1607(6)	2636(9)	1178(5)	64(6)*
N(4)	-652(7)	2807(10)	1296(5)	44(2)
O(4)	4405(7)	3135(10)	1690(5)	65(5)*
O(5)	5887(7)	2508(10)	1247(5)	75(7)*
O(6)	4586(8)	2604(11)	485(5)	79(7)*
N(5)	4976(8)	2776(10)	1142(5)	47(2)

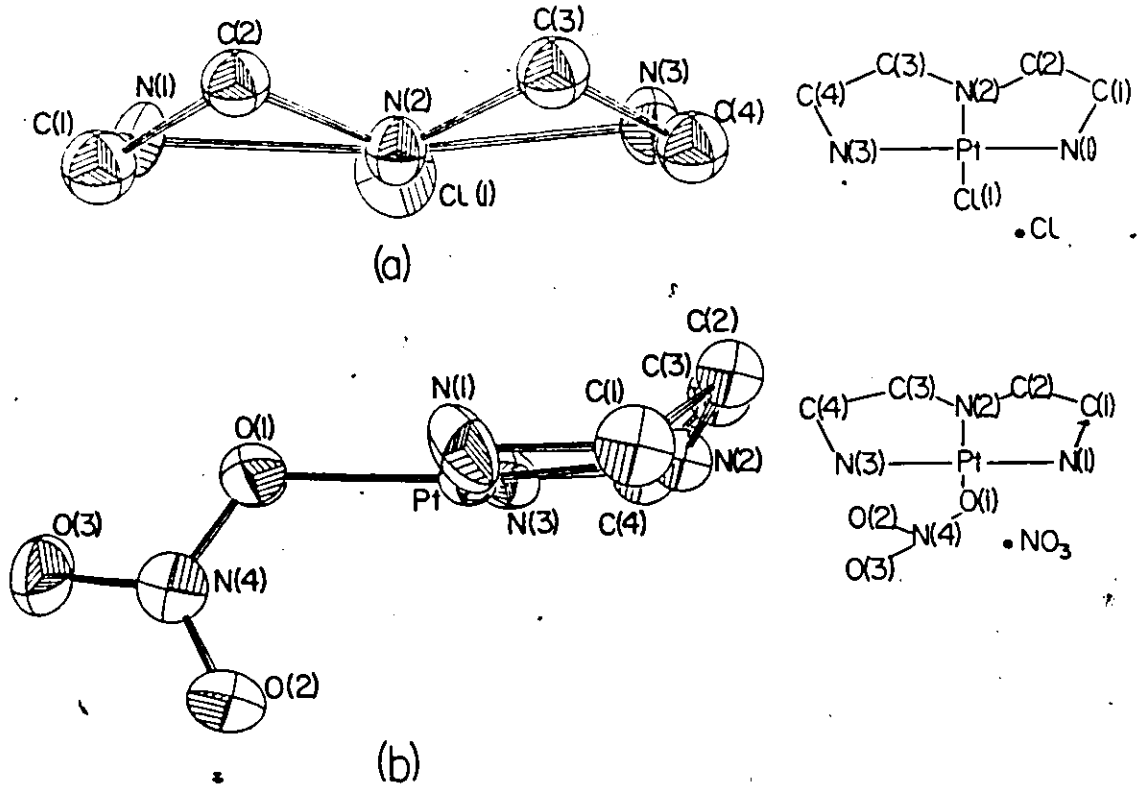

Figure 3.6. The molecular cations of 3C and 3D.

(a) The $[Pt(dien)Cl]^+$ cation viewed down the N(2)-Pt axis. Pt is hidden by N(2).

(b) The $[Pt(dien)ONO_2]^+$ cation showing the monodentate nitrate ion.

Table 3.8. Selected interatomic distances (Å) and angles (deg) for 3C and 3D.

	3C	3D		3C	3D
Pt-Cl(1)	2.313(3)	--	Pt-O(1)	--	2.030(8)
Pt-N(1)	2.057(8)	2.036(9)	Pt-N(2)	2.006(8)	1.984(8)
Pt-N(3)	2.063(9)	2.044(9)	N(1)-C(1)	1.49(1)	1.47(2)
C(1)-C(2)	1.52(2)	1.52(2)	C(2)-N(2)	1.49(1)	1.49(1)
N(2)-C(3)	1.49(2)	1.52(1)	C(4)-C(4)	1.52(2)	1.50(2)
C(4)-N(3)	1.46(1)	1.47(2)	O(1)-N(4)	--	1.31(1)
N(4)-O(3)	--	1.25(1)	N(4)-O(2)	--	1.23(1)
N(5)-O(4)	--	1.24(1)	N(5)-O(5)	--	1.21(1)
N(5)-O(6)	--	1.24(1)			

Possible hydrogen bonds

3C	Cl(2)...N(1)^{i}	3.347(9)	Cl(2)...N(2)^{ii}	3.272(9)
	Cl(2)...N(3)	3.385(9)	Cl(2)...N(3)^{iii}	3.384(9)
3D	N(1)...O(5)^{iv}	3.11(1)	N(1)-H(N11)	1.0(1)
	H(N11)...O(5)^{iv}	2.2(1)	N(2)...O(4)	2.89(1)
	N(2)-H(N2)	0.7(1)	H(N2)...O(4)	2.2(1)
	N(3)...O(4)^{v}	3.13(1)	N(3)-H(N31)	0.9(1)
	H(N31)...O(4)^{v}	2.2(1)	N(3)...O(5)^{v}	3.14(1)
	H(N31)...O(5)^{v}	2.4(1)	N(1)...O(1)^{vi}	2.93(1)
	N(3)...O(2)^{vii}	3.15(1)		

Table 3.8. (continued)

	3C	3D		3C	3D
Cl(1)-Pt-N(1)	95.8(2)	--	Cl(1)-Pt-N(2)	175.8(3)	--
Cl(1)-Pt-N(3)	96.8(3)	--	O(1)-Pt-N(1)	--	93.4(4)
O(1)-Pt-N(2)	--	173.7(3)	O(1)-Pt-N(3)	--	95.8(4)
N(1)-Pt-N(2)	84.3(3)	84.6(4)	N(1)-Pt-N(3)	165.9(4)	168.0(4)
N(2)-Pt-N(3)	83.5(4)	85.5(4)	Pt-N(1)-C(1)	107.5(6)	109.0(7)
N(1)-C(1)-C(2)	108.9(8)	109(1)	C(1)-C(2)-N(2)	105.5(8)	105.9(9)
C(2)-N(2)-Pt	109.0(6)	107.3(6)	Pt-N(2)-C(3)	108.0(7)	107.9(6)
C(2)-N(2)-C(3)	119.3(8)	116.0(8)	N(2)-C(3)-C(4)	106.6(7)	104.9(8)
C(3)-C(4)-N(3)	109.0(8)	111.5(9)	C(4)-N(3)-Pt	108.9(6)	106.9(7)
O(1)-N(4)-O(3)	--	115.5(9)	O(1)-N(4)-O(2)	--	120.4(9)
O(2)-N(4)-O(3)	--	124.1(9)	O(4)-N(5)-O(6)	--	121(1)
O(4)-N(5)-O(6)	--	119(1)	O(5)-N(5)-O(6)	--	120(1)
Pt-O(1)-N(4)	--	119.9(7)			

Atoms are related to those in Tables 3.6 and 3.7 by: (i) ½-x, y, z-½; (ii) -x, -y, z-½; (iii) x, y-1, z; (iv) x-½, ½-y, -z; (v) x-½, y, ½-z; (vi) -x, 1-y, -z; (vii) -x, ½+y, ½-z.

(see Table 3.9) and the averages quoted here refer to values based on those determinations.

The cation of 3C is almost identical to $[Pt(dien)Br]^+$. In the cation of 3D the nitrate ion is monodentate, being coordinated through O(1), and the dihedral angle between the nitrate ion and the ligand plane is 71(1)°. The Pt-O(2) distance of 3.020(8) Å is too long to be considered a bonding interaction (Lippert, Lock, Rosenberg, Zvagulis (1977)).

Pt-N(1) and Pt-N(3) [range: 2.036(9)-2.063(9) Å] in both 3C and 3D are longer than Pt-N(2) [2.006(8), 1.984(8)Å]. This was not detectable from previous results because of larger errors. It is not possible to state, because of the errors, that a given C-C bond is longer than a given C-N bond in 3C and 3D but the N(1,3)-C(1,4), C(1,4)-C(2,3), C(2,3)-N(2) averages of 1.47(1), 1.52(1), 1.50(1)Å for 3C and 3D agree well with the averages for previous results (1.48, 1.52, 1.48) and are consistent with a difference in the C and N covalent radii of about 0.04Å (Pauling (1960)). There are differences in some angles: the larger X-Pt-N(2) angle [175.8(3)°] for X = Cl [vs. 173.7(3)°, X = O] being compensated by the smaller N(1)-Pt-N(3) angle [165.9(4)° vs. 168.0(4)°]. These small differences are probably caused by packing constraints. That O,Cl-Pt-N(1,3) angles [range: 93.4(4)-96.8(3)°] are larger than N(1,3)-Pt-N(2) angles [range: 83.5(4)-85.5(4)°] has been noted previously (see references in Table 3.9).

Table 3.9. Comparison of the conformations of $Pt(dien)X^{n+}$ cations

Compound	Distance of C atoms from MNN plane (Å) N(1)N(2)M		N(2)N(3)M		Distance of atoms from NN<C> plane (Å) N(1)N(2) <C(1)C(2)>		N(2)N(3) <C(3)C(4)>		Torsional angles NCCN (°) N(1)C(1) C(2)N(2)	N(2)C(3) C(4)N(4)	Conformation	Ref
[Pt(dien)Cl]Cl	C(1)	-0.22(1)	C(3)	-0.49(1)	Pt	0.161(0)	Pt	-0.177(0)				
	C(2)	0.50(1)	C(4)	0.20(1)	C(1)	-0.36(1)	C(3)	-0.35(1)	-53.7(9)	52.8(9)	λδ	A
					C(2)	0.36(1)	C(4)	0.35(1)				
$[Pt(dien)NO_3]NO_3$	C(1)	0.06(1)	C(3)	0.54(1)	Pt	-0.322(0)	Pt	0.225(0)				
	C(2)	-0.62(1)	C(4)	-0.15(1)	C(1)	0.34(1)	C(3)	0.34(1)	51.7(9)	-52.7(9)	δλ	A
					C(2)	-0.34(1)	C(4)	-0.34(1)				
$[Pt(dien)Br]_2PtBr_4$,A	C(1)	0.00(8)	C(3)	0.60(10)	Pt	-0.355(2)	Pt	0.288(2)				
	C(2)	-0.58(6)	C(4)	-0.05(10)	C(1)	0.29(8)	C(3)	0.33(10)	45(6)	-46(6)	δλ	B
					C(2)	-0.29(8)	C(4)	-0.33(10				
$[Pt(dien)Br]_2PtBr_4$,B	C(1)	0.02(9)	C(3)	0.69(7)	Pt	-0.493(3)	Pt	0.459(3)				
	C(2)	-0.83(8)	C(4)	0.14(9)	C(1)	0.43(9)	C(3)	0.29(7)	59(6)	-42(6)	δλ	B
					C(2)	-0.43(8)	C(4)	-0.29(9)				
[Pt(dien)Br]Br	C(1)	0.21(2)	C(3)	0.49(1)	Pt	-0.203(1)	Pt	0.213(1)				
	C(2)	-0.57(2)	C(4)	-0.14(2)	C(1)	0.39(2)	C(3)	0.32(1)	58(2)	-50(2)	δλ	C
					C(2)	-0.39(2)	C(4)	-0.32(2)				
$[Pt(dien)Ino](NO_3)_2$	C(1)	-0.07(1)	C(3)	-0.52(1)	Pt	0.264(0)	Pt	-0.250(0)				
	C(2)	0.53(1)	C(4)	0.10(2)	C(1)	-0.31(1)	C(3)	-0.31(1)	-49(1)	49(1)	λδ	D
					C(2)	0.31(1)	C(4)	0.31(1)				
$[Pt(dien)Guo](NO_3)_2$	C(1)	-0.12(2)	C(3)	-0.55(1)	Pt	0.249(1)	Pt	-0.272(1)				
	C(2)	0.54(2)	C(4)	0.09(2)	C(1)	-0.34(2)	C(3)	-0.32(2)	-51(1)	50(1)	λδ	E
					C(2)	0.34(2)	C(4)	0.32(2)				

(A) this work; (B) Melanson, Rochon, Hubert (1979); (C) Melanson, Rochon, Hubert (1975); (D) Melanson, Rochon (1978); (E) Melanson, Rochon (1979).

Within the dien ligand angles are close to the tetrahedral angle but it appears that the N(1,3)-C(1,4)-C(2,3) angles (average 109.6°) are larger than N(2)-C(2,3)-C(1,4) angles (average 105.7°). Errors preclude this conclusion on the basis of an angle-for-angle comparison, but the averages for 3C and 3D agree well with the averages for previous results (110°, 106° respectively). The Pt-Cl(1) bond length is normal.

In Table 3.9 is presented a comparison of the conformations of $[Pt(dien)X]^{n+}$ cations. The conventions and definitions are the same as in Table 3.5. All Pt(II) cations (mer-configuration) adopt the λδ or δλ conformations predicted by Schmidtke and Garthoff (1968), so that each molecule looks like a sting-ray with the front edges of the 'wings' up and the X group forming the tail. An examination of the distances of the atoms from the least-squares planes formed by the Pt-bound ligand atoms (the 'ligand planes') shows different distortions. The nitrate complex is distorted towards a square pyramid [N(1) 0.014(9), N(2) -0.011(8), N(3) 0.014(10), O(1) -0.008(8), Pt -0.1160(3)Å], whereas the chloride, like the bromide, is distorted towards a tetrahedron [N(1) 0.13(1), N(2) -0.13(1), N(3) 0.14(1), Cl(1) -0.010(3), Pt 0.0080(3)Å] (Note: The Pt atoms were given no weight in calculating the planes). The direction and magnitude of these distortions appear to be determined by packing considerations, rather than intramolecular factors, since one $[Pt(dien)Br]^{+}$ cation

in the tetrabromide complex is essentially planar, tending to a square pyramid, and the other is distorted towards a square pyramid, and the guanosine and inosine complexes are planar (see references in Table 3.9)

For the fac-$[M(dien)X_3]^{n+}$ complexes, hydrogen-bonding caused changes in ligand conformation, significant variation in the distance the M atom was out of the N<C>N plane [range 0.01-0.58Å] and the NCCN torsional angles [36.6-50.3°] (see Table 3.5). The M distance range is less for the $[Pt(dien)X]^{n+}$ complexes, even including one of the rather distorted cations (B) in the $PtBr_4^{2-}$ complex [0.161(0)-0.493(3)Å]. The steric restraints on the tridentate dien ligands in the mer-configuration in the $[Pt(dien)X]^{n+}$ cations are greater and apparently hydrogen-bonding can cause less variation.

The packing of 3C is shown in Figure 3.7. Like the bromide it is a layer structure with the cations centered at y = 0 and the anions at y = 0.5. Cations along the **c** direction related by the c-glide at x = 0.25, 0.75 are oriented so that Cl(1) on each molecule is pointing into the same anion layer, but up the **a** direction the cations are related by the a-glide at y = 0 so that alternate molecules have Cl(1) pointing into anion layers on opposite sides. The cations are hydrogen-bonded to the anion layer through $Cl(2)...N(1)^{i}$, $Cl(2)...N(2)^{ii}$, Cl(2)...N(3), and $Cl(2)...N(3)^{iii}$.

The packing of 3D is shown in Figure 3.8. Surprisingly, because of the rather different shape of the cation, the

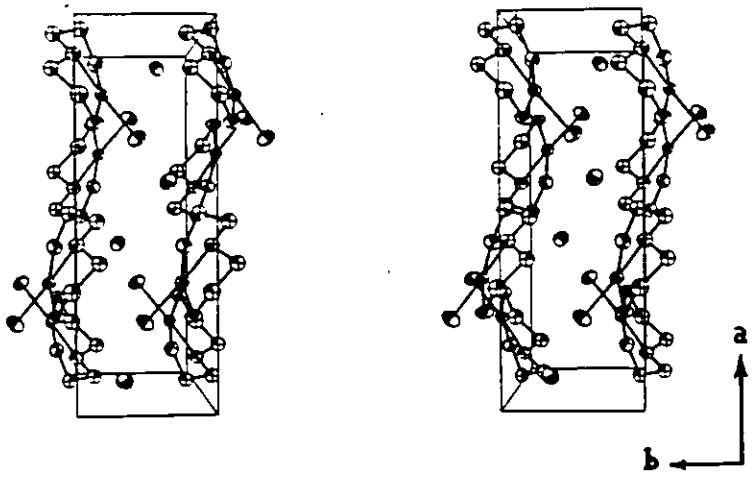

Figure 3.7. The packing of [Pt(dien)Cl]Cl (3C) in the unit cell showing the layer structure.

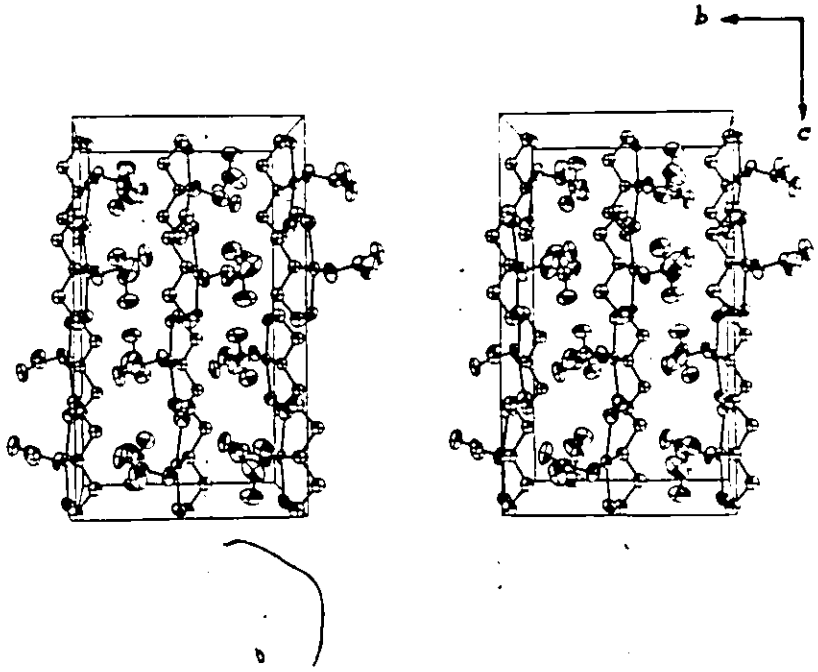

Figure 3.8. The packing of $[Pt(dien)ONO_2]NO_3$ (3D) in the unit cell showing the layer structure.

packing is again a layer structure, very similar to that of the chloride, but now the repeat distance along **b** is doubled, compared to 3C. Also, the **a** and **c** directions in 3C correspond to the **c** and **a** directions in 3D, respectively. The effects of orientation of the coordinated nitrate group are comparable to 3C. Cations in the **ac** layer form chains up **c** and the nitrate groups on alternate cations lie in opposite anion layers. In 3D, cations along the **a** direction are related by the a-glide, and the nitrate groups lie in the same anion layer. Each cation is hydrogen-bonded by a medium hydrogen-bond N(2)...O(4) [2.89(1)Å] and weak N(1)...O(5)^{iv} and N(3)...O(4)^{v},O(5)^{v} bifurcated hydrogen-bonds to nitrate ions in the same layer. There is a remaining weak cation-cation link along **c** through N(3)...O(2)^{viii}. The principal reason for the doubling of the b axis and the space group change is that in 3C all cations with the same x have the Pt-Cl(1) bonds pointing in roughly the same direction along **b**, whereas for 3D, cations with roughly the same z have Pt-O(1) bonds oriented in opposite directions in alternate layers along **b**. Of the other structures presented in Table 3.9, only $[Pt(dien)Br]_2 \cdot [PtBr_4]$ can be considered a layer structure and it is different from the structures here in that the cations are oriented so that the bound Br atoms all point into the same anion layer.

Although $[Pt(dien)ONO_2]NO_3$ was prepared, it was hoped that $[Pt(dien)OH_2] \cdot (NO_3)_2 \cdot xH_2O$ would crystallize from water,

where the nitrate ion is not coordinated. The Raman spectrum of solid 3D (Figure 3.9) shows vibrational bands both for the ionic and coordinated nitrate ions, but the solution spectrum shows that no coordinated nitrate atom is present, even when the spectrum was measured less than 2 min after the solid was dissolved in the minimum of water. (Spectra-physics 164 argon ion laser, 300 mW, λ = 5145Å; Spex Double Monochromater Model 14018; 295K). Only bands from ionic nitrate are observed in solution. This problem has been encountered previously (Lippert, Lock, Rosenberg, Zvagulis (1977)). Brown's bond valence concept (Brown (1981); Brown, Shannon (1973)) can be used to explain why attempts to prepare aqua-species of Pt(II) have been unsuccessful and to suggest conditions under which it may be possible to obtain terminal aqua- and hydroxo-Pt(II) species.

3.3.4 Bond Valence Considerations

Brown's bond valence model is an extension of Pauling's (1960) bond-order bond-length relationship, the main difference being that Brown assigns a bond valence to all nearest-neighbour interactions, regardless of whether they are covalent 'bonds', ionic or Van der Waals interactions. The only requirement is that the sums of the bond valences shall be equal to the modulus of the formal oxidation state of the atom under consideration: consider Figure 3.10(a). The N-O bond valence in the free nitrate ion is 1.67 (3 x 1.67 = 5) leaving a residual, unsatisfied valence of 0.33 (1.67 + 0.33 = 2)

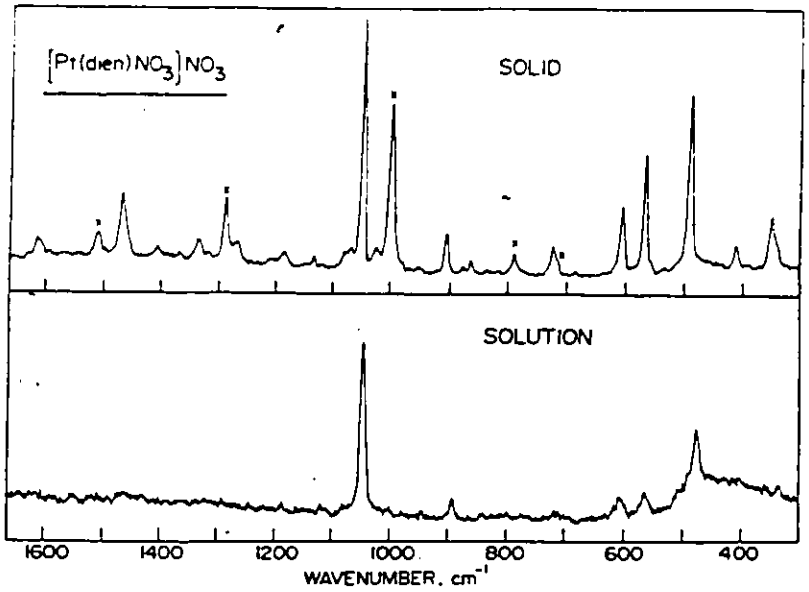

Figure 3.9. Raman spectra of 3D.

(a) Solid

(b) aqueous solution

Points marked x are characteristic of the coordinated nitrate ion.

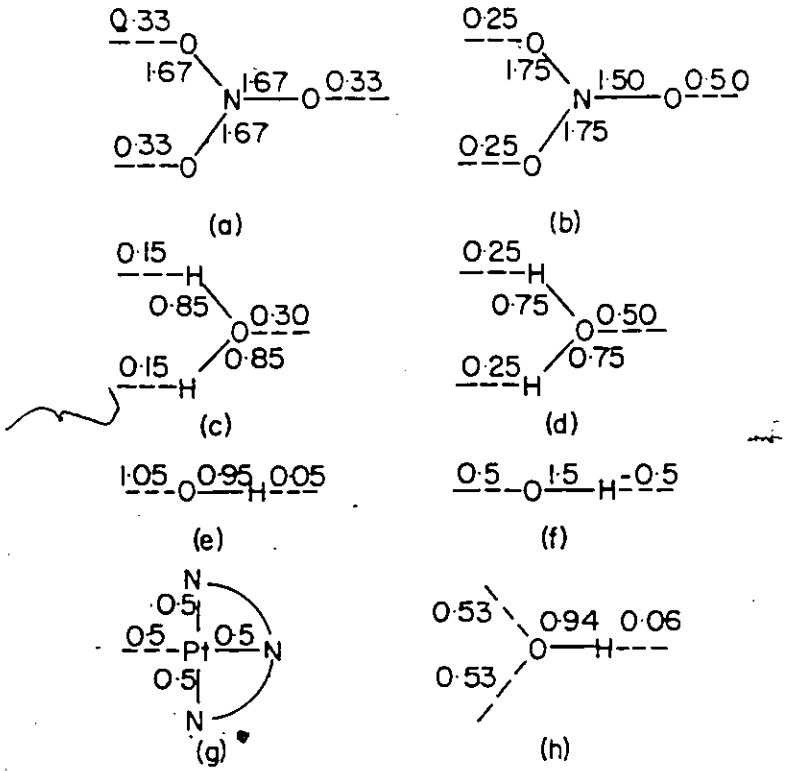

Figure 3.10. Bond valence distributions in various molecules and ions

on each O atom (its base strength), which will normally be satisfied by some ionic, covalent, or hydrogen bond. Similar figures are shown for water (c) and hydroxide (e) obtained from Brown's empirical relationships. For the $[Pt(dien)]^{2+}$ species, if it is assumed that Pt-N bonds are as strong as Pt-O bonds (a not unreasonable assumption since in a number of structures Pt-O bonds are as short or shorter than Pt-N bonds, although aqua- or hydroxo-Pt(II) monomers are needed to verify this), the situation shown in Figure 3.10(g) arises. The $[Pt(dien)]^{2+}$ fragment has an unsatisfied bond valence of 0.5. Since a bond can only have one bond valence, $[Pt(dien)]^{2+}$ cannot bond directly to either nitrate or water without some redistribution of the bond valence. Figures 3.10 (b) and (d) show how this might occur. The redistribution of bond valence can be tested by comparing observed bond lengths with values calculated from Brown's empirical bond-valence bond-length relationship and the excellent agreement for the nitrate ion is shown in Table 3.10.

One might expect a strong hydrogen bond to the uncoordinated O atoms of the nitrate ion, but, as Brown (1981) has shown, oxygen is normally four-coordinate, so the residual bond valence of 0.25 at each O atom will be distributed over three hydrogen-bonds of only 0.08 valence units, which would represent rather weak hydrogen-bonds. In addition, the hydrogen-bond to the coordinated O atom O(1) will increase the external bond valence at O(1), weakening O(1)-N(4), strength-

Table 3.10. Comparison of nitrate bond lengths (Å).

Molecule	Pt-O(1)	O(1)-N(1)	N(1)-O(2)	N(1)-O(3)
cis-$Pt(NH_3)_2(NO_3)_2$, (NO_3^-A)	1.99(1)	1.30(2)	1.22(2)	1.24(2)
cis-$Pt(NH_3)_2(NO_3)_2$, (NO_3^-B)	2.03(1)	1.28(2)	1.19(2)	1.22(2)
$[Pt(dien)NO_3]^{2+}$	2.038(8)	1.31(1)	1.23(1)	1.21(1)
average	-	1.30	1.21	1.22
Brown's calc. for Fig. 3.10(b)	-	1.29	1.24	1.24
$[Pt(dien)NO_3]NO_3$, (free NO_3^-)	-	1.24(1)	1.21(1)	1.24(1)

Except for the free nitrate ion the atoms are numbered as in Figure 3.6(b).

ening N(4)-O(2) and N(4)-O(3), and further reducing the base strength at O(2) and O(3).

For water coordinated to Pt(II) through oxygen there must be an increase in the residual valence at each H atom (acid strength) on the water molecule which must be satisfied by stronger proton-donation hydrogen-bonding. Since hydrogen is normally only two-coordinate (Brown (1981)) the residual bond valence of 0.25 will only be satisfied by one rather strong hydrogen-bond.

In aqueous solution this can take place, the water molecules acting as acceptors (and stabilizers). In the solid, coordination of the nitrate ion seems to be preferred, insufficient strong hydrogen-bonds being formed to stabilize water coordination. Clearly, if one wants to stabilize water coordinated to Pt(II) in the solid state, one must use small counter-ions which are good hydrogen-bond acceptors but poor ligands, such as fluoride, or salts which are extensively hydrated and have counter-ions which are poor ligands.

For the hydroxide ion there is no simple arrangement to allow monofunctional bonding to Pt(II) since it results in a negative unsatisfied bond valence at hydrogen (Figure 3.10(f)), which is impossible. The residual bond valence at oxygen of 1.05 can easily be split into 2 x 0.53, each matching the valence at Pt(II) (h) and it is easy to see why hydroxide bridges Pt(II) so readily. An alternative way of satisfying the ~0.5 base strength at oxygen would be to form

two strong proton-acceptor hydrogen-bonds, 0.25 v.u. each. This can only occur in aqueous solution or in an extensively hydrated salt. To stabilize such a system the bond valence of the OH bond should approach 1.0 v.u. and thus the residual acid strength of the hydrogen will be near 0.0 and will not be involved in any significant hydrogen-bond. This arrangement is seen in hydroxo-cis-diammine(1-methylcytosine-N^3)-platinum(II) nitrate dihydrate (Pilon (1984)).

3.4 cis-Diammineaqua(1-methylcytosine-N^3) Platinum(II) Dinitrate Hydrate, 3E

For several years our laboratory has been systematically studying the interactions of the $[Pt(NH_3)_2]^{2+}$ moiety, both cis and trans, with model nucleobases of DNA (Lock (1980) and references therein). This work has been carried out in conjunction with the laboratory of Bernhard Lippert at the Anorganisch-Chemisches Institut, Technische Universität München, 8046 Garching, Federal Republic of Germany. In a reaction of cis-$[Pt(NH_3)_2(1\text{-Me-Cyt})Cl]Cl\cdot H_2O$ (where 1-Me-Cyt ≡ 1-methylcytosine, $C_5H_7N_3O$) with two equivalents of $AgNO_3$ (Britten, Lippert, Lock, Pilon (1982)), Lippert obtained cis-$[Pt(NH_3)_2(1\text{-Me-Cyt})(OH_2)]\cdot(NO_3)_2\cdot H_2O$, 3E, and several other components. The fact that the aqua-complex was not isolated as the exclusive product clearly shows that there must be a delicate balance of conditions leading to its crystallization. There are two main reasons for the formation of 3E: first, the specific hydrogen-bonding conditions (see

§3.3.4) which stabilize the coordinated water (see below), and second, the poor nucleophilicity of O(2) of 1-Me-Cyt toward Pt(II) in aqueous solution. With Ag, for example, N(3), O(2) bridging occurs rather than aqua-complex formation (Kistenmacher, Rossi, Marzilli (1979)), and bidentate (N(3); O(2)) binding is also observed in complexes of Cd(II) (Gagnon, Beauchamp, Tranqui (1979)), Hg(II), and Cu(II) (Authier-Martin, Beauchamp (1977); Marzilli, Wilkowski, Chiang, Kistenmacher (1979)). Many more examples of varying degrees of O(2) involvement in metal binding are known (Martin, Mariam (1979); Gellert, Bau (1979); Marzilli, Kistenmacher, Eichhorn (1980), p.181).

To prepare 3E, Lippert reacted cis-$Pt(NH_3)_2Cl_2$ and 1-Me-Cyt in 1:1 ratio in H_2O to give cis-$[Pt(NH_3)_2(1\text{-Me-Cyt})Cl]\cdot Cl\cdot H_2O$ (Britten, Lippert, Lock, Speranzini). 1.0 mmol of this product was reacted with 2.0 mmol of $AgNO_3$ in 15 mL H_2O at room temperature for 24 h, and the solution was then concentrated to a 1.5 mL volume (pH 1.8). Upon cooling, 230 mg of 3E were obtained. Further concentration of the filtrate and cooling gave a mixture of 3E (150 mg) and 10 mg of cis-$[Pt(NH_3)_2(OH)_2Pt(NH_3)_2]\cdot(NO_3)_2$ (Faggiani, Lippert, Lock, Rosenberg (1977)). Warming during the concentration process had to be avoided in order to prevent darkening of the solution and formation of a brown glassy material. The addition of 1 equivalent of base to a solution of 3E gave crystals of cis-$[Pt(NH_3)_2(1\text{-Me-Cyt})(OH)]\cdot NO_3\cdot 2H_2O$ (Pilon (1984)), while

0.5 equivalents of base yielded $[Pt_2(NH_3)_4(1\text{-Me-Cyt})_2(OH)]\cdot(NO_3)_3$, a Pt dimer with a single hydroxo-bridge. The structural formulations were based on IR and Raman data, and elemental analyses (Britten, Lippert, Lock, Pilon (1982)).

3.4.1 The Crystal Structure of 3E

cis-$[Pt(NH_3)_2(C_5H_7N_3O)(OH_2)]\cdot(NO_3)_2\cdot H_2O$, $C_5H_{15}N_5O_2Pt^{2+}\cdot 2NO_3^-\cdot H_2O$; 514.32 $g\cdot mol^{-1}$; $P\bar{1}$; Nicolet P3 diffractometer; 15 refl. ($27^\circ<2\theta<35^\circ$) for cell; a=12.380(6), b=6 [illegible], c=10.895(3)Å, α=90.39(3), β=110.26(3), γ=114.68(V=744.5(5)Å^3, Z=2; D_x=2.29, D_m=2.31 $g\cdot cm^{-3}$ in CH [illegible] Br_3; $2\theta_{max}=55^\circ$, h, ±k, ±l; N_{meas}=3603, min. R_{scan}=3.91 $deg\cdot min^{-1}$; 22°C; standards: 2 1 1 (1.4%), 1 1 -1 (1.3%); Bond abs.corr., μ=91.0 cm^{-1}, sphere, r=0.10 mm, $3.45<A_\theta^*<3.66$; N_{unique}=3442, N_{used}=3317; NP=191; F(000)=492, $\omega=(\sigma_F^2 + 0.00120F^2)^{-1}$, S=undet, g(SHELX)=0.00039; max.nc [illegible]-H shift/error=.312, R [illegible], R_ω=0.061; diff. map: -2.8, 4.2 $e\cdot Å^{-3}$, both near Pt; XRAY76, SHELX, NRC-22, ORTEPII.

The coordinates of the Pt atom were found from a three-dimensional Patterson map, and a series of full-matrix least-squares refinements followed by three-dimensional electron density difference syntheses revealed all other atoms, including hydrogens. Statistical tests were used to determine which atoms should have anisotropic temperature factors (Hamilton (1965)). The final atomic parameters for the non-hydrogen atoms are listed in Table 3.11.

The molecular cation is illustrated in Figure 3.11

Table 3.11. Atomic positional coordinates ($x10^3$) and temperature factors ($Å^2$) ($x10^3$) for 3E.

Atom	x	y	z	U_{iso} or U_{eq} *
Pt	53.63(3)	114.44(6)	217.16(3)	28.4(2)*
O(3)	112.0(8)	448(1)	288.6(8)	48(4)*
N(5)	-11.3(9)	-213(2)	137(1)	40(2)
N(6)	-130.9(9)	68(2)	161.7(9)	31(4)*
N(1)	431.7(8)	299(1)	241.3(8)	38(2)
C(2)	302.3(9)	238(2)	195.2(9)	34(2)
N(3)	240.4(7)	169(1)	283.3(8)	32(2)
C(4)	302.8(9)	145(2)	406(1)	38(2)
C(5)	437(1)	205(2)	451(1)	44(2)
C(6)	496(1)	280(2)	369(1)	43(2)
C(1)	499(1)	385(3)	154(1)	56(3)
O(2)	245.5(7)	251(1)	80.5(7)	38(4)*
N(4)	237(1)	73(2)	483(1)	52(2)
N(7)	133(1)	441(2)	606(1)	49(2)
O(71)	197.1(8)	566(2)	545.1(9)	53(5)*
O(72)	173(1)	515(2)	728.7(9)	76(7)*
O(73)	41(1)	262(2)	547(1)	83(8)*
N(8)	706.7(9)	263(2)	875.7(9)	43(2)
O(81)	670.2(8)	285(1)	754.9(8)	52(5)*
O(82)	822.2(8)	320(2)	939.8(9)	47(5)*
O(83)	626.5(9)	184(2)	926.5(9)	59(5)*
O(7)	358.2(9)	13(2)	749.6(9)	57(2)

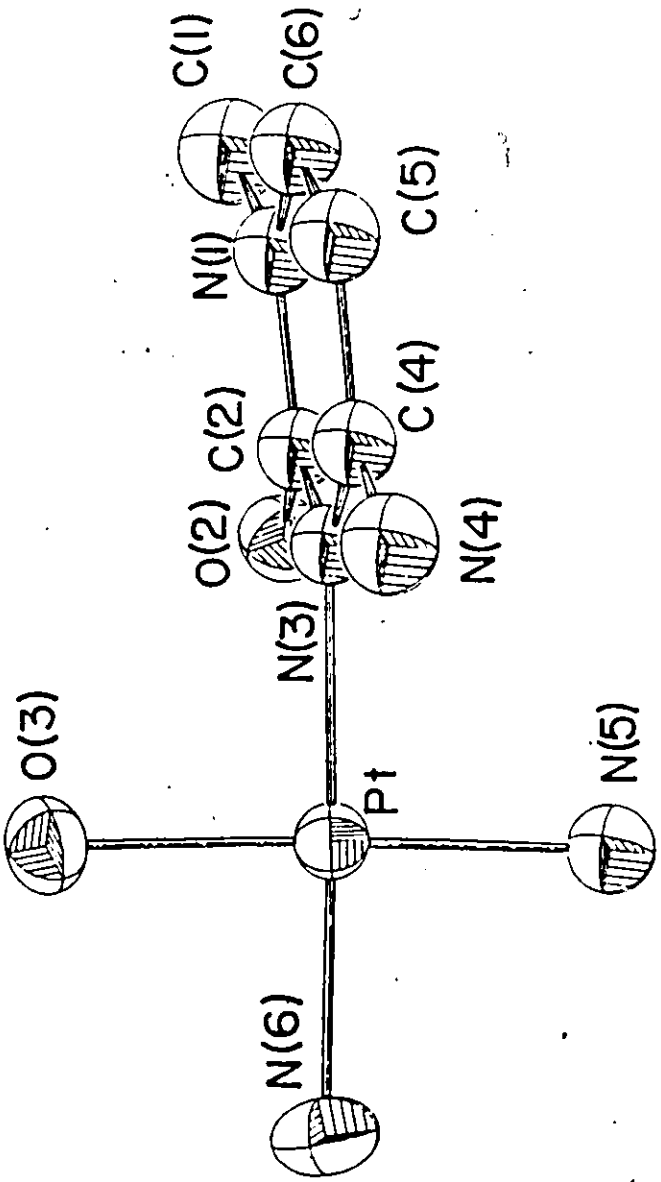

Figure 3.11. The molecular cation of 3E

and selected interatomic distances and angles are given in Table 3.12. The bond lengths and angles agree well with previously reported values (Lippert, Lock, Speranzini 1981a,b). The cation is very similar to the hydroxo-analogue (Pilon (1984)), having no significant differences in bond lengths or angles. The principal difference is in the square plane-ring dihedral angle, which is 90.9(5)° for the aqua-complex but only 79.8(5)° for the hydroxo-complex, probably a result of the hydrogen-bonding requirements. Neither the Pt-OH_2 distance [2.052(8)Å] nor the Pt-OH distance [2.027(9)Å] are unduly long, and are comparable to the Pt-N distances. Thus the Pt-OH_2 distance gives no indication of weakness of the Pt-O bond which has been suggested by the rapid rate of reaction of square-planar d^8 complexes. This work suggests, therefore that the rapid rate of reaction of OH^- and OH_2 groups on Pt(II) is associated with a marked weakening of the Pt-O bond in the five-coordinate state. Such weakening of a metal-oxygen bond in a d^8 system has been demonstrated previously in Rh(I) complexes when the Rh-O distance to an acetylacetonate ion increased from 2.025(5) and 2.037(5)Å in the square planar complex (Allen, Lock, Turner, Powell (1975)) to 2.217(9) and 2.235(8)Å in the five-coordinate complex (Hughes, Krishnamachari, Lock, Powell, Turner (1977)).

The packing of 3E is shown in Figure 3.12. It is characterized by a series of 3 parallel layers, formed by the cytosine ring, the N(7) nitrate ions, and the water molecules,

Table 3.12. Selected interatomic distances (Å) and angles (deg) for 3E.

Pt-N(3)	2.034(9)	Pt-N(5)	2.02(1)	Pt-N(6)	2.03(1)
Pt-O(3)	2.052(8)	N(1)-C(2)	1.37(1)	C(2)-N(3)	1.39(2)
N(3)-C(4)	1.34(1)	C(4)-C(5)	1.43(2)	C(5)-C(6)	1.31(2)
C(6)-N(1)	1.38(1)	N(1)-C(1)	1.45(2)	C(2)-O(2)	1.23(1)
C(4)-N(4)	1.33(2)	N(7)-O(71)	1.26(2)	N(7)-O(72)	1.26(1)
N(7)-O(73)	1.21(1)	N(8)-O(81)	1.27(1)	N(8)-O(82)	1.24(1)
N(8)-O(83)	1.23(2)	C(1)-H(11)	1.0(2)	C(1)-H(12)	0.8(2)
C(1)-H(13)	1.0(1)	C(5)-H(5)	0.6(2)	C(6)-H(6)	0.8(2)
N(4)-H(41)	1.0(2)	N(4)-H(42)	1.2(2)	O(7)-H(71)	1.1(2)

Hydrogen-bond distances

O(3)-O(81)^{i}	2.74(1)	O(3)-H(32)	0.8(2)	H(32)-O(81)^{i}	2.0(2)
O(3)-O(71)	2.60(1)	O(3)-H(31)	0.9(2)	H(31)-O(71)	1.8(1)
N(5)-O(72)^{ii}	2.98(2)	N(5)-H(51)	0.9(2)	H(51)-O(72)^{ii}	2.1(2)
N(5)-O(2)^{iii}	2.95(1)	N(5)-H(52)	1.1(2)	H(52)-O(82)^{iv}	2.0(2)
N(5)-O(82)^{iv}	3.07(2)	N(5)-H(53)	0.9(1)	H(53)-O(2)^{iii}	2.2(1)
N(6)-O(2)^{iii}	2.87(1)	N(6)-H(61)	1.0(1)	H(61)-O(2)^{iii}	2.0(2)
N(6)-O(7)^{ii}	3.13(2)	N(6)-H(62)	0.9(2)	H(62)-O(7)^{ii}	2.8(2)
N(6)-O(82)^{v}	2.97(2)	N(6)-H(63)	1.1(2)	H(63)-O(82)^{v}	2.0(2)
O(7)-O(72)	3.07(1)	O(7)-H(72)	0.9(2)	H(72)-O(72)	2.2(1)

N(3)-Pt-N(5)	92.2(4)	N(3)-Pt-N(6)	176.7(4)
N(3)-Pt-O(3)	90.3(4)	N(5)-Pt-N(6)	90.1(5)
N(5)-Pt-O(3)	176.6(4)	N(6)-Pt-O(3)	87.6(4)
Pt-N(3)-C(2)	116.6(6)	Pt-N(3)-C(4)	122.6(8)
C(6)-N(1)-C(2)	120(1)	N(1)-C(2)-N(3)	118.0(8)
C(2)-N(3)-C(4)	120.8(9)	N(3)-C(4)-C(5)	120(1)
C(4)-C(5)-C(6)	118(1)	C(5)-C(6)-N(1)	122(1)
C(6)-N(1)-C(1)	121(1)	C(1)-N(1)-C(2)	118.5(9)

Table 3.12. (continued)

N(1)-C(2)-O(2)	120(1)	O(2)-C(2)-N(3)	122(1)
N(3)-C(4)-N(4)	118(1)	N(4)-C(4)-C(5)	122(1)
O(71)-N(7)-O(72)	115.6(8)	O(71)-N(7)-O(73)	119(1)
O(72)-N(7)-O(73)	125(1)	O(81)-N(8)-O(82)	119(1)
O(81)-N(8)-O(83)	119.3(9)	O(82)-N(7)-O(83)	122(1)

Atoms are related to those in Table 3.11 by the transformations:
(i) 1-x, 1-y, 1-z; (ii) -x, -y, 1-z; (iii) -x, -y, -z; (iv) 1-x, -y, 1-z;
(v) x-1, y, z-1.

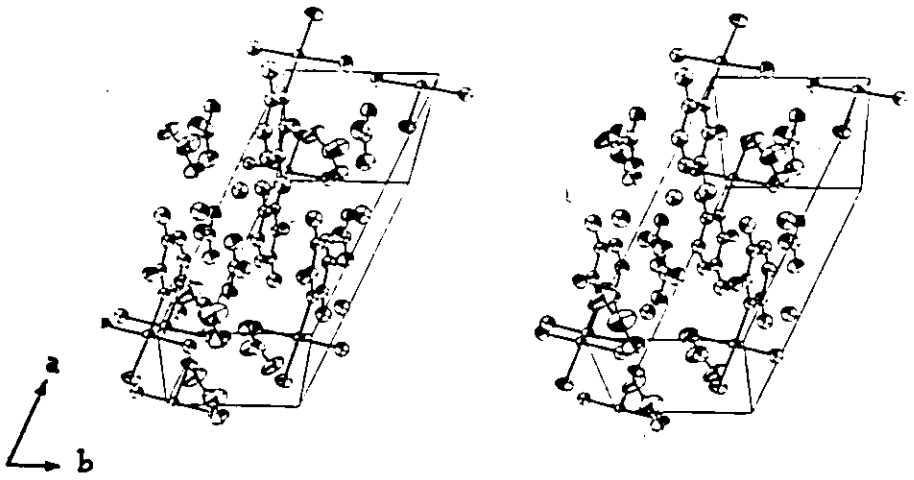

Figure 3.12. The unit cell contents for 3E

lying roughly parallel to the **ac** face. Surprisingly there is no hydrogen bonding within these layers. In particular, the amino group $N(4)H_2$ is not involved in hydrogen bonds. The layers are arranged such that the cytosine ring of a molecule related to another by the **c** translation is in the next layer. The platinum atoms lie close to the y = 0 plane and here there is extensive hydrogen-bonding. Two cations related by the 0, 0, 0 inversion center lie with the square planes separated by roughly 3.4Å, a feature seen extensively before for cis-amine complexes (Lock, Speranzini, Zvagulis (1980)). This cation pair is hydrogen-bonded together through $N(5)\ldots O(2)^{iii}$, $N(6)\ldots O(2)^{iii}$. Hydrogen-bonding in the **c**-direction is through N(5)...O(72), O(3)...O(71) and in both the **a** and **c** direction through $N(5)\ldots O(82)^{iv}$, $N(6)\ldots O(82)^{v}$. Other hydrogen-bonds stabilizing the structure and providing cation-anion links are $O(3)\ldots O(81)^{i}$, $N(6)\ldots O(7)^{ii}$, and O(7)...O(72).

In section 3.3.4, it was predicted, using Brown's (1981) bond valence relationships, that the coordinated water molecule would have to form two strong hydrogen-bonds, where it donates the protons, and a hydrogen-bond to a proton donor would be very weak or non-existent. Clearly both requirements are fulfilled: the only hydrogen-bond distances are $O(3)\ldots O(81)^{i}$ [2.74(1)Å] and O(3)...O(71) [2.60(1)Å]. Both interactions are strong and the hydrogen atoms are in the correct positions. The closest proton donor [3.35(2)Å] is N(5) on a

symmetry related molecule (x, 1+y, z).

3E is the first definite example of a Pt(II)-OH_2 bond stabilized in the solid state. It also suggests that a cis-[Pt(OH_2)(nucleobase)(NH_3)$_2$] model for the preliminary DNA lesion is a reasonable one.

CHAPTER 4

SOME REACTIONS OF TRANS-$Pt(NH_3)_2Cl_2$

4.1 Introduction

The anticancer drug cis-$Pt(NH_3)_2Cl_2$ has been shown to yield several different hydrolysis products after removal of the chloride ligands by the action of silver salts (Lock (1980); Rosenberg (1978)). The cis-$Pt(NH_3)_2(NO_3)_2$ complex has been characterized by infrared spectroscopy and X-ray crystallography (Lippert, Lock, Rosenberg, Zvagulis (1977)), as have several hydroxo-bridged complexes (Lock (1980), Bushnell (1978), Pilon (1984)). As a result of these findings, toxicity studies on fresh cis-$Pt(NH_3)_2(NO_3)_2$ were repeated and the results were found to differ from previous studies (Rosenberg (1978)). The hydroxo-bridged compounds were found to be very toxic, while the pure cis-dinitrato complex (aquated) was active.

The inactive isomer trans-$Pt(NH_3)_2Cl_2$ is often used, either halogenated or hydrolysed, for comparison tests in chemical and clinical studies of the cis drug (see §6.1). It was decided that solutions of trans-$Pt(NH_3)_2(NO_3)_2$ at various pH's should be examined to determine if any more complex species were present. Three questions needed answering.

Firstly, is the starting material trans-$Pt(NH_3)_2(NO_3)_2$

or trans-$[Pt(NH_3)_2(OH_2)_2](NO_3)_2$? The cis-isomer exists as the neutral molecule cis-$Pt(NH_3)_2(NO_3)_2$ in the solid but is rapidly hydrolysed to cis-$[Pt(NH_3)_2(H_2O)_2]^{2+}$ in solution. Similarly $[Pt(dien)(OH_2)](NO_3)_2$ could not be isolated as a solid (Chapter 3).

Secondly, is there only one Pt species in solution, or is it a mixture as found in the case of the cis-analogue? Are pure compounds being used for clinical testing?

Thirdly, what type or types of hydroxo compound(s) can be formed? Since they must be geometrically different from the cis-hydroxo-bridged complexes, any proposed mechanism of anti-cancer action involving the formation of hydroxo-bridged oligomers may rule out trans-$Pt(NH_3)_2Cl_2$ activity on this basis.

4.2 Trans-Diamminedinitratoplatinum(II) Bis(tetraammineplatinum(II)) Tetranitrate, 4A

The preparation of K_2PtCl_4 from Pt waste residues was done according to the procedures of Kauffman, Teter (1963) and Kauffman, Cowan (1963). Large red crystals were obtained. trans-$Pt(NH_3)_2Cl_2$ was prepared by the method of Kauffman and Cowan (1963). 0.5 g K_2PtCl_4 was dissolved in 9 mL of water and 0.3 mL of concentrated HCl. 1.2 mL of concentrated aqueous ammonia was added to convert the K_2PtCl_4 to $[Pt(NH_3)_4]Cl_2$ and KCl, and the volume was reduced to 2.5 mL. 50 mL 6M HCl was added and the solution was evaporated to a

volume of 4 mL, cooled on an ice bath for 15 min , and filtered. The 6M HCl treatment of the remaining solution was repeated. The solid trans-$Pt(NH_3)_2Cl_2$ was air dried. It was pale yellow-green. The X-ray powder diffraction pattern revealed no impurities.

Because of the greenish color, indicating Magnus's Green Salt ($[Pt(NH_3)_4][PtCl_4]$) as an impurity, the product was redissolved in the minimum amount of concentrated aqueous ammonia to convert back to $[Pt(NH_3)_4]^{2+}$ and the 6M HCl treatment was repeated. The resulting powder was straw-yellow in colour. This preparation of trans-$Pt(NH_3)_2Cl_2$ was repeated several times with fresh K_2PtCl_4 (scaled by mole ratios), and the products combined.

trans-$Pt(NH_3)_2(NO_3)_2$ was prepared by suspending 1.000 g (3.33 mmol) trans-$Pt(NH_3)_2Cl_2$ in 750 mL warm water and slowly adding an aqueous solution containing 1.131 g (6.66 mmol) $AgNO_3$ with constant stirring in the dark. AgCl was removed from the vessel after 24 h and the solution was allowed to evaporate to dryness at room temperature in the dark. Three visually distinguishable products were obtained: amorphous yellow semi-spheres, small twinned cross-shaped yellow crystals, and large, thick colourless, needle-shaped crystals of trans-$[Pt(NH_3)_2(NO_3)_2][Pt(NH_3)_4]_2(NO_3)_4$, 4A. Samples of these needles were separated from the solid residues for X-ray study, density determination, and elemental analysis. (Analysis: Found: N, 20.63%. Calc: N, 19.87%)

4.2.1 Crystal Data for 4A

$[Pt(NH_3)_2(NO_3)_2]\cdot 2[Pt(NH_3)_4]\cdot(NO_3)_4$, $H_6N_4O_6Pt\cdot 2H_{12}N_4Pt^{2+}\cdot 4NO_3^-$; 1127.61g·mol^{-1}; Pnma; Syntex $P2_1$ diffractometer, 15 refl. ($22.0^\circ<2\theta<30.1^\circ$) for cell; a=21.170(4), b=10.946(2), c=10.946(2)Å; V=2536.4(8)Å^3, Z=12; D_x=2.92, D_m=2.96g·cm^{-3} in CH_2I_2/CCl_4; $2\theta_{max}=55^\circ$, +h, ±k, +l; N_{meas}= 5837, min. R_{scan}=2.93 deg·min^{-1}; 23°C; standards: 0 2 0 (1.9%), 8 2 2 (3.7%); Psi-scan, Bond abs. corr., μ=160cm^{-1}, approx. cyl.: r=.10 mm, l=.14 mm, $9.5<A^*_\theta<12.3$; N_{unique}=3076, N_{used}=2747; NP=194, F(000)=2080; $\omega=\sigma^{-2}$, s= 2.43 , g(SHELX)= 0.00004; max. shift/error(ave.)=2.07 (0.28), R=0.104, R_ω= 0.039; Diff. map: -4.7, 5.9e·Å^{-3}, ~.375,.25,0 ; PSI, XRAY76, SHELX, ORTEP-II.

The precession photographs of 4A indicated that the space group was either Pnma or the non-centrosymmetric $Pn2_1a$ (non-standard for $Pna2_1$), thus the +h ±k +l reflections were collected. Tetragonal symmetry was ruled out on the basis of reflection intensities. Initially Pnma symmetry was used for structure solution and this proved to be the correct choice. The Patterson map was solved for three symmetry independent Pt atoms, using the assumption that they all had the same y coordinate (y = ¼, special position 4c). The remaining non-hydrogen atoms were found from electron density difference syntheses, indicating that the previous assumption was valid. No disorder in the nitrate moieties, bound or free, could be detected in Pnma or $Pn2_1a$.

It was expected that tetragonal pseudo-symmetry (b = c) may have caused refinement problems. There were serious convergence problems, but the source was a pseudo-inversion center at Pt(1), (.375, .25, .50). (There were high correlations between the following atom pairs: N(12), N(13); O(2), O(5); O(3), O(6); Pt(2), Pt(3); N(22), N(23); N(22), N(31); N(1), N(2); O(12), O(21).) For example, a large temperature factor for N(1) was compensated by a small one for N(2). The problem was minimized by using blocked-matrix refinement for an even number of cycles for each parameter set. The full parameter matrix was used for the final refinement cycles. Hydrogen atoms could not be located. The final atomic parameters are given in Table 4.1, and selected bond distances and angles are given in Table 4.2.

4A contains discrete $[Pt(NH_3)_4]^{2+}$ and NO_3^- ions, with normal molecular geometry. The trans-$Pt(NH_3)_2(NO_3)_2$ molecule, the compound sought, is also found in the lattice and is shown in Figure 4.1. The nitrate moieties are coordinated to the Pt atom, as found in the cis analogue. Only monodentate interaction is seen. The Pt(1)-N(11) bonds are perpendicular to the plane containing Pt(1) and the nitrate ligands. The trans-dinitrato complex has a non-crystallographic center of symmetry, because O(3) and O(6) lie on opposite sides of Pt(1). The cis compound was found to have the corresponding oxygen atoms on the same side of the ligand square plane, giving it non-crystallographic mirror symmetry.

Table 4.1. Atomic Positional Parameters ($x10^3$) and Isotropic Temperature Factors ($Å^2$) ($x10^2$) for 4A

	x	y	z	U_{eq}
Pt(1)	374.66(6)	250	490.7(1)	3.42(4)
N(11)	374.7(7)	436.5(8)	492(2)	4.7(6)
N(12)	360(2)	250	739(3)	7(2)
O(1)	404(1)	250	667(2)	7(2)
O(2)	382(2)	250	857(2)	14(3)
O(3)	306(1)	250	726(3)	11(3)
N(13)	378(2)	250	234(4)	10(2)
O(4)	339(1)	250	318(3)	12(2)
O(5)	364(2)	250	130(2)	16(3)
O(6)	431(2)	250	258(2)	13(3)
Pt(2)	120.62(6)	250	493.20(9)	3.08(4)
N(21)	120.7(7)	438.1(8)	495(2)	4.5(6)
N(22)	24.8(9)	250	486(2)	3(1)
N(23)	217(1)	250	500(3)	6(1)
Pt(3)	131.71(5)	250	-6.69(9)	2.48(4)
N(31)	226(1)	250	-39(2)	5(1)
N(32)	36.6(9)	250	26(2)	3(1)
N(33)	152(1)	250	177(2)	3(1)
N(34)	107.4(9)	250	-186(2)	3(1)
N(1)	258(1)	14(2)	233(2)	6(1)
O(11)	248.1(7)	19(1)	119(1)	5.9(9)
O(12)	306(1)	-56(2)	249(1)	10(2)
O(13)	229(1)	40(2)	317(3)	14(2)
N(2)	9(1)	4(2)	241(2)	6(1)
O(21)	61(1)	51(3)	240(2)	11(2)
O(22)	-17(1)	-32(2)	148(2)	14(2)
O(23)	-13(1)	-35(3)	338(2)	15(3)

Table 4.2. Selected interatomic distances (Å) and angles (deg) for 4A.

bonds

Pt(1)-N(11)	2.041(9)	Pt(2)-N(23)	2.05(2)
Pt(1)-O(1)	2.03(3)	Pt(3)-N(31)	2.02(2)
Pt(1)-O(4)	2.04(3)	Pt(3)-N(32)	2.05(2)
N(12)-O(1)	1.22(4)	Pt(3)-N(33)	2.06(2)
N(12)-O(2)	1.37(4)	Pt(3)-N(34)	2.03(2)
N(12)-O(3)	1.17(5)	N(1)-O(11)	1.27(3)
N(13)-O(4)	1.24(5)	N(1)-O(12)	1.29(4)
N(13)-O(5)	1.17(5)	N(1)-O(13)	1.14(4)
N(13)-O(6)	1.16(6)	N(2)-O(21)	1.21(4)
Pt(2)-N(21)	2.059(9)	N(2)-O(22)	1.23(3)
Pt(2)-N(22)	2.03(2)	N(2)-O(23)	1.23(3)

possible hydrogen-bonds

N(11)...O(11)^{i}	3.08(2)	N(23)...O(13)^{iii}	3.06(3)
N(11)...O(22)^{ii}	2.96(3)	N(31)...O(3)^{v}	3.07(4)
N(21)...O(12)^{i}	3.18(3)	N(31)...O(11)	3.10(2)
N(21)...O(13)^{iii}	3.03(3)	N(32)...O(22)^{vi}	3.09(3)
N(21)...O(21)^{iii}	3.07(3)	N(33)...O(21)	2.99(3)
N(21)...O(23)^{iv}	2.94(3)	N(34)...O(12)^{vii}	2.89(3)
N(22)...O(23)^{iv}	3.06(3)	N(34)...O(22)^{vi}	3.10(3)
N(23)...O(3)	3.11(4)		

angles

N(11)-Pt(1)-N(11)^{iii}	179.2(8)	N(21)-Pt(2)-N(23)	89.9(4)
N(11)-Pt(1)-O(1)	89.6(5)	N(22)-Pt(2)-N(23)	180(1)
N(11)-Pt(1)-O(4)	90.4(5)	N(31)-Pt(3)-N(32)	180.0(9)
O(1)-Pt(1)-O(4)	176(1)	N(31)-Pt(3)-N(33)	88.0(9)

Table 4.2. (continued)

Pt(1)-O(1)-N(12)	112(2)	N(31)-Pt(3)-N(34)	94.5(9)
Pt(1)-O(4)-N(13)	116(3)	N(32)-Pt(3)-N(33)	92.0(8)
O(1)-N(12)-O(2)	110(3)	N(32)-Pt(3)-N(34)	85.5(8)
O(1)-N(12)-O(3)	133(3)	N(33)-Pt(3)-N(34)	177.5(8)
O(2)-N(12)-O(3)	117(3)	O(11)-N(1)-O(12)	107(1)
O(4)-N(13)-O(5)	124(4)	O(11)-N(1)-O(13)	134(3)
O(4)-N(13)-O(6)	119(4)	O(12)-N(1)-O(13)	117(2)
O(5)-N(13)-O(6)	117(4)	O(21)-N(2)-O(22)	122(2)
N(21)-Pt(2)-N(21)^{iii}	178.7(7)	O(21)-N(2)-O(23)	120(2)
N(21)-Pt(2)-N(22)	90.1(4)	O(22)-N(2)-O(23)	116(3)

Atoms are related to those in Table 4.1 by:
(i) ½-x, ½+y, ½+z; (ii) ½+x, ½-y, ½-z; (iii) x; ½-y, z; (iv) -x, ½+y, 1-z;
(v) x, y, z-1; (vi) -x, ½+y, -z; (vii) ½-x, ½+y, z-½.

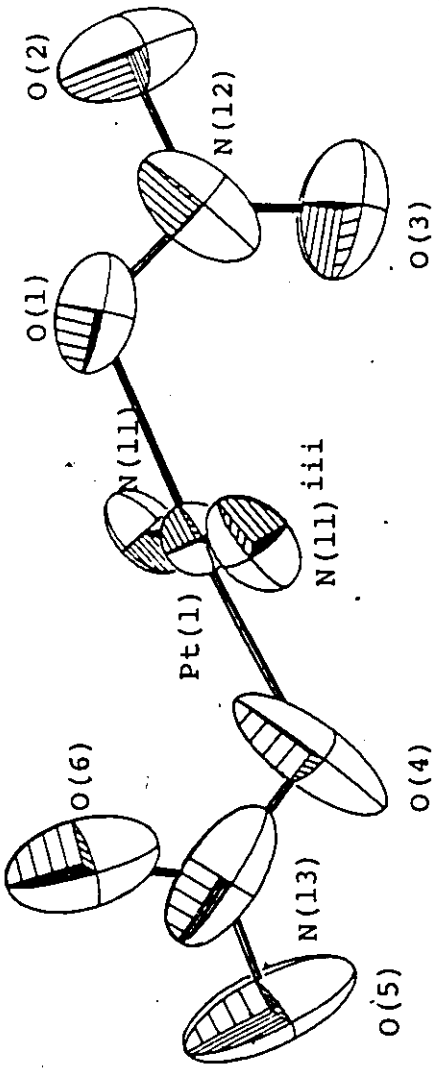

Figure 4.1. The trans-$[Pt(NO_3)_2(NH_3)_2]$ molecule of 4A

The high errors in bond lengths preclude any discussion of the relative trans influence of the ammine and nitrate ligands. N-O bond lengths in 4A cannot be compared for the same reason.

The packing of 4A is shown in Figure 4.2 with the view down **b**. The platinum complexes form layers at z = 0 and z = 0.5, and are separated by layers of nitrate ions at z = 0.25 and z = 0.75. The nitrate ligands are packed into the anion layer, similar to the packing for 3D (§3.3.3), $[Pt(dien)(NO_3)]NO_3$.

The trans-$Pt(NH_3)_2(NO_3)_2$ molecule lies with the Pt atom and nitrate ligands in the mirror plane at y = 0.25. The platinum ligand plane is roughly parallel to the **bc**-face. Each bound nitrate is surrounded by four anions oriented to minimize contact. The nitrate ion planes are approximately $\pm 32^{\circ}$ from the mirror plane, forming an 'open pocket' for the coordinated nitrate. The nitrate layer is stabilized by relatively weak hydrogen-bonding to the ammine ligands in the platinum layers (N(11), N(21), N(22), N(23), N(31), N(32)) and to the ammines sitting in the 'closed pocket' (N(33), N(34)) of the nitrate layer. This three-dimensional array of hydrogen-bonds and the ionic interactions serve to hold the crystal together.

The Pt(2) and Pt(3) cations pack parallel to the **ab**- and **ac**-faces, respectively. The Pt(2) square plane has its Pt-N bonds roughly parallel to the cell edges, and N(33) and N(34) ammines block the vacant octahedral sites. The N(23)

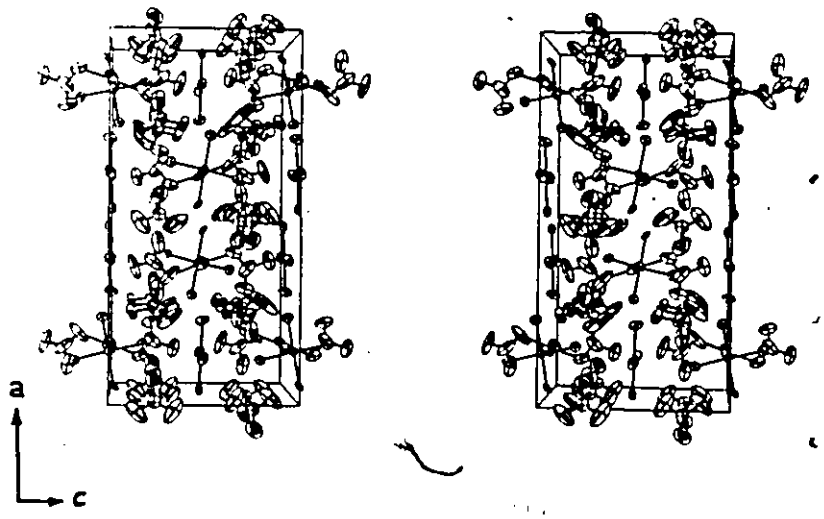

Figure 4.2. The packing of 4A in the unit cell

ammine in turn sits above the Pt(1) square plane. The sixth site on Pt(1) is blocked by N(32). The Pt(3) square plane, which is capped above and below by N(11) ammines, is slightly rotated (approx. 5°) around **b** to maximize hydrogen-bonding. The range of Pt...H_3N contacts observed [3.36(2)-3.53(2)Å] does not permit any conclusions on the possibility of proton interaction with filled $5d_{xy}$ and $5d_{yz}$ orbitals of platinum. Was it these contacts or the nitrate-ammine hydrogen-bonding network which determined the similarity in cell axial lengths? Because the normal hydrogen-bonding can account for this observation, platinum-ammine hydrogen-bonds cannot be verified.

Three other points are of note. Firstly, there are no water molecules in the lattice, similar to the cis-analogue and 3D. Only the aqua complex (3E) formed a hydrate, and the nitrates were not coordinated. Thus the competition between amine-nitrate and amine-water hydrogen-bonds seems to be readily won by the nitrate ions (at least in these Pt(II) systems). The cytosine ligand of 3E (§3.4) provided the necessary environment for water molecules to be incorporated in the cell.

Secondly, the pseudo-symmetry problem is clearly evident in the packing. Not only does the trans-$Pt(NH_3)_2(NO_3)_2$ molecule have a center of symmetry, but the planes parallel to the **bc**-face which contain Pt(1) are also centrosymmetric at the Pt sites and in between them. The anions above and

below these planes are approximately related by these pseudo-centers. This 'symmetry' is only destroyed because the next layer of molecules along +**a** (another plane containing pseudo-centers) has its cations rotated by 90° relative to the corresponding tetraammines in the -**a** direction (see Figure 4.2).

Finally, since the environment of the dinitrato complex is made up of ammines and nitrates, it is very likely that pure trans-$Pt(NH_3)_2(NO_3)_2$, with no $[Pt(NH_3)_4]\cdot 2\ NO_3$ in solution, will crystallize as the neutral molecule and not a nitrate salt of an aqua complex. A similar environment could be provided by symmetry related molecules. This hypothesis is currently being examined by Brenda Brown in our research group. The source of the ions in 4A will be discussed in section 4.4.

4.3 Trans-Dichlorotetraammineplatinum(IV) Dinitrate, 4B

A fresh batch of trans-$Pt(NH_3)_2Cl_2$ (1.756 g) was prepared (§4.2). The infrared spectrum of a sample from this lot matched that found by Poulet, Delorme, Mathieu(1964). Two experiments were then performed, using a Corning 130 pH meter with glass (#476022) and calomel (#476002) electrodes.

The first experiment was an attempt to reproduce Jensen's (1939) titration curve of aqueous trans-$[Pt(NH_3)_2(OH_2)_2]\cdot(NO_3)_2$. 0.300 g (1.00 mmol) trans-$Pt(NH_3)_2Cl_2$ was dissolved in 1 L of warm water and 0.340 g $AgNO_3$ was added

with stirring in the dark. After 24 h the AgCl was removed by filtration, and the solution was concentrated to 100 mL (now 0.01 M in Pt) to give the same concentration Jensen used, but a 20-fold volume. Titration with 0.0999 N NaOH (standardized using potassium hydrogen phthalate) with constant stirring did not give the same results as those reported by Jensen. The pH readings were consistently lower than the published results, by approximately one pH unit. The starting pH was 2.36, compared to 3.20. As the experiment progressed, the readings were found to be less stable. For example, after the addition of 6.33 mL NaOH, the pH was 4.857. Twenty-five minutes later it had decreased to 4.700. At 6.67 mL NaOH the pH was 5.400, but after 24 hours the reading was 4.516 pH units. The titration was therefore stopped.

In the second experiment 0.6003 g <u>trans</u>-$Pt(NH_3)_2Cl_2$ was dissolved in water and stirred with 0.6795 g $AgNO_3$. The AgCl was removed by filtration and the solution was allowed to evaporate for three weeks at room temperature in the dark. The pH dropped steadily. A white solid which precipitated from the yellow solution, was removed by filtration and dried. At this point, the pH was 1.3 and still dropping. Also, a fine stream of yellow powder was observed descending from the calomel electrode in the still solution.

The white precipitate was examined under the stereomicroscope, revealing a colourless microcrystalline powder,

some yellow material, and some colourless single crystals. The bulk sample contained a surprising 10% Cl by weight. The single crystals were of two types: needle-shaped and rhombohedral-shaped. The latter was determined to be trans-$[PtCl_2(NH_3)_4]\cdot(NO_3)_2$, 4B, by X-ray crystallography. (Analysis: Found: Cl, 15.45; N, 18.4; H, 2.6%. Calc: Cl, 15.48; N, 18.3; H, 2.6%)

4.3.1 Crystal Data for 4B

$[PtCl_2(NH_3)_4]\cdot(NO_3)_2$, $H_{12}N_4Cl_2Pt^{2+}\cdot 2NO_3^-$; 458.13g·mol^{-1}, $P\bar{1}$, Syntex $P2_1$ diffractometer; 15 refl. ($32.1^\circ<2\theta<46.5^\circ$) for cell; a=6.635(1), b=7.114(2), c=6.548(1)Å, α=114.41(2), β=95.52(2), γ=100.33(2)°, V=271.8(1)Å^3, Z=1; D_x=2.80, D_m=2.79g·cm^{-3} in CH_2I_2/CCl_4; $2\theta_{max}$=70.13°, ±h, ±k, ±l; N_{meas}=4795, min. R_{scan}=3.66deg·min^{-1}; 23°C; standards: 3 0 1 (1.3%), 1 3 0 (1.5%), 0 3 1 (1.8%); Psi-scan, Bond abs. corr., μ=129cm^{-1}, approx. sphere, r=0.08mm, $5.00<A^*_\theta<5.98$; N_{unique}=2398, N_{used}=2398; NP=89, F(000)=214; $\omega=(\sigma^2+0.00109F^2)^{-1}$, s=1.00, g(SHELX)=0.00007, max. shift/error(ave)=0.051(0.002), R=0.0216, R_ω=0.0276; Diff. map: -1.0, 1.6e·Å^{-3}, both near Pt; PSI, XRAY76, SHELX, ORTEPII.

Precession photographs of 4B revealed only a triclinic cell, and Delauney reduction revealed no hidden symmetry. The polaroid rotation photograph showed fairly intense reflections at high angle, so the 2θ limits were extended from 0-55° to 0-70°. All reflections measured had

$I>0$, so it was assumed that the Pt atom was on the origin, and that the space group was $P\bar{1}$. These assumptions proved to be correct, and the remaining atoms (including H atoms) were found from electron density difference synthesis. The weighting function was refined for this structure. The atomic parameters are given in Table 4.3 and selected bond lengths and angles are presented in Table 4.4.

The molecular ions and their packing are shown in Figure 4.3. The cation, which is on the inversion center, has bond lengths which are within the ranges previously found in Pt(IV) complexes (Pt-Cl, 2.26 to 2.309(6); Pt-N, 1.97(4) to 2.07(2) Å) (Bjorling (1941); Craven, Hall (1961); Liu, Ibers (1970); Faggiani, Howard-Lock, Lock, Lippert, Rosenberg (1982)), although they lie at the longer end of the range. The Pt-NH_3 distances in 4B are significantly longer than those found in cis-dichlorodiammine-trans-dihydroxoplatinum(IV) (2.00(1) Å, Faggiani et al. (1982)), but not significantly longer than the 'normal' Pt-NR_3 distance of 2.03 Å (Shustorovich, Porai-Koshits, Buslaev (1975)). The nitrate ion was found to have the expected (see §3.3.4) bond lengths and angles, although the N(3)-O(3) bond is 3.7σ longer than the N(3)-O(2) bond.

The packing of the ions is completely determined by the ammine-nitrate hydrogen-bonding. Each ammine is hydrogen-bonded to the three non-equivalent nitrate oxygen atoms in bonds involving all hydrogen atoms. The hydrogen bonds are

Table 4.3. Atomic positional parameters ($x10^3$) and temperature factors ($Å^2$)($x10^3$) for 4B.

	x	y	z	U_{iso} or U_{eq} *
Pt	0	0	0	17.80(7)*
Cl	255.1(1)	-60.4(1)	215.2(2)	28.6(3)*
N(1)	170.1(4)	-61.2(4)	-258.3(5)	25(1)*
N(2)	-146.5(4)	-317.4(4)	-137.4(5)	26(1)*
N(3)	680.5(5)	552.5(4)	284.4(5)	26(1)*
O(1)	598.2(6)	388.0(5)	300.7(8)	41(2)*
O(2)	570.2(5)	659.2(5)	239.2(6)	38(2)*
O(3)	876.8(5)	611.4(6)	309.7(7)	42(2)*
H(1)	88(10)	-105(10)	-373(11)	37
H(2)	243(10)	-149(10)	-253(10)	37
H(3)	223(10)	55(10)	-279(11)	37
H(4)	-156(10)	-351(10)	-17(11)	38
H(5)	-90(10)	-417(10)	-275(11)	38
H(6)	-309(10)	-371(10)	-262(11)	38

U_{iso} for H atoms set to approximately 1.5 U_{eq} of bonded atom.

Table 4.4. Intramolecular Bond Distances (Å) and Angles (deg) for 4B.

Pt-Cl	2.310(1)	Pt-N(1)	2.064(3)	Pt-N(2)	2.054(2)
N(3)-O(1)	1.231(5)	N(3)-O(2)	1.242(5)	N(3)-O(3)	1.266(4)
N(1)-H(1)	0.79(7)	N(1)-H(2)	0.87(8)	N(1)-H(3)	0.91(8)
N(2)-H(4)	0.92(8)	N(2)-H(5)	1.04(6)	N(2)-H(6)	1.19(6)

Cl-Pt-N(1)	89.90(9)	Cl-Pt-N(2)	88.79(9)	N(1)-Pt-N(2)	90.2(1)
O(1)-N(3)-O(2)	120.3(3)	O(1)-N(3)-O(3)	120.9(4)	O(2)-N(3)-O(3)	118.8(4)
Pt-N(1)-H(1)	106(5)	Pt-N(1)-H(2)	109(5)	Pt-N(1)-H(3)	114(4)
H(1)-N(1)-H(2)	114(6)	H(1)-N(1)-H(3)	89(7)	H(2)-N(1)-H(3)	123(7)
Pt-N(2)-H(4)	107(3)	Pt-N(2)-H(5)	115(4)	Pt-N(2)-H(6)	116(4)
H(4)-N(2)-H(5)	118(6)	H(4)-N(2)-H(6)	113(5)	H(5)-N(2)-H(6)	88(5)

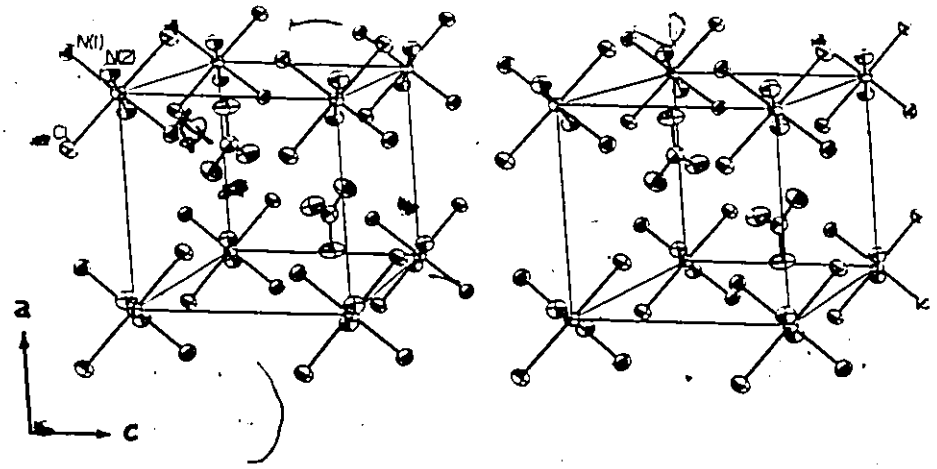

Figure 4.3. The packing of 4B in the unit cell

indicated in Figure 4.4. The chlorine atom is not involved in any significant hydrogen-bonding.

Brown's bond valence model (§3.3.4) can be used to explain the difference in bond lengths seen in the nitrate ion of 4B [$r_{2,obs}$ = 1.242(5) Å for N(3)-O(2) and $r_{3,obs}$ = 1.266(4) Å for N(3)-O(3)]. Figure 4.4 shows that O(3) is hydrogen-bonded to three ammines via H(5), H(1), and H(4), while O(2) interacts with H(3) and H(6). Using Brown's O-H bond valence (s) versus distance (r) curve (Brown (1981)), and the assumption that the N-H bonds are all 1.1 Å, the calculated Lewis acid strength of the hydrogen-bonding environment of O(3) is 0.39 valence units (vu); for O(2) s = 0.22 vu. This leaves O(3) with a base strength of 1.61 vu and O(2) with 1.78 vu for bonding to the central nitrogen. Empirically, $r = 1.43s^{-0.25}$ Å for an N-O bond. Thus $r_{3,calc}$= 1.269 Å and $r_{2,calc}$=1.240 Å, in excellent agreement with the measured values. Table 4.5 shows hydrogen-bonding distances, selected angles, adjusted distances, and individual bond valences.

4.4 Source of Impurities

The attempts to prepare trans-$Pt(NH_3)_2(NO_3)_2$ outlined in this chapter did produce and verify the structure of this complex, but unwanted complex ions were also observed, $[Pt(II)(NH_3)_4]^{2+}$ and trans-$[Pt(IV)Cl_2(NH_3)_4]^{2+}$, as nitrate salts.

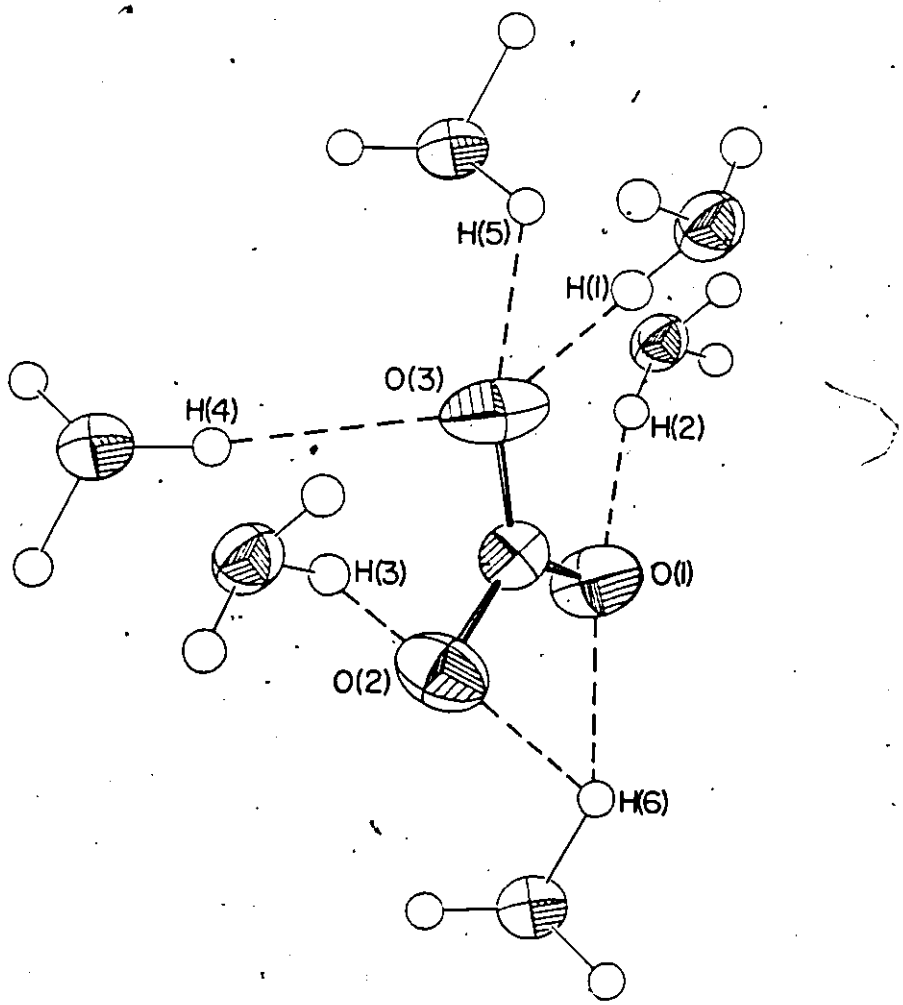

Figure 4.4. The hydrogen-bonding about the nitrate group shown in the upper left corner of Figure 4.3.

Table 4.5. Hydrogen-Bonding Distances, Angles, and Bond Valences(S)

H-Bond*	H---O	N-H···O	N····O	Adj.	S***
	Å	deg	Å	H··O**	
$N(1)^{i}$-$H(2)^{i}$···O(1)	2.09(7)	170(6)	2.945(5)	1.86	0.19
$N(2)^{ii}$-$H(6)^{ii}$···O(1)	1.88(7)	149(5)	2.963(5)	1.96	0.16
$N(1)^{iii}$-$H(3)^{iii}$···O(2)	2.14(7)	161(5)	3.010(5)	1.96	0.16
$N(2)^{ii}$-$H(6)^{ii}$···O(2)	2.50(7)	114(5)	3.179(4)	2.54	0.07
$N(2)^{i}$-$H(5)^{i}$···O(3)	2.12(7)	134(6)	2.939(5)	2.08	0.13
$N(1)^{iv}$-$H(1)^{iv}$···O(3)	2.31(5)	150(7)	3.014(4)	2.05	0.13
$N(2)^{v}$-$H(4)^{v}$···O(3)	2.26(8)	170(3)	3.165(6)	2.08	0.13

*Symmetry operators to transform from coordinates in Table 4.3:
(i) 1-x, -y, -z; (ii) -x, -y, -z; (iii) 1-x, 1-y, -z; (iv) 1+x, 1+y, 1+z;
(v) 1+x, 1+y, z.

**O···H distance recalculated with consideration of the angle at H to adjust for a 1.1Å N-H bond (Brown, 1982).

***For the O···N hydrogen bond, 0.02 valence units are added to the S value from the O-H curve (Brown, 1982).

There are two likely sources of the $[Pt(NH_3)_4]^{2+}$ ion, both of them contaminants of trans-$Pt(NH_3)_2Cl_2$. The first is Magnus' Green Salt, $[Pt(NH_3)_4][PtCl_4]$, which may not have been completely removed in the preparation (Kauffman, Cowan (1963)). The $[PtCl_4]^{2-}$ ion, or some halogenated derivative, may be present in one or more of the unidentified products. The second possibility is $[Pt(NH_3)_4]Cl_2$, formed either by adding too much concentrated aqueous ammonia (to destroy Magnus' Salt), or by condensing the trans-$Pt(NH_3)_2Cl_2$/6M HCl solution too much before filtering. The presence of this impurity would also result in a low Cl percentage in the solid, and therefore an excess of $AgNO_3$ in the 'stoichiometric' reaction.

The tetravalent platinum complex may have formed at any stage in the preparation, but there is evidence to suggest that the trans-$Pt(NH_3)_2Cl_2$ is again the source of the impurity. When dissolving the K_2PtCl_4 in dilute HCl, a small amount of black precipitate was sometimes observed and removed by filtration. On one occasion a temporary faint yellow cloud in the red solution was noticed. Thus a small amount of the K_2PtCl_4 appears to have disproportionated in the HCl solution to give Pt metal and K_2PtCl_6. Treatment with concentrated NaOH and then 6M HCl would likely give $[Pt(NH_3)_{6-n}Cl_n]Cl_{4-n}$ as a contaminant in the trans-$Pt(NH_3)_2Cl_2$. The structure of 4B suggests that n = 2. This would result in an underestimate of the amount of $AgNO_3$ required

to remove all of the Cl. This cannot, however, explain the presence of Cl both in 4B and as 10% of the remaining solid.

This excess chloride was found to come from the saturated KCl solution in the calomel electrode of the pH meter, via the porous ceramic salt bridge. This fact explains the stream of yellow solid below the electrode (trans-$Pt(NH_3)_2Cl_2$ is not very soluble) and may also explain the failure of the titration experiment. Jensen (1939), however, claims that addition of Cl^- ion to the solution causes the pH to rise. It is possible that the slow formation of hydroxo-bridged oligomers caused the pH to decrease.

For future studies, careful preparation and analysis of the trans-$Pt(NH_3)_2Cl_2$ is required. Elemental analyses and gravimetric determination of chloride with silver salts are not very sensitive techniques, considering the types of impurities and the small quantities used. Infrared and X-ray powder studies are also ineffective, without a great deal of analysis. Conductivity measurements could be useful because most of the possible impurities are ionic. Any cis-$Pt(NH_3)_2Cl_2$ contaminant gives an intense violet colour in the presence of phenoxytellurine di(hydrogen sulfate).

The calomel electrode problem can be solved by using a second salt bridge of KNO_3 in order to keep the reference electrode in a separate beaker.

The study of the reactions of trans-$Pt(NH_3)_2Cl_2$ with other small inorganic molecules, and its possible hydrolysis

products, is currently being continued by Brenda Brown in our laboratory.

CHAPTER 5

MIXED-VALENCE HALOGEN-BRIDGED CHAIN COMPOUNDS OF Pt

5.1 Introduction

The two preceding chapters have discussed the chemistry and crystallography of (1) platinum(II) aqua and (2) trans-$A_2L_2Pt(II)$ compounds. Problems with (3) impure starting materials and (4) oxidation of Pt(II) to Pt(IV) have been outlined. The work presented in this chapter resulted from a convergence of all four of these aspects of Pt chemistry through the synthesis of a mixed-valence halogen-bridged chain compound. It was hoped that the removal of one equivalent of chloride from trans-$Pt(NH_3)_2Cl_2$ with $AgClO_4$ would yield trans-$[Pt(OH_2)(NH_3)_2Cl](ClO_4)$, since perchlorate is not well suited for coordination to Pt. However, a hard, yellow crystalline compound was obtained which was determined to be $[Pt(NH_3)_4Cl_2]_{0.87}\cdot[Pt(NH_3)_4]_{4.13}\cdot(ClO_4)_{10}$, 5A.

5A belongs to a class of compounds exhibiting linear chains of halogen-bridged metal atoms in which the metal atoms appear in two different oxidation states. For comparison, the structures of two other mixed-valence Pt-halogen chain compounds were determined: $2K\cdot[Pt(NH_3)Br_3]\cdot[Pt(NH_3)Br_5]\cdot 2H_2O$, 5B, and $2(NH_4)\cdot[Pt(NH_3)Br_3]\cdot[Pt(NH_3)Br_5]\cdot 2H_2O$, 5C. 5B and 5C were prepared by T. Theophanides and D. Layek at the Université de Montréal, Montréal, P.Q., Canada.

The crystal structures of 5A, 5B, and 5C show some interesting order-disorder features in the packing. In this chapter an outline of common physical and optical properties of this class of compounds and the interpretation in terms of crystal packing are presented.

5.2 Dichlorotetraammineplatinum(IV) Tetrakis(tetraammineplatinum(II)) Decaperchlorate, 5A.

1.0000 g (3.333 mmol) of trans-$PtCl_2(NH_3)_2$ was stirred in 50 mL hot water. 0.6910 g (3.333 mmol) $AgClO_4$ in 5 mL water was added dropwise, and stirred for 24 h. AgCl was filtered from the solution, and after slow evaporation, several hard yellow crystals of 5A were obtained. The white microcrystalline residue which co-precipitated with 5A turned green after several weeks exposure to the air in the dark.

Precession photographs of spherically-ground single crystals of 5A revealed a primitive tetragonal cell with no systematic absences. The possible space groups were P4, $P\bar{4}$, P422, P4mm, $P\bar{4}2m$, $P\bar{4}m2$ (noncentrosymmetric) or P4/m, P4/mmm (centrosymmetric). Because the crystal chosen was aligned along the unique axis (**c**), rotation and Weissenberg (hk0) photographs were taken to verify the four-fold symmetry. Analyses: Found: N, 11.87; H, 2.46%. Calculated for $[Pt(NH_3)_4Cl_2]_{0.87}\cdot[Pt(NH_3)_4]_{4.13}\cdot(ClO_4)_{10}$: N, 11.81; H, 2.55%. Not enough sample for Cl analysis.

5.2.1 Crystal Data for 5A

$[Pt(NH_3)_4Cl_2]_{0.87}\cdot[Pt(NH_3)_4]_{4.13}\cdot(ClO_4)_{10}$, $0.87H_{12}Cl_2N_4Pt^{2+}\cdot 4.13H_{12}N_4Pt^{2+}\cdot 10ClO_4^-$; 2372.26 $g\cdot mol^{-1}$, P4/mmm, Syntex $P2_1$ diffractometer; 15 refl. ($22.0^\circ<2\theta<35.2^\circ$) for cell; a=11.500(2), c=11.147(2)Å, V=1474.2(5)$Å^3$, Z=1; D_x=2.67, D_m=2.66 $g\cdot cm^{-3}$ in CH_2I_2/CCl_4; $2\theta_{max}=55^\circ$, +h, +k, ±l; N_{meas}= 3751, min. R_{scan}=4.88 $deg\cdot min^{-1}$; 23°C; standards: 2 -4 -2 (2.1%), 2 0 6 (2.3%); Psi-scan, Bond abs. corr., μ=120 cm^{-1}, sphere: r=0.151 mm, $10.22<A_\theta^*<13.59$; N_{unique}=1050, N_{used}=1039; NP=74, F(000)=1114; $\omega=\sigma_F^{-2}$, S=4.17, g(SHELX)=0.00015, max. shift/error(ave)=0.012(0.001), R=0.065, R_ω=0.042; Diff. map: $-3.7\ e\cdot Å^{-3}$ near Pt, $4.5\ e\cdot Å^{-3}$ at (0,0,0.5); PSI, XRAY76, SHELX, ORTEPII.

The Patterson map for 5A was highly symmetric, and showed several Pt...Pt vectors. It was solved with four independent Pt's at special positions 1a, 1d, 2e, and 1c in space group P4/mmm. The remaining non-hydrogen atoms were found from electron density difference syntheses. The perchlorate (Cl(1), O(1)) at position 2f appeared with eight half-oxygen atoms forming a cube around the chlorine atom, indicating a two-fold disorder. The symmetry independent perchlorate at position 8r showed large temperature factors for the oxygen atoms, but could not be resolved into two different orientations. Hydrogen atoms were not found, since they are highly disordered. The $4.5\ e\cdot Å^{-3}$ residual peak at position 1b was tested as a water molecule, but the enormous tempera-

ture factor ruled this out (U_{iso}=3.3 Å^2). Possible disordered water positions around (0,0,0.5) were similarly ruled out. Furthermore, the elemental analyses do not suggest that water is present. The peak is likely an aberration caused by the high symmetry of the position.

The raw data were then averaged in both P4 and P$\bar{4}$ space groups to determine if lowering the symmetry would remove any of the disorder in the perchlorates. A model containing only Pt, N and Cl atoms showed no further ordering of the oxygen atoms in the difference maps, and refinement with the half-oxygen atoms gave correlations which indicated the full P4/mmm symmetry. Again, residual electron density was observed near (0,0,0.5), but an oxygen atom was not acceptable in that area.

At this point in the refinement, it was clear that there were chains of Pt(II)...Cl-Pt(IV)-Cl...Pt(II)... etc. parallel to **c**, with an unsymmetric Cl bridge. It is common for structures of this type (cf. §5.4) to have these ordered chains disordered relative to one another because of random shifting of the chains along **c** by a Pt(IV)...Pt(II) distance, resulting in a symmetry equivalence of the two platinums, and a symmetric disordering of Cl atoms about the Pt...Pt midpoint. No evidence of this type of disorder was found. However, it was found that there is a three-dimensional disorder at the position of the Pt(IV). It was suspected that the $[Pt(NH_3)_4]^{2+}$ ion could occasionally replace the <u>trans</u>-

$[Pt(NH_3)_4Cl_2]^{2+}$. The evidence for this was the similarities of the charge and the ammine square-planes for the two ions, the lack of any strong interaction of the chloride atom (only a weak interaction with Pt(II)), the (approximately) four to one ratio of $[Pt(NH_3)_4]^{2+}$ to $[Pt(NH_3)_4Cl_2]^{2+}$, and the slightly high temperature factors of the Cl atom. The occupancy of Cl was subsequently refined, and both the temperature factors and R factors improved. The 0.87 occupancy of Cl also improved the elemental analyses fit. The final atomic parameters are given in Table 5.1, and bond distances and angles are given in Table 5.2.

5A comprises discrete trans-$[Pt(NH_3)_4Cl_2]^{2+}$, $[Pt(NH_3)_4]^{2+}$ and ClO_4^- ions. The Pt-N bond lengths are relatively long in general, but because of large errors are not significantly different from the identical ions examined in 4A and 4B. The Pt-Cl bond length is normal. All angles around the Pt atoms are fixed at the ideal 90° or 180° by symmetry. The geometry of the disordered perchlorate at (0,0.5,0) is normal for each of the superimposed species. The perchlorate at roughly (.25,.25,.25) has an ill-defined disorder, with very large oxygen temperature factors, and not so ideal geometry.

The packing of these ions is shown in Figure 5.1. The Pt(II)...Cl-Pt(IV)-Cl...Pt(II)... chain runs parallel to **c**, centered in the **ab**-face. Pt(IV) is found only in the **ab**-face, with the Pt-N bonds parallel to **a** and **b**. The [Pt(II)-

Table 5.1. Positional parameters ($x10^3$) and isotropic temperature factors ($x10^3$) ($Å^2$) for 5A.

	x	y	z	U_{eq}
Pt(1)	0	0	0	30.0(7)
N(1)	179(1)	0	0	62(14)
Pt(2)	500	500	500	26.5(7)
N(2)	316(2)	500	500	78(16)
Pt(3)	0	500	500	41.3(9)
N(3A)	0	317(2)	500	62(15)
N(3C)	0	500	688(2)	65(14)
Pt(4)	500	500	0	30.4(8)
N(4)	500	319(2)	0	55(13)
Cl*	500	500	205.9(9)	65(6)
Cl(1)	0	500	0	58(7)
O(1)	73(1)	428(1)	75(1)	55(9)
Cl(2)	246.4(4)	246.4(4)	254.6(6)	64(2)
O(2)	262(1)	262(1)	131(1)	180(15)
O(3)	166(1)	166(1)	249(2)	455(42)
O(4)	347(2)	221(2)	300(2)	312(24)

*refined site occupancy for Cl: 0.87(2)

Table 5.2. Selected interatomic distances (Å) and angles (deg) for 5A.

bonds

Pt(1)-N(1)	2.06(2)
Pt(2)-N(2)	2.11(2)
Pt(3)-N(3A)	2.11(2)
Pt(3)-N(3C)	2.09(2)
Pt(4)-N(4)	2.08(2)
Pt(4)-Cl	2.30(1)
Cl(1)-O(1)	1.44(1)
Cl(2)-O(2)	1.41(2)
Cl(2)-O(3)	1.31(2)
Cl(2)-O(4)	1.29(2)

hydrogen-bonds

N(1)...O(1)^{i}	3.10(2)
N(2)...O(4)^{i}	3.04(2)
N(3C)...O(1)^{ii}	2.89(2)
N(3C)...O(4)^{iii}	3.10(2)
N(4)...O(1)^{i}	3.07(2)
N(4)...O(2)	3.17(2)

contacts

Pt(2)...Cl	3.28(1)
Cl...O(2)	3.96(2)
Cl...O(4)	3.81(2)

angles

O(1)-Cl(1)-O(1)^{iv}	109(1)	O(2)-Cl(2)-O(3)	98(1)
O(1)-Cl(1)-O(1)^{v}	110(1)	O(2)-Cl(2)-O(4)	107(1)
O(1)-Cl(1)-O(1)^{vi}	109(1)	O(3)-Cl(2)-O(4)	119(1)
		O(4)-Cl(2)-O(4)^{i}	104(1)

Atoms are related to those in Table 5.1 by:
(i) y, x, z; (ii) -x, y, 1-z; (iii) -y, x, 1-z;
(iv) -x, 1-y, z; (v) -x, y, -z; (vi) x, 1-y, -z.

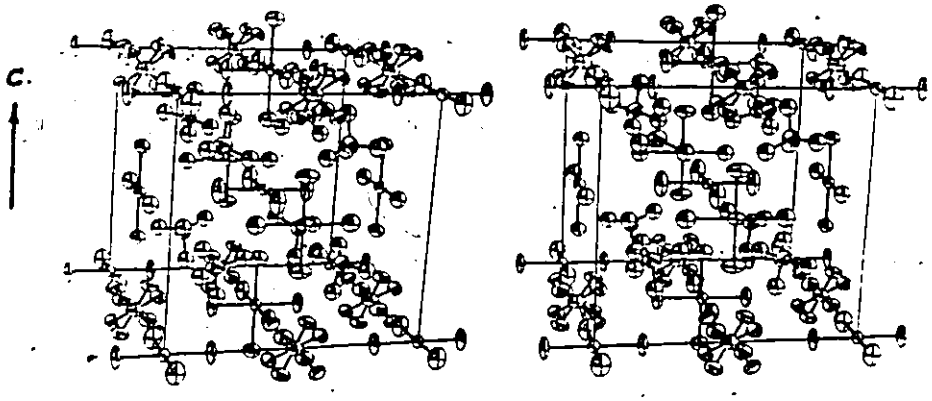

Figure 5.1. The unit cell contents of 5A

The thermal elipsoids of the oxygen atoms (O(2), O(3), O(4)) of the internal perchlorate ions have been reduced for clarity.

$(NH_3)_4]^{2+}$ ion is found at (0,0,0) and (0.5,0.5,0.5), with the same orientation as the Pt(IV)$(NH_3)_4$ group. Two symmetry related $[Pt(II)(NH_3)_4]^{2+}$ ions are centered in the **ac** and **bc** faces, with the Pt-N bonds parallel to the axes defining each respective face. The disordered perchlorate ions centered on the **a** and **b** cell edges serve to hold the structure together rigidly. The cation at the origin is linked via these edge perchlorates to the cations centered on each of the three faces. Each oxygen (O(1)) is hydrogen-bonded to N(1) [3.10(1) Å], N(3C) [2.89(2)Å], and N(4) [3.07(1)Å]. The eight interior perchlorates, one centered in each of the eight octants of the cell, are held in place mainly by the ionic lattice surrounding them, and are loosely oriented by weak hydrogen-bonds [O(2)...N(4), 3.17(2); O(4)...N(3C), 3.10(2); O(4)... N(2), 3.04(2)Å]. The $[Pt(II)(NH_3)_4]^{2+}$ ion at the center of the cell is held in place by the surrounding eight perchlorate ions, and has a very weak interaction with the chloride ligands of Pt(IV) [Pt(2)...Cl, 3.28(1)Å] (cf. §5.4). It should be noted that there is a cavity centered at (0,0,0.5), surrounded by eight perchlorate oxygens (O(2)) and four ammines (N(3A)). This space could easily accommodate a disordered water molecule, although one could not be located. The generally high thermal parameters of the nitrogen atoms and the relatively high errors on the bond lengths are a result of the slight positional disorders of the cations required for hydrogen-bonding to the disordered perchlorate

ions. This can be seen in the anisotropy of the thermal ellipsoids in Figure 5.1. Thus the hydrogen-bonding may be slightly stronger than is indicated by the distances given in Table 5.2. X-ray analysis at low temperature might resolve these disorders.

5.3 Dipotassium and Diammonium[Tribromo(ammine)platinate(II)] [Pentabromo(ammine)platinate(IV)] Dihydrate, 5B and 5C.

The two bromo-compounds were prepared by the oxidation of an aqueous solution of $M^{I}[Pt(NH_3)Br_3]$ with Br_2 according to the methods described by Werner (1896), Elleman, Rishus, and Martin (1958), Fanwick and Martin (1973) and Layek (1981), where $M^{I} = K^+$, NH_4^+. The oxidation yielded red crystals of the type $M^{I}[Pt(NH_3)Br_5]$. A mixture of hot aqueous solutions of equivalent amounts of $M^{I}[Pt(NH_3)Br_3]$ and $M^{I}[Pt(NH_3)Br_5]$ yielded bronze crystals with metallic appearance. Large crystals of 5B and 5C in the form of dark, shiny, rectangular needles were obtained by slow evaporation of an aqueous solution in the presence of $M^{I}Br$. Chemical analyses for H, C, N, and Br were reported by Layek (1981).

The isomorphous crystals of 5B and 5C were found to have the needle axis coinciding with the **a** axes of the orthorhombic cells. The distances between the (010) and (0$\bar{1}$0) faces ranged from about one (in the crystals chosen for study) to one tenth times the distances between the (001) and (00$\bar{1}$) faces, indicating slightly weaker intermolecular interactions in the **b** direction. Precession photographs of

5B, the potassium salt, indicated the space group Pbca. The very weak odd-h reflections corresponded to the weak, diffuse layer-lines observed interleaving the stronger Bragg lines on the rotation photograph aligned along a. These weak, odd-h reflections for the ammonium salt, 5C, did not appear on the precession photographs, suggesting a cell of approximately half the volume in space group Cmcm, $Cmc2_1$, or Cmc2 (non-standard form of Ama2). Diffuse interleaving layer-lines were seen on a week-long rotation photograph of 5C, but a week-long precession photograph of a large crystal was necessary to reveal the Bragg reflections which doubled the a-axis. Thus X-ray data were collected for both compounds in the Pbca cell.

5.3.1 Crystal Data for 5B

2 K·$[PtBr_3(NH_3)]$·$[PtBr_5(NH_3)]$·$2H_2O$, $2K^+ \cdot H_3Br_3NPt^- \cdot H_3Br_5NPt^- \cdot 2H_2O$; 1177.71 g·$mol^{-1}$, Pbca; Syntex $P2_1$ diffractometer; 15 refl. ($32.1^\circ < 2\theta < 51.8^\circ$) for cell; a=11.068(2), b=20.296(10), c=8.292(1)Å; V=1863(1)$Å^3$, Z=4; D_x=4.20, D_m>3.33 g·cm^{-3}; $2\theta_{max}=55^\circ$, +h, +k, ±l; N_{meas}=4135, min. R_{scan}=3.66 deg·min^{-1}; 23°C; standards: 0 2 1 (0.9%), 2 -1 0 (1.0%); Psi scan, Bond abs. corr., μ=317 cm^{-1}, approx. cyl.: r=0.035, l=0.100 mm, $5.76 < A^*_\theta < 6.57$; N_{unique}=2145, N_{used}=1866; NP=81; F(000)=2056; $\omega=\sigma^{-2}$; S=2.47 ; g(SHELX)=0.00022, max. shift/error(ave)=0.430(0.088), R=0.128, R_ω=0.056; Diff. map: -3.4, 4.0 e·$Å^{-3}$, both near the K^+, H_2O chain; PSI, XRAY76, SHELX,

ORTEPII.

The Pt coordinates for 5B deduced from a Patterson synthesis were for the general position (.125, .402, .750). A series of least-squares refinements followed by three-dimensional electon-density syntheses revealed all the non-hydrogen atoms. The Br atom bridging the two platinum atoms in the **a** direction was found to be disordered, and was represented by two Br's (Br(4) and Br(5)), each with half occupancy. Refinement in space groups of lower symmetry (eg. $P2_1/c$ or $P2_12_12_1$) which allowed adjacent platinums along the chain to be symmetry independent, revealed no ordering of this Br atom. The potassium and oxygen atoms were completely ordered in general positions.

In the early stages of structure refinement, it was necessary to use blocked least-squares calculations to avoid high correlations between the two half bromines and between the two Br atoms (Br(2) and Br(3)) trans to one another, parallel to **c**. The final refinements used full-matrix least-squares procedures. Two peaks in the final difference map corresponded to the hydrogen atoms of the water molecule and were in chemically sensible positions. Nevertheless it was not possible to refine the positions. They did not reach a stable minimum in chemically sensible positions, so they were not retained, especially since other peaks on the map, presumably caused by the high absorption problems, were much larger. The final R and R_ω values were 0.128 and 0.056,

respectively, with the σ_c^{-2} weighting greatly improving the residual. The high value of R is a result of the inclusion of the very weak odd-h data. (With removal of the odd-h data, the refinement converged to R = 0.075.) The positional parameters and temperature factors for 5B are listed in Table 5.3.

5.3.2 Crystal Data for 5C and a Comparison of 5B and 5C

2 $NH_4 \cdot [PtBr_3(NH_3)] \cdot [PtBr_5(NH_3)] \cdot 2H_2O$, $2H_4N^+ \cdot H_3Br_3N\text{-}Pt^- \cdot H_3Br_5NPt^- \cdot 2H_2O$; 1135.58 $g \cdot mol^{-1}$, Pbca; Syntex $P2_1$ diffractometer; 15 refl. ($29.5^\circ < 2\theta < 41.3^\circ$) for cell; a=11.162(1), b=20.765(3), c=8.3166(9)Å; V=1927.5(4)$Å^3$, Z=4; D_x=3.91, D_m>3.33 $g \cdot cm^{-3}$; $2\theta_{max}=55^\circ$, +h, +k, ±l; N_{meas}=4422, min. R_{scan}= 2.44 $deg \cdot min^{-1}$; 23°C; standards: 4 0 0 (1.4%), 0 -2 1 (1.6%); Psi scan, Bond abs. corr., μ=302 cm^{-1}, cube: l=0.10 mm, $5.75 < A_\theta^* < 6.57$; N_{unique}=2230, N_{used}=1855; NP=78; F(000)=1992, $\omega=\sigma^{-2}$; S=1.86 ; g(SHELX)=0.00027; max. shift/error(ave)= 0.433(0.090), R=0.148, R_ω=0.046; Diff. map: -4.4, 5.1 $e \cdot Å^{-3}$, both near Pt; PSI, XRAY76, SHELX, ORTEPII.

Since the early precession photographs of the ammonium salt, 5C, indicated the Cmcm cell (a=5.58Å) and the potassium salt of the pyridine (py) analogue ($2\,K \cdot [PtBr_3(py)] \cdot [PtBr_5(py)] \cdot 2H_2O$; Beauchamp, Layek, Theophanides (1982a)) had previously been solved in Cmcm, the initial data set was collected for this cell. Normal Patterson synthesis, least-squares refinements, and electron density difference syntheses yielded a crystal structure (discussed below) isomorphous to

Table 5.3. Atomic positional parameters ($x10^3$) and temperature factors ($Å^2$) ($x10^3$) for 5B.

	x	y	z	U_{eq}
Pt	125.1(2)	402.54(3)	748.8(2)	21.5(3)
Br(1)	124.6(7)	282.02(9)	754.8(6)	43(1)
Br(2)	117.0(5)	408.0(2)	1042.8(4)	47(2)
Br(3)	142.4(3)	403.3(2)	453.1(4)	33(2)
Br(4)	-101(1)	410.7(5)	730(1)	29(5)
Br(5)	349(1)	398.4(5)	764(1)	38(5)
N	123(4)	506.4(9)	740(4)	39(10)
K	621(1)	788.5(3)	29.1(8)	61(4)
O	125(3)	675(1)	647(3)	67(13)

to the pyridine compound, with the Pt atom on special position 4c at (0, .3443, .25), having 2mm point symmetry. The ammonia nitrogen and water oxygen atoms were found to be disordered on the mirror plane at 8f, (0, .044, .038) and (0, .078, .131) respectively. The coordinated nitrogen atom and trans-bromine atoms were on the 4c mm axis (y = .246 and .462 respectively), the disordered Br atom on special position 8g (.446, .341, .25) and the final Br atom on 8f (0, .341, .544). The final residuals were R = 0.041 and R_ω = 0.027, with $\omega=\sigma^{-2}$, for 662 unique, non-zero reflections. The maximum peak on the final difference map was 1.9 $e\cdot\AA^{-3}$, near the disordered ammonium-water chain. s = 2.80.

Because the Pbca cell for 5B resulted in ordered cation-water chains, but was otherwise packed similarly to 5C and the pyridine analogue, the ammonium salt was examined more carefully to check for a doubling of the a-axis (ie. the one week exposure precession photograph). Since the cation was involved in the scattering which caused the doubling, the odd-h Bragg spots were harder to detect for the lighter ammonium salt.

With proof of a doubled cell, the cell parameters were redetermined and the data for 5C were recollected, as described above. The coordinates for the atoms of 5B were used (replacing the N scattering curve for that of K) and the structure refined to R and R_ω values of 0.1482 and 0.0463. The final difference map was again very noisy in regions of

high electron density. It should be noted that for both 5B and 5C it was necessary to fix $U_{13} = U_{23} = 0$ for Br(4) to keep both Br(4) and Br(5) from refining to hyperbolic temperature factor tensors. N(1) of 5C was restricted to $U_{12} = U_{13} = U_{23} = 0$ for the same reason. The applied restrictions were borrowed from the corresponding atomic special positions in the Cmcm cell in order to retain some degree of anisotropy. The positional parameters and isotropic temperature factors for 5C are listed in Table 5.4. Selected interatomic distances and angles for both 5B and 5C are listed in Table 5.5. The cation geometries are normal and indistinguishable.

For comparison, the even-h data for 5B were used to do a structure calculation in Cmcm. The transformation from the Pbca cell to the higher symmetry C-centered cell is x' = 2x-0.25, y' = y+0.25, z' = z. After slight positional adjustments to fix all of the atoms on the previously described Cmcm mirror positions, the refined structure gave residuals R = 0.040 and R_ω = 0.043 with $\omega=(\sigma_F^2 + 0.0001F_o^2)^{-1}$, s=2.53 for 627 I 0 reflections. When the unadjusted positions were used, and occupancy factors modified to fit the resulting disorder, the refinement would not converge.

When the even-h data for 5B were used for refinement in Pbca, convergence was reached with R = 0.075 and R_ω = 0.049. Removal of the 257 non-zero even-h reflections with (0.5h + k) odd (systematically extinct with Cmcm symmetry) from the even-h data set caused divergence of the refinement

Table 5.4. Atomic positional parameters ($x10^3$) and temperature factors ($Å^2$)($x10^3$) for 5C (Pbca).

	x	y	z	U_{eq}
Pt	123.9(2)	405.74(3)	748.7(2)	23(3)
Br(1)	124.8(6)	288.08(8)	752.8(7)	40(1)
Br(2)	118.2(5)	411.7(2)	1042.2(4)	43(2)
Br(3)	138.5(4)	405.4(2)	454.7(4)	38(2)
Br(4)	-98.7(8)	415.5(3)	737.5(9)	21(3)
Br(5)	346.8(9)	402.5(4)	766(1)	49(5)
N(1)	111(3)	503.7(6)	739(4)	25(10)
N(2)	606(2)	800(1)	43(3)	57(17)
O	113(3)	673(1)	626(2)	62(14)

Table 5.5. Selected bond distances (Å) and angles (deg) for 5B and 5C.

	(5B)	(5C)		(5B)	(5C)		(5B)	(5C)
Pt-Br(1)	2.447(2)	2.433(2)	Pt-N,N(1)	2.11(2)	2.04(1)	K,N(2)···Br(1)^{iii}	3.60(1)	3.61(3)
Pt-Br(2)	2.422(3)	2.445(4)	Br(4)···Br(5)^{ii}	0.61(2)	0.67(1)	K,N(2)···Br(1)^{x}	3.63(1)	3.91(3)
Pt-Br(3)	2.460(3)	2.450(3)	O···Br(2)^{iii}	3.43(3)	3.54(3)	K,N(2)···Br(1)^{xi}	3.55(1)	3.54(3)
Pt-Br(4)	2.51(1)	2.494(9)	O···Br(3)^{iv}	3.46(3)	3.31(3)	K,N(2)···Br(2)^{xi}	3.58(1)	3.41(3)
Pt···Br(4)^{i}	3.04(1)	3.106(9)	O···K^{v},N(2)^{v} or K,N(2)···O^{vii}	2.74(2)	3.01(4)	K,N(2)···Br(3)^{ix}	3.51(1)	3.59(3)
Pt-Br(5)	2.48(1)	2.49(1)	O···K^{vi},N(2)^{vi} or K,N(2)···O^{viii}	2.79(2)	2.81(3)	K,N(2)···Br(4)^{xi}	3.51(1)	3.49(3)
Pt···Br(5)^{ii}	3.06(1)	3.10(1)	K,N(2)···Br(1)^{ix}	3.67(1)	3.90(3)	K,N(2)···Br(5)^{ix}	3.31(1)	3.38(3)

	(5B)	(5C)		(5B)	(5C)		(5B)	(5C)
Br(1)-Pt-Br(2)	91.4(2)	92.1(2)	Br(3)-Pt-Br(4)	90.9(2)	91.7(2)	Br(3)^{iv}···O···K^{v},N(2)^{v}	104.1(9)	108.2(9)
Br(1)-Pt-Br(3)	91.5(2)	90.6(2)	Br(3)-Pt-Br(5)	88.4(3)	89.5(3)	Br(3)^{iv}···O···K^{vi},N(2)^{vi}	110(1)	106(1)
Br(1)-Pt-Br(4)	93.8(3)	94.9(2)	Br(3)-Pt-N,N(1)	87.7(8)	88(1)	K^{v},N(2)^{v}···O···K^{vi},N(2)^{vi}	106.8(7)	106(1)
Br(1)-Pt-Br(5)	88.1(3)	88.1(3)	Br(4)-Pt-Br(5)	178.0(4)	176.7(3)	O^{vii}···K,N(2)···O^{viii}	137.9(7)	129(1)
Br(1)-Pt-N,N(1)	179(1)	176(1)	Br(4)-Pt-N,N(1)	85(1)	81.3(9)	O^{vii}···K,N(2)···Br(4)^{xi}	102.7(5)	105.3(7)
Br(2)-Pt-Br(3)	176.2(2)	176.4(2)	Br(5)-Pt-N,N(1)	93(1)	95.7(9)	O^{vii}···K,N(2)···Br(5)^{ix}	100.1(5)	101.1(7)
Br(2)-Pt-Br(4)	91.8(3)	90.4(2)	Br(2)···O···Br(3)^{iv}	115.4(6)	116.0(7)	O^{viii}···K,N(2)···Br(4)^{xi}	119.4(5)	125(1)
Br(2)-Pt-Br(5)	89.3(3)	88.2(3)	Br(2)···O···K^{v},N(2)^{v}	106.9(9)	111.6(9)	O^{viii}···K,N(2)···Br(5)^{ix}	121.6(5)	128(1)
Br(2)-Pt-N,N(1)	89.4(8)	89(1)	Br(2)···O···K^{vi},N(2)^{vi}	113(1)	108.5(9)	Br(4)^{xi}···K,N(2)···Br(5)^{ix}	9.8(3)	11.0(2)

Atoms are related to those in Tables 5.3 and 5.4 by: (i) ½+x,y,1½-z; (ii) x-½,y,1½-z; (iii) ½-x,1-y,z-½; (iv) -x,1-y,1-z; (v) x-½,y,½-z; (vi) x-½,1½-y,1-z; (vii) ½+x,y,½-z; (viii) ½+x,1½-y,1-z; (ix) 1-x,½+y,½-z; (x) 1-x,1-y,1-z; (xi) ½-x,½-y,z-1.

in the Pbca cell. The latter calculation was modeled after the data set (Cmcm) collected for the pyridine analogue, which would not converge in a refinement in Pbca (Britten, Faggiani, Gayowski, Harvey, Lock, Montgomery, Beauchamp, Layek, Theophanides (in press)).

The packing for 5B (analogous to 5C) in the Cmcm cell is shown in Figure 5.2. Figure 5.2(a) shows the Pt-Br chains parallel to **a**, with four chains cutting the **bc**-face. Both equivalent positions for the disordered Br (Br(4) and Br(5) in Pbca) are shown. Two symmetry equivalent Br atoms (Br(2) and Br(3) in Pbca) extend from the Pt atom in the plus and minus **c** directions. The final Br atom (Br(1) in Pbca) is trans to the nitrogen atom, bonding parallel to **b**. The ammines (or pyridines in the (py) analogue) are found in layers at $y = 0.25$ and $y = 0.75$. Disordered chains of water molecules and potassium (or ammonium) ions centered at $x = 0.0$, $y = 0.0$ and $x = 0.5$, $y = 0.5$ run parallel to **c**, binding adjacent layers of Pt-Br chains. These double-layers are hydrogen-bonded to each other via ammine-bromine interactions (negligible for the pyridine analogue). Figure 5.2(b) gives the view down the chain axis, showing the 'sinusoidal' K^+-OH_2 (NH_4^+-OH_2) chains disordered in the mirror plane.

Figure 5.3 is a stereo view of 5B through the **bc**-face of the Pbca cell. The major improvement is the ordering of the K-O chains. The disordered chains which were related by a two-fold axis in Cmcm are now related by a two-fold

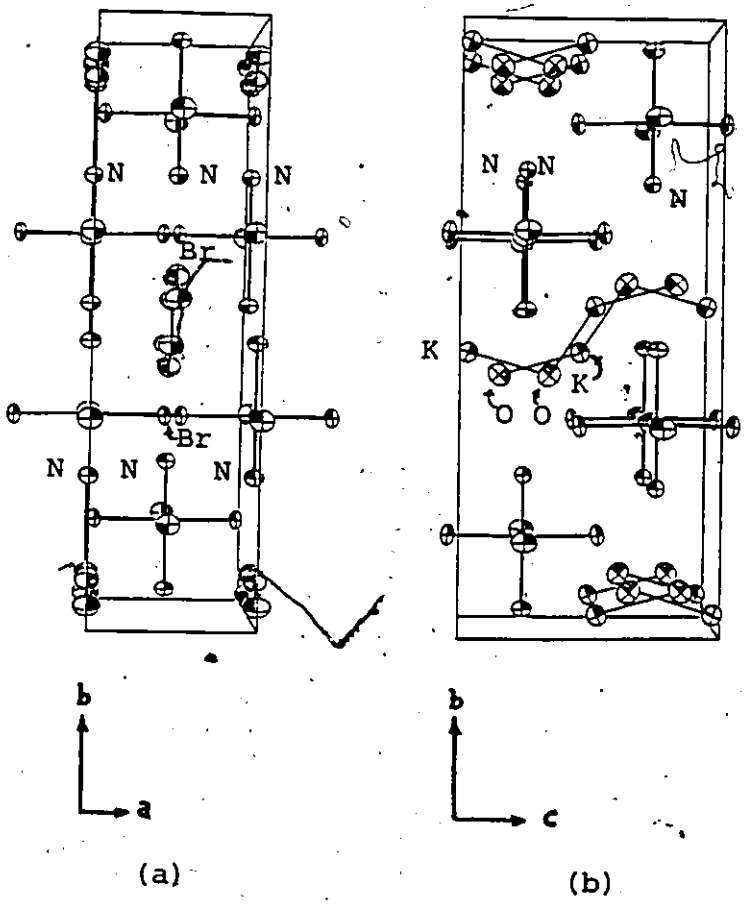

Figure 5.2. The unit cell contents for 5B with Cmcm symmetry. (a) the ab projection
(b) the bc projection

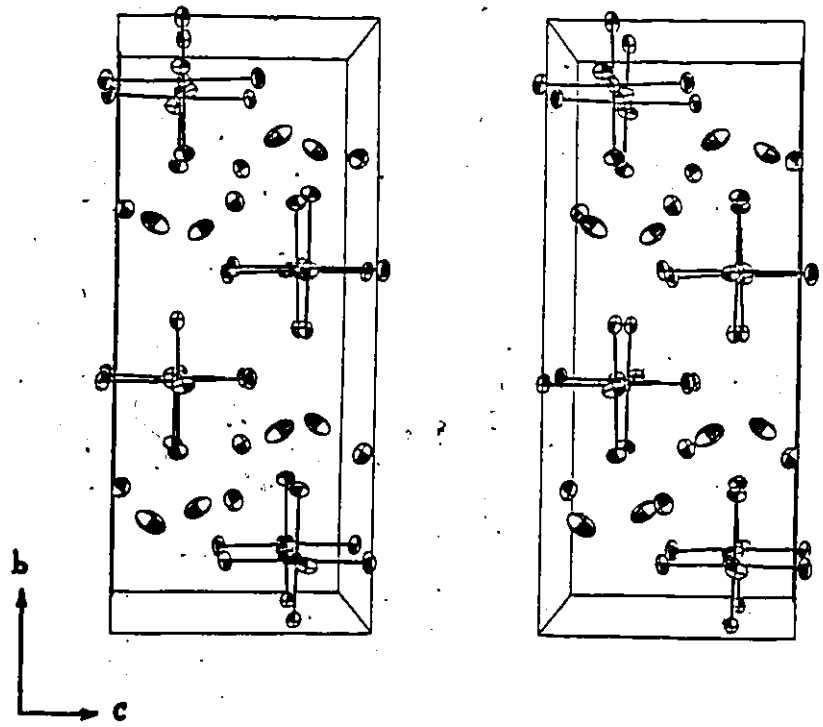

Figure 5.3. The unit cell contents for 5B (with Pbca symmetry)

screw axis. Another important change is that all atoms are now in general positions and no longer have any point-symmetry restrictions. The result is a noticeable twist in the Pt-Br chain.

Figure 5.4 shows this twist from another angle, and also illustrates the coordination of the water molecule and the cation. The oxygen atom is at the center of an approximate tetrahedron, with coulombic interactions to two cations and hydrogen-bonds to Br(2) and Br(3) on adjacent Pt's along a chain, holding the Br's at a separation of 5.816(4)Å for 5B and 5.809(5)Å for 5C. The cation is centered in a trigonal prism, made up of four Br(1)'s (from 2 chains, one in each layer) and an adjacent Br(2), Br(3) pair. The Br(2)-Br(3) distance in this case is 5.254(4)Å for 5B and 5.356(5)Å for 5C. The prism is face-capped by the disordered bridging Br atom and two water molecules. Again, this almost parallels what was found for the packing in Cmcm. However, the removal of the mirror planes revealed the true packing details, which explain why the cation/water chain is ordered. The different geometric requirements of the water molecule and cations for the Br(2)-Br(3) clips cause a twist along the Pt-Br chain, since these two Br atoms alternate along opposite sides of the chain. Thus information of packing order is transmitted along the **a** and **c** directions for double layers of Pt-Br chains (see schematic drawing, Figure 5.5. Br(1), Br(4), Br(5) and N have been omitted). These double layers are stacked in the

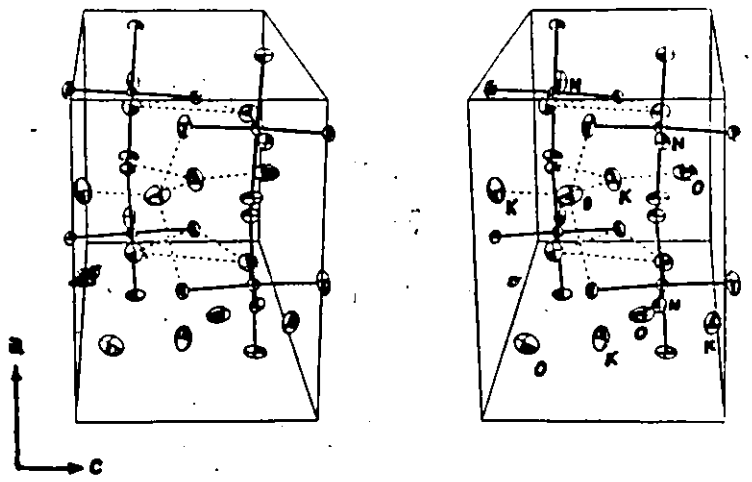

Figure 5.4., The water and cation coordination for 5B. The packing in 5C is similar.

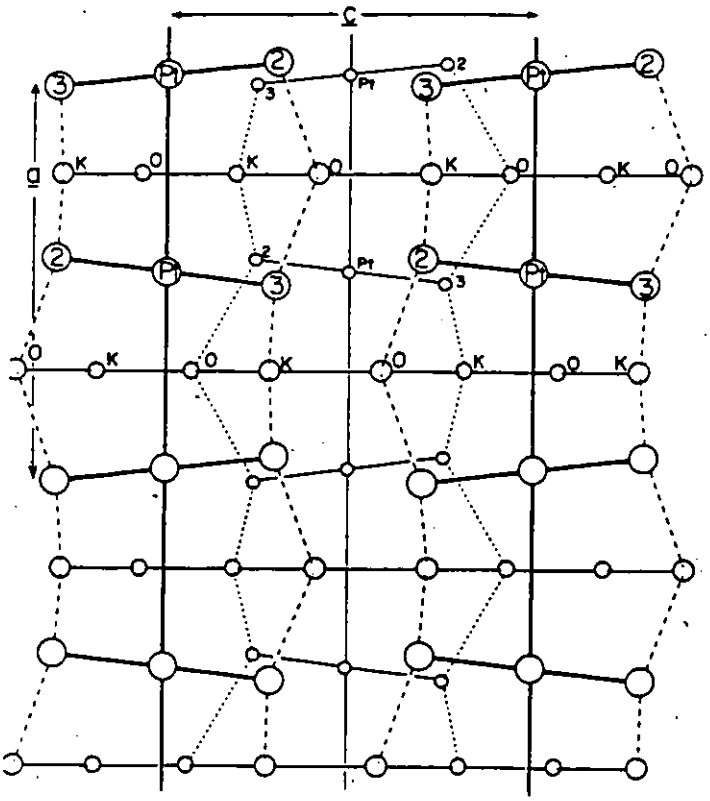

Figure 5.5. Schematic drawing showing the transmission of the packing twist in the **a** and **c** directions. (2 ≡ Br(2), 3 ≡ Br(3))

b direction (see Figure 5.3). They retain order relative to one another because packing information is transmitted at the interface by the ordered zig-zag rows of ammines via interaction with neighbouring Br's. These interactions are relatively weak, especially in the case of the pyridine analogue which has little, if any, hydrogen-bonding capacity (although steric factors may be important). This interface is a potential source of crystallographic disorder in these systems.

Table 5.6 illustrates the transformation from the (symmetrically bridged) Cmcm model to the final Pbca solution, and its effect on the F's for some of the odd-h data.

The packing differences between 5B and 5C are a result of the larger ionic radius of NH_4^+ relative to K^+ (1.48 vs 1.33Å, Pauling (1960)). The most important of these are the larger $Br(4)^{i}$, $Br(5)^{ii}$...Pt distances, the larger Br(2), Br(3) cation clip, and the longer cell axes for 5C.

5.4 Linear Platinum-Halide Chain Compounds: Order vs. Disorder

Mixed valence compounds have been grouped into three general classes, (Robin, Day (1967)). Class I includes compounds in which two oxidation states of the same metal exist in completely different environments, such that exchange is energetically forbidden. An example is $GaCl_2$, which has Ga(III) in a tetrahedral site, and Ga(I) in a dodecahedral site. Class II compounds are those which have two disting-

Table 5.6. Dependence of Odd-h Structure Factors on Ordering and Packing Twist for K salt in Pbca.

h k l	$F_{obs}(\sigma)$	F_{calc} A	B	C	D	E
3 4 1	93(2)	0	0	7	44	104
7 4 1	90(2)	0	0	17	6	89
3 5 1	121(2)	0	0	7	58	127
7 5 1	106(2)	0	0	20	41	109
1 7 1	95(2)	0	0	5	87	96
5 7 1	88(2)	0	0	15	43	90
5 2 3	87(2)	1	1	6	36	93
3 7 4	86(3)	0	0	9	27	92
5 0 6	111(3)	0	0	11	33	97
5 3 6	95(4)	0	0	10	25	85

A. No twist, disordered K-O, isotropic T, symmetric Br bridge.
B. No twist, disordered K-O, isotropic T, disordered Br bridge.
C. No twist, disordered K-O, anisotropic T.
D. No twist, ordered K-O.
E. Twist in Pt-Br chain. Final solution.

uishable but very similar sites, and exchange is possible. The Pt(II)...X-Pt(IV)-X...Pt(II)...X-Pt(IV)-X... compounds are of this type. Class III mixed valence solids have indistinguishable metal sites, but the chemical formulae indicate mixed valences (eg. $2\,K\cdot[Pt(CN)_4]\cdot(Br)_{0.3}\cdot 3H_2O$), which can often be represented by MO band theories.

The Pt(II,IV), X chain compounds exhibit some interesting optical and physical properties, which can be interpreted in terms of the packing of the molecules. Figure 5.6(a) shows a one dimensionally ordered (and chemically sensible) chain of PtL_4 and trans-PtX_2L_4 molecules, where r is the Pt(II)-Pt(IV) distance. For X = Cl, Br, I the (Pt(IV)-X/Pt(II)...X) distance ratios average 0.74, 0.83, 0.93, respectively (Keller, Keppler, Ledezma-Sanchez, Steiger (1981); Endres, Keller, Martin, Traeger, Novotny(1980);Matsumoto, Yamashita, Ueda, Kida (1978); Craven, Hall (1961); Beauchamp, Layek, Theophanides (1982a)). The ratio for 5A is 0.70, indicating a fairly weak Pt(II)...Cl interaction. This is a result of the crystal packing (see §5.2.1). For 5B the ratio for the Br(4) and Br(5) distances are 0.83 and 0.81 respectively. The corresponding values for 5C are 0.80 and 0.80; smaller because of the NH_4^+, K^+ radius difference.

These halogen bridged mixed oxide chains are responsible for the dark, metallic lustre of the Br and I compounds. Some Cl compounds are dark, while others are yellow or orange. The light ones, however show sharp dichroism. 5A, for example,

is bright yellow when incident polarized light is parallel to the chain axis, but colourless when the light is perpendicular. Compounds of this type also show anisotropic conductivity (300 times greater in the chain direction) and are pressure and temperature sensitive one-dimensional semiconductors (Clark (1980)). They have a strong absorbance around 23000 cm^{-1} which is attributed to electronic charge transfer between the metal atoms via the halogen, possibly from X to the empty p_z orbital of Pt(II). This accounts for the lustre, dichroism, and other anisotropic properties. Furthermore, the Pt(II)...X distances are close enough that a concerted symmetric stretch (planar) throughout the chain could result in an exchange of oxidation states (Figure 5.6(a)→(b)). This symmetric X-Pt(IV)-X (ν_1) vibration is used in resonance Raman studies. Excitation with a beam around 23000 cm^{-1}, polarized parallel to the chain axis, results in resonance enhancement of ν_1 (312±4, chlorides; 176±7, bromides; 123±8 cm^{-1}, iodides; Clark (1980); Papavassilion, Layek, Theophanides (1980)), thus verifying the charge transfer assignment in the visible spectra.

X-ray photoelectron spectra have been used to verify the fact that Pt(II) and Pt(IV) both exist in the crystals (Matsumoto et al. (1978)), as opposed to Pt(III). $4f^{5/2}$ and $4f^{7/2}$ binding energies clearly show the two oxidation states, with the Pt(IV), Pt(II) differences decreasing as the Pt(IV)-X/Pt(II)...X ratio increases. X-ray PES was attempted for 5A

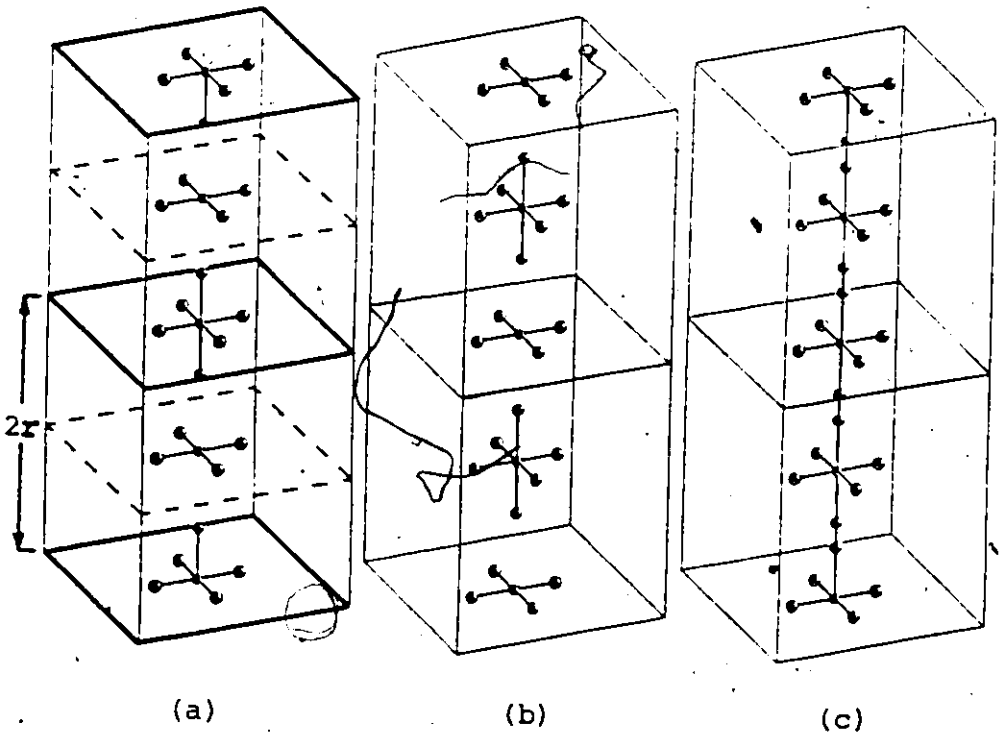

Figure 5.6. Order vs. disorder for halogen-bridged Pt(II), Pt(IV) chains.
(a) one-dimensionally ordered chain
(b) neighbouring chain shifted by r
(c) crystallographic disorder
(The Pt(II)-Pt(IV) distance is r)

(Tammy Chan, University of Western Ontario, London, Ontario, Canada) but good spectra were not obtained. This was likely because of the three (if not five) different environments of Pt(II).

A full review of mixed valence compounds is presented by D. B. Brown (1980).

Although X-ray crystallography has proven invaluable in explaining the properties of Pt(II,IV)-X chain compound, it has also shown that several types of packing disorder can exist in these crystals. The most common disorder occurs when equivalent chains in different cells have been randomly shifted by r along the chain axes (Figure 5.6(a) vs. Figure 5.6(b)). This could be a packing fault or it could arise from concerted halogen transfer from Pt(IV) to Pt(II), resulting in a switch in oxidation states. The crystallographic result is shown in Figure 5.6(c), where each of the disordered halogen atoms has half-occupancy. A consequence of this two dimensional disorder is a supercell with period 2r along the chain axis. Because there is periodicity in only one dimension, only one of the three Laue conditions (see Chapter 2) is met, and diffuse diffraction planes, rather than diffraction spots, are seen. The intensity for the diffuse diffraction is derived only from the asymmetrically bridging halogens, and is a function of halogen atomic number and the separation of the disordered positions. Thus Br gives more easily observed diffuse diffraction than either Cl or I,

since Cl is lighter and I forms a nearly symmetric bridge. Furthermore, the even diffuse layers (not the Bragg reflections) of the supercell are extinguished. For example, for any one chain with origin at Pt(IV) an odd indexed set of reflection planes contains the Pt(IV) atoms and has X's nearby (Figure 5.6(a), solid lines). Interleaving this set of planes is a set which is centered on Pt(II), and differs because of the greater distance to the halogen atoms (dashed lines). Thus an odd reflection is almost, but not quite, extinguished. Any even-indexed set of planes would contain both regions of electron density (solid and dashed lines), and the interleaving set would be identical, thus completely extinguishing it. This phenomenon was observed for 5B and 5C in the rotation photographs, proving that the chains are disordered relative to one another. For 5A, no diffuse lines were observed in a 10 d photograph, indicating (not proving) that the chains were three dimensionally ordered.

This type of disorder has resulted in some problems in interpreting crystallographic data. Three examples are noteworthy. In one iodine compound (example one) (Endres, Keller, Martin, Traeger, Novotny (1980)) the chains were found to be disordered, but no diffuse layer lines were observed. This was interpreted in terms of a breakdown of the one dimensional ordering of the chain, involving intermediate states of the (unlikely) type I-Pt...I, or rapid I exchange. It is very possible that a much longer exposure time for the

photograph is required (details were not given), as has been found in the case of bis(ethylenediamine)palladium(II) dichloro-bis(ethylenediamine)palladium(IV) tetraperchlorate (Beauchamp, Layek, Theophanides (1982b)). This disordered palladium structure has also been used to refute the claim that its Pt analogue (example two) is 3-dimensionally ordered with distinct Pt(II) and Pt(IV) sites (Matsumoto et al. (1978)). A close examination of the environment of the Cl atom in the $Pt(en)_2$ structure shows the closest oxygen (perchlorate) contact at 3.646 Å. The unoccupied disordered site is 3.71 Å from the nearest oxygen atom and the Pt(IV)-Cl/Pt(II)...Cl ratio of 0.75 suggests normal chain axial interactions. It seems, therefore, that there is no apparent reason for an ordered model. In the case of 5A, the bridging Cl has perchlorate contacts (closest) 3.81(2) Å, while the unoccupied Cl (on Pt(2)) site has 3.69(2) Å contacts. The distance ratio of 0.70 suggest weak interaction, and occupancy refinement reached 98% ordering. Thus for 5A the ordered state seems reasonable. It does, however, show a three dimensional disorder in that, 13% of the $[PtCl_2(NH_3)_4]^{2+}$ is replaced by $[Pt(NH_3)_4]^{2+}$.

An ordered structure has been reported for bis(1,2-diaminopropane)platinum(II,IV) tribromide (example three) (Endres, Keller, Martin, Nötzel (1980)). Although diffuse interleaving layer lines were observed in the rotation photograph, and the bridging Br was found to be unsymmetric and

disordered in the early stages of refinement (distance ratio = 0.89), the final solution is reported to have a symmetric Br bridge statistically distributed over four sites around the Pt-Pt midpoint: This indicates a Pt(III) structure with a Pt-Br bond length of 2.673(1) Å. Again, no reason for this anomaly is presented. The diffuse diffraction giving a super-cell is suggested to arise from ligand configuration, but no details are given.

Another type of disorder in systems involves the ligands. For example, the pyridine in the 5B analogue is disordered over two positions. The hydrogen atoms of the ammines in 5A, 5B, and 5C are likely disordered. This packing ambiguity thus has little effect on the physical properties of the system. The packing of counter-ions and lattice waters, however, may have some effect. The switch from Cmcm to Pbca on the basis of an ordered cation model revealed a non-linearity in the Pt(II,IV)-Br chain. This indicates that orbital overlap for charge transfer may not be ideal, nor are the chain vibrations. The problem is,therefore, slightly more complicated than was assumed. Thus from the crystallographer's point of view, it is very important to examine the diffuse layer-lines for evidence of Bragg reflections resulting from counter-ion ordering with the period of the supercell. Otherwise the imposition of the wrong symmetry restrictions may result in the loss of information.

CHAPTER 6

A MODEL COMPLEX OF A POSSIBLE CROSS-LINKING PRODUCT OF TRANS-$Pt(NH_3)_2^{2+}$ WITH CYTOSINE AND GUANINE

6.1 Introduction

The well established similarities and differences in the physiological activity between cis and trans-diammine platinum(II) coordination complexes have been outlined in Chapter 1. Both dichloro isomers bind to DNA, either by coordination to a single strand (the majority of lesions) or by interstrand crosslinking, and cause shortening, disruption of base stacking, and unwinding at high platinum binding levels. However, the cis complex is antitumor active and mutagenic, whereas the corresponding trans isomer is inactive and less mutagenic (Rosenberg (1980)). Another interesting difference is that at low Pt/nucleobase ratios, the thermal stabilities of DNA and synthetic double-stranded poly C·poly I are increased by trans-$Pt((NH_3)_2Cl_2$ but decreased by the cis analogue. The same experiment using [Pt(dien)Cl]Cl (3C) showed stabilization at very low ratios, then subsequent destabilization at higher doses (see Figure 6.1).

Various differences in the properties of the cis and trans isomers may be relevant to the observed physiological and chemical activity. The first one refers to the kinetics

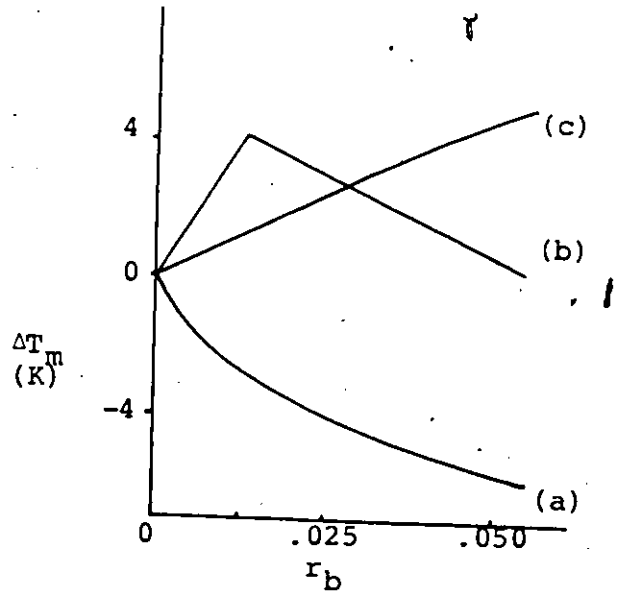

(Macquet, Butour, Johnson (1983))

Figure 6.1. The melting curve changes for DNA treated with

(a) cis-$PtCl_2(NH_3)_2$

(b) trans-$PtCl_2(NH_3)_2$

(c) [Pt(dien)Cl]Cl

(ΔT_m ≡ temperature change in melting point;

r_b = bound Pt/nucleobase)

of reaction: with the hydrolysis of the chloro complexes believed to be the rate-limiting step in the reaction with DNA, the difference in the rate of aquation (cis faster than trans , (Filipski, Kohn, Bonner (1980))) is noteworthy. A second one possibly related to the first, concerns the selectivity of both isomers for certain donor atoms in DNA. From model studies with mixtures of the four nucleotides of DNA it has become clear that cis and trans isomers exhibit somewhat different selectivities (Moller, Bruck, O'Connor, Armatis, Knolinski, Kottmair, Tobias (1980)). While the cis isomer appears to prefer guanine(N7) over any other base, the trans isomer also shows substantial reaction with adenine. Another remarkable feature of trans-$Pt(NH_3)_2Cl_2$ in this respect is the fact that it reacts with $tRNA^{Phe}$, despite a variety of potential donor atoms, in a monodentate fashion through the N7 site of guanine34, with the NH_3 groups acting as hydrogen donors in hydrogen-bonds with O6 of guanine and the oxygen atoms of the phosphate group (Jack, Ladner, Brown, Klug (1977)). These hydrogen-bonds can help stabilize the local geometry of the sugar-phosphate linkage in the RNA. A similar binding pattern with DNA (initial lesions are likely monodentate for both isomers), with hydrogen-bonding to the sugar-phosphate backbone by either t-$Pt(NH_3)_2^{2+}$ or $Pt(dien)^{2+}$, might be an explanation for the initial increase in thermal stability. A third major difference between the two isomers concerns the degree of distortion of the DNA secondary

structure on binding. This stereochemical aspect, possibly the most important, has been examined (Kistenmacher, Orbell, Marzilli (1983); Hitchcock, Lippert, Lock, Pratt (1983)) using the X-ray structural results of nucleobase complexes of cis- and trans- Pt(II) as models. In particular, the crystal structures of the bis(1-methylcytosine) (Orbell, Marzilli , Kistenmacher (1981); Faggiani, Lippert, Lock (1982); Lippert, Lock, Speranzini (1981b)) and bis(7,9-dimethylhypoxanthine) (Kistenmacher, Wilkowski, de Castro, Chiang, Marzilli (1979); Orbell, Wilkowski, Marzilli, Kistenmacher (1982)) complexes have been used for this purpose. A fourth possible explanation of the biological difference of the two isomers relates to the difference in the tumor cell's capacities to repair the different lesions (Roberts (1981)). Strictly speaking, this question comes back to the possibilities of different sites and modes of binding of the two isomers.

In this chapter is presented the preparation (by B. Lippert, Technische Universität München, FRG) and crystal structure of a complex containing the nucleobases 1-methylcytosine (1-MeC), and 9-ethylguanine (9-EtG), coordinated to the trans-$Pt(NH_3)_2^{2+}$ moiety: trans-$[Pt(NH_3)_2(1\text{-MeC})(9\text{-EtG})]^{2+}$. The results are compared with those of the respective cis-complex (Faggiani, Lippert, Lock, Speranzini (1982)), and the possible relevance of cytosine, guanine cross-linking in DNA will be discussed (§ 6.4). First, the structure of its

laboratory precursor is examined.

6.2 Chloro-trans-diammine (1-methylcytosine)platinum(II) Chloride Sesquihydrate, 6A

Trans-$Pt(NH_3)_2Cl_2$, prepared as described by Kauffman and Cowan (1963), was reacted with one equivalent of 1-MeC to give trans-$[Pt(NH_3)_2(1\text{-}MeC)Cl]\cdot Cl\cdot 1.5H_2O$, 6A, among other products. The colorless crystals of 6A decomposed to a white powder when cleaved or dried in air. A spherically-shaped crystal was sealed in a 0.2 mm capillary and used for data collection.

6.2.1 Crystal structure of 6A

trans-$[Pt(NH_3)_2(C_5H_7N_3O)Cl]\cdot Cl\cdot 1.5H_2O$, $C_5H_{13}ClN_5OPt^+\cdot Cl^-\cdot 1.5H_2O$; 452.21 $g\cdot mol^{-1}$; $P2_1/c$; Syntex $P2_1$ diffractometer; 15 refl. ($21^\circ<2\theta<35^\circ$) for cell; a=10.085(2), b=9.169(2), c=28.865(4)Å, β=99.83(1)°, V=2629.9(8)$Å^3$, Z=8; D_x=2.28, D_m=2.29$g\cdot cm^{-3}$ in $CHCl_3/CHBr_3$; $2\theta_{max}=55^\circ$, +h, +k, ±l; N_{meas}= 6381, min R_{scan}=3.66deg·min^{-1}; 22°C; standards: -1 2 1(1.5%), 1 0 4 (1.2%); Bond abs. corr, μ=106.7cm^{-1}, sphere, r=0.091 mm, $3.8 < A^*_\theta < 4.1$; N_{unique}=6043, N_{used}=5313; NP=281; F(000)= 1704, $\omega=\sigma^{-2}$, s= 2.34 , g(SHELX)=0.00012; max shift/error(ave)= 0.43 (0.07), R=0.101, R_ω=0.063; Diff. map: -0.8, 1.3e·$Å^{-3}$, both near PtA ; XRAY76, SHELX, NRC-22, ORTEP-II.

The coordinates of the two independent Pt atoms were found from a three-dimensional Patterson map. The remaining non-hydrogen atoms were located using electron density

difference methods. No hydrogen atoms in refinable positions were found. All atoms were given anisotropic temperature factors. A ψ-scan of the crystal was performed, but not used for the final data set. The ψ-scan correction brought equivalent reflections to slightly better agreement (averaging residual = 0.0702 vs. 0.0759), but this included only the 0 k $\pm$1 set for the data collected. Removal of the ψ-correction improved R and R_w by 0.005 for the refined structure. This check was made because data from a crystal of spherical shape should not require an empirical absorption correction. The A^*_θ correction made an improvement of only 0.001 in the residuals.

The cis analogue of this compound is currently being investigated in our lab, and it too shows a fairly high R-factor (Britten, Lippert, Lock, Speranzini). Low temperature data may have to be taken to improve the results for these two compounds. The final atomic parameters are listed in Table 6.1, and selected bond lengths and angles are given in Table 6.2.

The molecular cation (A) is illustrated in Figure 6.2. The chloro ligand is trans to the N(3)A atom of the planar 1-MeC ligand. The interatomic distances and bond angles are normal, although C(2)A-N(3)A [1.42(2)Å] and N(3)A-C(4)A [1.42(1)] are 3.2σ and 3.8σ, respectively, longer than the standard neutral cytosine residue values (Taylor, Kennard (1982)). The ligand-square-plane/ring dihedral angle

Table 6.1. Atomic positional parameters ($x10^3$) and temperature factors (A^2)($x10^2$) for 6A

	x	y	z	U_{eq} or U_{iso}*
PtA	417.28(6)	391.85(7)	245.76(3)	2.46(4)
Cl(1)A	198.7(4)	377.1(7)	256.8(2)	4.5(3)
N(2)A	361(2)	330(2)	177.5(6)	4(1)
N(5)A	468(1)	448(2)	314.4(6)	3.3(5)*
N(1)A	756(1)	532(2)	188.4(6)	3.3(9)
C(2)A	626(2)	521(2)	198.6(7)	2.5(9)
N(3)A	607(1)	421(1)	234.7(7)	2.4(3)*
C(4)A	711(2)	326(2)	254.9(7)	2.4(4)*
C(5)A	846(2)	359(2)	245.3(6)	4(1)
C(6)A	863(2)	451(2)	211.7(7)	3(1)
C(1)A	771(2)	633(2)	149.5(7)	4(1)
O(2)A	533(1)	589(1)	179.3(4)	3.0(7)
N(4)A	691(1)	232(1)	287.0(5)	3.0(9)
PtB	638.84(6)	371.82(8)	429.56(2)	2.47(4)
Cl(1)B	424.0(5)	329.2(6)	443.3(2)	4.0(3)
N(2)B	645(1)	154(2)	410.2(6)	4.0(9)
N(5)B	618(1)	586(1)	446.4(5)	2.9(8)
N(1)B	979(2)	523(2)	373.8(6)	3.3(9)
C(2)B	845(2)	491(2)	379.6(7)	3(1)
N(3)B	833(1)	414(1)	417.6(5)	2.8(8)
C(4)B	939(2)	360(2)	451.0(7)	4(1)
C(5)B	1075(2)	384(2)	441.7(8)	5(1)
C(6)B	1085(2)	470(2)	402.4(7)	3(1)
C(1)B	995(2)	619(2)	334.8(7)	4(1)
O(2)B	750(1)	537(1)	351.7(4)	3.3(8)
N(4)B	915(2)	283(2)	488.2(6)	5(1)
Cl(2)	373.4(5)	732.8(6)	372.8(2)	4.9(3)
Cl(3)	95.7(5)	528.8(6)	127.8(2)	4.6(3)
O(W1)	162(1)	311(1)	50.3(6)	5(1)
O(W2)	177(2)	867(2)	433.0(5)	7(1)
O(W3)	320(2)	467(2)	-1.0(7)	9(1)

Table 6.2. Selected interatomic distances (Å) and angles (deg) for 6A

bonds

	A	B		A	B
Pt-Cl(1)	2.284(5)	2.302(5)	C(4)-C(5)	1.46(3)	1.45(3)
Pt-N(2)	2.04(2)	2.07(1)	C(5)-C(6)	1.32(3)	1.40(3)
Pt-N(5)	2.03(1)	2.04(1)	C(6)-N(1)	1.38(2)	1.33(2)
Pt-N(3)	2.01(1)	2.08(1)	N(1)-C(1)	1.49(3)	1.46(3)
N(1)-C(2)	1.40(2)	1.42(3)	C(2)-O(2)	1.18(2)	1.22(2)
C(2)-N(3)	1.42(2)	1.34(2)	C(4)-O(2)	1.31(2)	1.34(3)
N(3)-C(4)	1.41(3)	1.40(2)			

possible hydrogen-bonds

N(2)A...O(2)B^{i}	2.98(2)	N(2)B...O(2)A^{i}	2.94(2)
N(2)A...Cl(3)	3.35(2)	N(2)B...O(W3)^{i}	3.10(2)
N(2)A...Cl(2)^{i}	3.38(2)	N(2)B...Cl(3)^{i}	3.22(2)
N(5)A...O(2)B	2.98(2)	N(5)B...O(W1)^{iii}	3.02(2)
N(5)A...Cl(2)	3.33(2)	N(5)B...Cl(1)B^{iv}	3.37(2)
N(4)A...O(2)A^{i}	2.92(2)	N(5)B...Cl(2)	3.26(1)
N(4)A...Cl(3)^{i}	3.52(1)	N(4)B...O(W1)^{v}	2.94(2)
O(W1)...O(W3)	2.75(3)	N(4)B...O(W2)^{iv}	2.94(2)
O(W1)...Cl(3)	3.16(2)	O(W3)...O(W2)^{vi}	2.67(2)
O(W2)...Cl(2)	3.11(2)	O(W3)...Cl(1)B^{vii}	3.41(2)
O(W2)...Cl(3)^{ii}	3.34(2)		

angles

	A	B
Cl(1)-Pt-N(2)	90.1(5)	87.4(4)
Cl(1)-Pt-N(5)	88.0(5)	89.1(4)
Cl(1)-Pt-N(3)	175.6(4)	179.1(3)
N(2)-Pt-N(5)	177.7(7)	175.7(5)
N(2)-Pt-N(3)	90.0(6)	93.5(6)
N(5)-Pt-N(3)	92.1(6)	90.0(5)
C(6)-N(1)-C(2)	123(2)	122(2)
C(6)-N(1)-C(1)	122(2)	121(2)
C(1)-N(1)-C(2)	115(1)	117(1)
N(1)-C(2)-N(3)	116(1)	116(2)
N(1)-C(2)-O(2)	124(2)	121(2)
O(2)-C(2)-N(3)	120(2)	124(2)
C(2)-N(3)-C(4)	121(1)	126(2)
C(2)-N(3)-Pt	117(1)	117(1)
Pt-N(3)-C(4)	121(1)	117(1)
N(3)-C(4)-C(5)	117(2)	117(2)
N(3)-C(4)-N(4)	120(2)	121(2)

Table 6.2. (continued)

	A	B
N(4)-C(4)-C(5)	122(2)	122(2)
C(4)-C(5)-C(6)	120(2)	116(2)
C(5)-C(6)-N(1)	121(2)	123(2)

Atoms are related to those in Table 6.1 by:
(i) 1-x, y-½, ½-z; (ii) -x, ½+y, ½-z; (iii) 1-x, ½+y, ½-z;
(iv) 1-x, 1-y, 1-z; (v) 1+x, ½-y, ½+z; (vi) x, 1½-y, z-½;
(vii) x, ½-y, z-½.

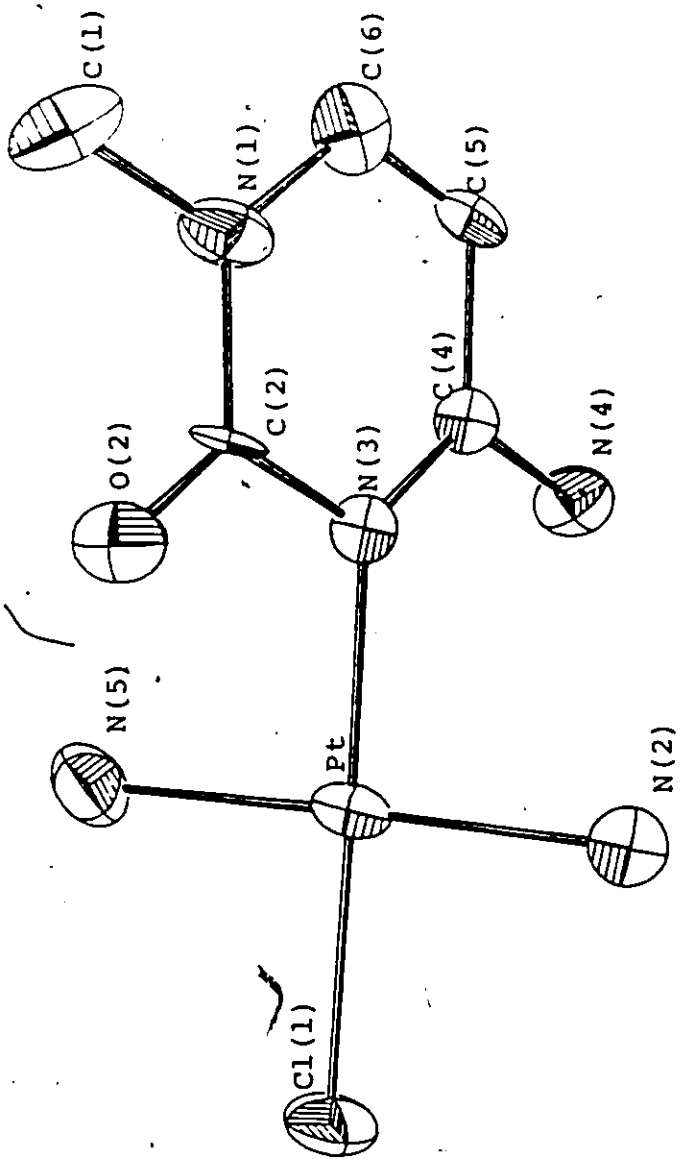

Figure 6.2. The molecular cation (A) of 6A

is 61.1(5)°; lower than observed for 3E and lower than the ranges previuosly observed (63°-79°, Kistenmacher, Orbell, Marzilli (1983), for bis(base) complexes; 64.4°-89.1°, Lippert, Lock, Speranzini (1981ab) and 3E, for monobase) for pyrimidine ligands. The symmetry independent cation (B) of 6A is almost identical to cation A. The only differences are found in the interligand angles Cl(1)B-PtB-N(2)B, -4.2σ, Cl(1)B-PtB-N(3)B, $+7.0\sigma$, and N(2)B-PtB-N(3)B, $+4.1\sigma$; and the square plane-ring dihedral angle [71.4(5)° for B]. The variation in dihedral angle is likely a result of intermolecular hydrogen-bonding for these two cations.

The packing diagram (Figure 6.3) shows stacks of A cations spiraling down the 2_1 axes at (0.5, y, 0.25) and (0.5, y, 0.75), with the square planes 16.2(5)° from the axes. They are directly hydrogen-bonded along the column by N(4)A...O(2)A^{i} contacts [2.92(2)Å]. There are no π-π interactions. The B cations stack on either side of each A cation stack, but the B-B separation along **b** is the full 9.169 Å. O(2)B atoms form hydrogen-bond bridges between alternate A cations via N(5)A and N(2)A links. The N(2)B ammines are also hydrogen-bonded to the O(2)A atoms. This bundle of three stacks is further stabilized by the chloride ions, Cl(2) and Cl(3). There is one contact linking these bundles in the **c** direction: the N(5)B...Cl(1)B^{iv} hydrogen-bond [3.37(3)Å].

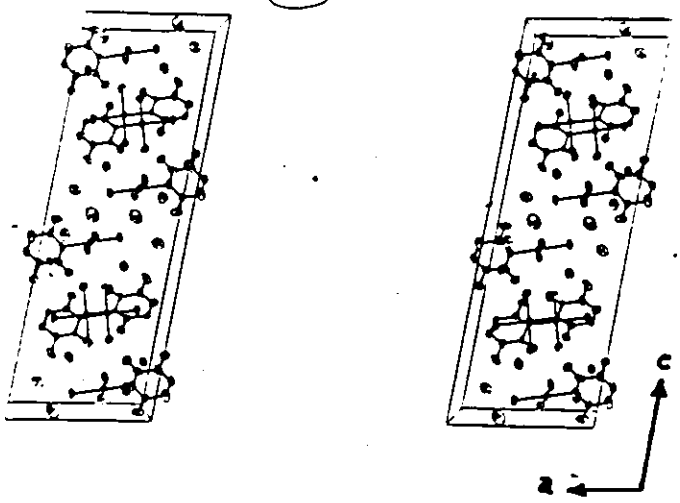

Figure 6.3. The contents of the unit cell for 6A

The three symmetry independent water molecules (O(W1) O(W2), and O(W3)) serve to stabilize the crystal lattice in the **a** and **c** directions. Each one is surrounded by an approximate tetrahedron consisting of two proton donors and two proton acceptors. The important role played by these water molecules in holding the crystal together explains the decomposition of the crystals in air, and lends credence to the hope that low temperature data will result in an improvement in the structure determination.

Although the structure of the cis analogue of 6A is not yet available, the crystal structures of two forms of the anhydrous nitrate salt of chloro-cis-diammine(1-MeC)-platinum(II) have been published (Lippert, Lock, Speranzini (1981a). As with 6A, no significant intramolecular hydrogen-bonding was observed. The crystal packing, of course, was completely different. The range of Pt-N and Pt-Cl bond lengths and their errors do not allow any discussion of the possible structural trans influence of the nucleobase ligands (Orbell, Wilkowski, Marzilli, Kistenmacher (1982)).

6.3 trans-Diammine(9-ethylguanine-N^7)(1-methylcytosine-N^3)-platinum(II) Diperchlorate Hydrate, 6B.

Lippert reacted a 0.03 M solution of 6A with two equivalents of $AgClO_4 \cdot H_2O$ and one equivalent of 9-EtG (24 h, 40°C), filtered the AgCl, and crystallized the colorless product at 50°-80°C (pH 5) with a 65% yield. The crystals decompose in air. X-ray and elemental analyses revealed the

structure trans-$[Pt(NH_3)_2(9\text{-EtG})(1\text{-MeC})]\cdot(ClO_4)_2\cdot 1.4H_2O$, 6B. (Analysis: Found: C, 18.8; H, 3.4; N, 18.6; O, 24.4%. Calculated: C, 19.0; H, 3.3; N, 18.5; O, 24.1%).

6.3.1 The Crystal Structure of 6B

trans-$[Pt(NH_3)_2(C_7H_9N_5O)(C_5H_7N_3O)]\cdot(ClO_4)\cdot 1.4H_2O$, $C_{12}H_{22}N_{10}O_2Pt^{2+}\cdot 2ClO_4^-\cdot 1.4H_2O$; 757.58g·mol^{-1}; $P2_1/c$; Syntex $P2_1$ diffractometer; 15 refl. ($18.9°<2\theta<31.3°$) for cell; a=13.988(2), b=12.040(4), c=15.752(3)Å, β=112.24(1)°, V=2455.5(9)Å^3, Z=4; D_x=2.05, D_m=2.05g·cm^{-3} in $CHCl_3/CHBr_3$; $2\theta_{max}$=55°, +h, +k, ±l; N_{meas}=5898, min R_{scan}=2.44deg·min^{-1}; 22°C; standards: 6 0 2 (2.04%), 2 - -8 (1.76%); Psi scan; Bond abs. corr., μ=57.5cm^{-1}, ground cylinder, r=0.085mm, l=0.42mm, not applied ; N_{unique}=5674, N_{used}=5072; NP=307; F(000)=1479, $\omega=(\sigma^2 + 0.0007F_o^2)^{-1}$, s=undet., g(SHELX)=-0.00031; max shift/error(ave)=0.411(0.042), R=0.063, R_ω=0.056; Diff. map: -1.0, 1.1e·Å^{-3}, both near Pt; PSI, XRAY76, SHELX, NRC-22, ORTEP-II.

— The platinum atom position was chosen after examination of the three-dimensional Patterson map. Electron density difference syntheses revealed the positions of all remaining non-hydrogen atoms. However, the refinement residual remained at .27 and purine and pyrimidine ring geometries were far from ideal. The atom positions were then shifted to (x, y+0.5, z+0.25), which gave the same gross packing features, but molecules previously related by a 2_1 axis were then related

by an inversion center, and vice versa. This had the effect of altering the relative orientation of the ethyl groups, removing a slight disorder of the ammines, and significantly changing the dihedral angles between molecules centered near the bc-face. The refinement residual dropped to 0.08. The necessity of a similar shift as a result of ligand orientation has previously been noted (Zvagulis (1980)) for this space group.

In the remaining refinement cycles the Pt, O, and N atoms were given anisotropic temperature factors. Eleven positionally refinable hydrogen atoms were found from the difference syntheses. The water molecules were found to be disordered, and packing considerations (discussed below) permitted nonstoichiometry of the water. The independently refined water occupancies gave a Pt:water ratio of 1:1.4, using a common isotropic temperature factor for all fractional O atoms. This brought the calculated density into better agreement with the measured density. The atom parameters for the non-hydrogen atoms are listed in Table 6.3.

The molecular cation of 6B is illustrated in Figure 6.4 and selected interatomic distances and angles are given in Table 6.4. The bond lengths and angles involving the platinum atom are within the ranges previously observed (Lippert, Lock, Speranzini 1981ab); Faggiani, Lippert, Lock, Speranzini (1981, 1982); Faggiani, Lock, Pollock, Rosenberg, Turner (1981); Lock, Speranzini, Zvagulis (1980)) with the

Table 6.3. Atomic Positional Parameters ($x10^4$) and Isotropic Temperature Factors (A^2) ($x10^3$) for 6B

	x	y	z	U_{iso} or U_{eq}*
Pt	-172.3(2)	7585.8(2)	3480.7(2)	30.5(2)*
N(5)	-280(6)	7421(6)	2154(5)	50(4)*
N(6)	-32(5)	7737(6)	4829(5)	48(4)*
N(1)	2406(5)	10487(5)	4620(5)	36(4)*
C(2)	3424(6)	10221(6)	4819(5)	39(2)
N(3)	3732(4)	9211(5)	4717(4)	35(3)*
C(4)	2940(5)	8492(5)	4407(5)	30(1)
C(5)	1910(5)	8691(6)	4176(5)	33(2)
C(6)	1566(6)	9792(6)	4280(5)	40(2)
N(7)	1360(4)	7702(5)	3902(4)	34(3)*
C(8)	2072(6)	6931(6)	3989(5)	35(2)
N(9)	3024(4)	7358(5)	4287(4)	31(3)*
N(2)	4107(6)	11047(6)	5107(7)	57(5)*
O(6)	686(4)	10135(5)	4131(5)	51(4)*
C(9)	3971(7)	6719(7)	4475(6)	43(2)
C(10)	4540(9)	6516(10)	5486(8)	61(3)
O(W1)+	200(41)	-555(33)	1069(33)	117(6)
O(W2)+	-75(23)	-198(24)	1782(22)	117(6)
O(W3)+	278(22)	-339(22)	326(21)	117(6)
O(W4)+	687(42)	-838(33)	1372(30)	117(6)
N(1)'	-3336(5)	6664(6)	2606(5)	46(4)*
C(2)'	-2284(6)	6642(6)	2752(6)	42(2)
N(3)'	-1737(4)	7613(5)	3066(4)	36(3)*
C(4)'	-2219(6)	8563(6)	3119(6)	43(2)
C(5)'	-3298(7)	8578(7)	2933(6)	52(2)
C(6)'	-3795(7)	7624(7)	2698(6)	48(2)
C(1)'	-3920(9)	5595(8)	2346(7)	69(3)
O(2)'	-1881(5)	5806(5)	2625(5)	57(4)*
N(4)'	-1638(7)	9484(6)	3378(7)	54(5)*
Cl(1)	2781(2)	7690(2)	6786(1)	49(1)*
O(11)	2353(7)	7007(7)	5997(5)	80(6)*
O(12)	1973(7)	8043(8)	7068(6)	95(7)*
O(13)	3560(7)	7111(8)	7493(6)	92(6)*
O(14)	3230(8)	8660(6)	6553(7)	96(7)*
Cl(2)	-2564(2)	6272(2)	5158(2)	46(1)*
O(21)	-1953(6)	7214(5)	5149(6)	67(5)*
O(22)	-3635(5)	6524(7)	4603(6)	80(6)*
O(23)	-2250(7)	5388(7)	4743(7)	94(7)*
O(24)	-2409(10)	5986(10)	6054(7)	131(9)*

+The site occupancy factors for the water oxygen atoms were refined: O(W1), 0.36(4); O(W2), 0.34(2); O(W3), 0.37(2), O(W4), 0.33(4).

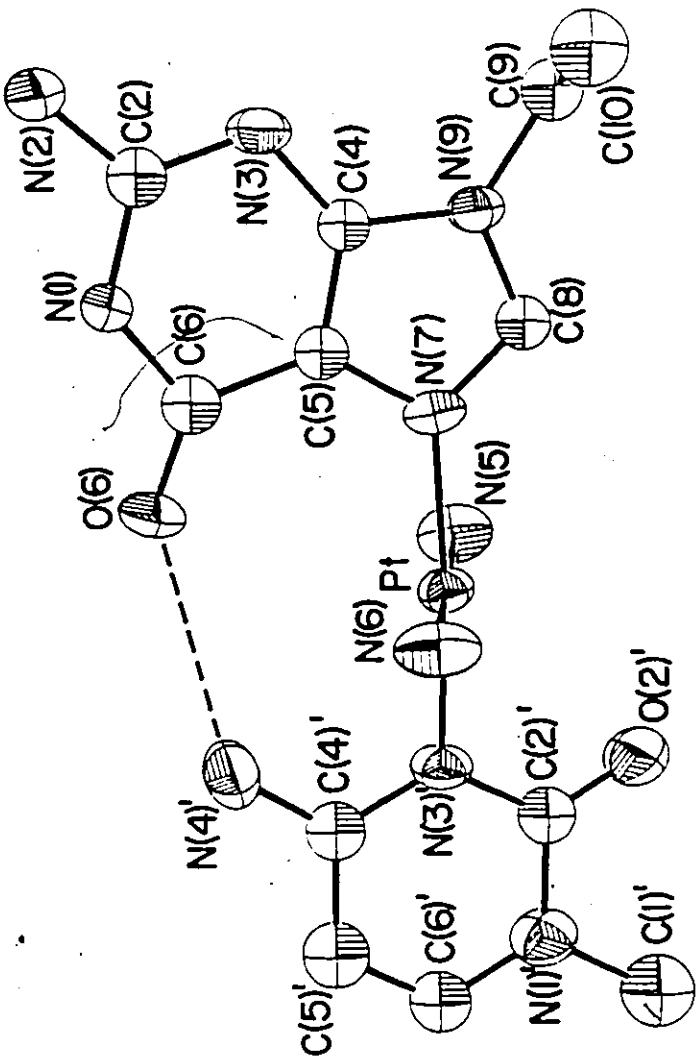

Figure 6.4. The molecular cation of 6B showing the intramolecular hydrogen-bond

Table 6.4. Selected bond distances (Å) and angles (deg) for 6B.

Bond Lengths

Pt-N(5)	2.047(8)	C(6)-N(1)	1.38(1)	N(1)'-C(2)'	1.40(1)	Cl(1)-O(11)
Pt-N(6)	2.066(7)	C(5)-N(7)	1.394(9)	C(2)'-N(3)'	1.38(1)	Cl(1)-O(12)
Pt-N(3)'	2.034(6)	N(7)-C(8)	1.33(1)	N(3)'-C(4)'	1.35(1)	Cl(1)-O(13)
Pt-N(7)	1.995(6)	C(8)-N(9)	1.336(9)	C(4)'-C(5)'	1.43(1)	Cl(1)-O(14)
N(1)-C(2)	1.38(1)	N(9)-C(4)	1.391(9)	C(5)'-C(6)'	1.32(1)	Cl(2)-O(21)
C(2)-N(3)	1.32(1)	N(9)-C(9)	1.33(1)	C(6)'-N(1)'	1.34(1)	Cl(2)-O(22)
N(3)-C(4)	1.344(9)	O(6)-C(6)	1.23(1)	C(1')-N(1)'	1.50(1)	Cl(2)-O(23)
C(4)-C(5)	1.37(1)	C(9)-N(9)	1.46(1)	O(2')-C(2)'	1.21(1)	Cl(2)-O(24)
C(5)-C(6)	1.44(1)	C(10)-C(9)	1.51(1)	N(4')-C(4)'	1.34(1)	

Possible Hydrogen-bond Lengths

$N(5)-O(12)^{i}$	3.25(1)	O(6)-N(4)'	3.11(1)	$O(W1)-O(23)^{v}$	3.28(5)	$O(W3)-O(23)^{vi}$	2.93(4)
$N(5)-O(21)^{i}$	3.17(1)	$N(4')-O(12)^{ii}$	3.05(1)	$O(W2)-N(5)^{iv}$	2.96(3)	$O(W4)-N(5)^{iv}$	3.00(5)
N(6)-O(11)	3.26(1)	$N(4')-O(14)^{ii}$	3.19(1)	$O(W2)-O(2')^{vi}$	2.81(3)	O(W4)-N(6)^{v}	3.21(4)
N(6)-O(21)	2.98(1)	$O(W1)-N(5)^{iv}$	3.19(5)	$O(W2)-O(24)^{v}$	3.17(3)	$O(W4)-O(2')^{vi}$	2.68(4)
$N(1)-O(21)^{ii}$	2.893(9)	$O(W1)-N(6)^{v}$	3.22(5)	$O(W2)-O(W3)^{vii}$	3.29(5)	O(W4)-O(11)^{v}	2.97(6)
$N(3)-N(2)^{iii}$	2.95(1)	$O(W1)-O(2')^{vi}$	2.96(4)	O(W2)-O(W3)	2.53(5)	O(W4)-O(12)^{v}	3.16(4)
$N(2)-O(22)^{ii}$	3.07(1)			$O(W3)-N(6)^{v}$	2.98(3)		

Bond Angles

N(5)-Pt-N(6)	178.7(3)	C(5)-C(6)-O(6)	129.7(7)	Pt-N(3)'-C(4)'	119.8(5)
N(5)-Pt-N(7)	90.1(3)	O(6)-C(6)-N(1)	121.0(7)	N(3)'-C(4)'-C(5)'	121.0(7)
N(5)-Pt-N(3)'	91.1(3)	C(5)-N(7)-C(8)	105.1(6)	N(3)'-C(4)'-N(4')	117.5(8)
N(6)-Pt-N(7)	88.8(3)	C(5)-N(7)-Pt	124.1(5)	N(4')-C(4)'-C(5)'	121.5(8)
N(6)-Pt-N(3)'	90.0(3)	Pt-N(7)-C(8)	130.8(5)	C(4)'-C(5)'-C(6)'	116.7(9)
N(7)-Pt-N(3)'	175.0(2)	N(7)-C(8)-N(9)	112.1(6)	C(5)'-C(6)'-N(1)'	123.5(9)
C(6)-N(1)-C(2)	127.3(7)	C(8)-N(9)-C(4)	107.4(6)	O(11)-Cl(1)-O(12)	108.9(5)
N(1)-C(2)-N(3)	123.0(7)	C(8)-N(9)-C(9)	125.2(6)	O(11)-Cl(1)-O(13)	110.4(5)
N(1)-C(2)-N(2)	116.8(7)	C(9)-N(9)-C(4)	127.3(6)	O(11)-Cl(1)-O(14)	109.1(6)
N(2)-C(2)-N(3)	120.2(8)	N(9)-C(9)-C(10)	112.3(9)	O(12)-Cl(1)-O(13)	111.5(6)
C(2)-N(3)-C(4)	112.1(6)	C(6)'-N(1)'-C(2)'	120.6(7)	O(12)-Cl(1)-O(14)	108.2(6)
N(3)-C(4)-C(5)	128.7(6)	C(6)'-N(1)'-C(1')	122.1(8)	O(13)-Cl(1)-O(14)	108.7(6)
N(3)-C(4)-N(9)	125.6(6)	C(1')-N(1)'-C(2)'	117.3(8)	O(21)-Cl(2)-O(22)	108.3(5)
N(9)-C(4)-C(5)	105.7(6)	N(1)'-C(2)'-N(3)'	116.6(7)	O(21)-Cl(2)-O(23)	107.8(6)
C(4)-C(5)-C(6)	119.6(6)	N(1)'-C(2)'-O(2')	121.1(7)	O(21)-Cl(2)-O(24)	110.1(6)
C(4)-C(5)-N(7)	109.6(6)	O(2')-C(2)'-N(3)'	122.3(8)	O(22)-Cl(2)-O(23)	108.2(5)
N(7)-C(5)-C(6)	130.7(7)	C(2')-N(3)'-C(4)'	121.2(7)	O(22)-Cl(2)-O(24)	113.1(7)
C(5)-C(6)-N(1)	109.4(7)	C(2')-N(3)'-Pt	118.9(5)	O(23)-Cl(2)-O(24)	109.3(7)

Atoms are related to those in Table 6.3 by:
(i) x, 1½-y, -½+z; (ii) -x, 2-y, 1-z; (iii) 1-x, 2-y, 1-z;
(iv) x, -1+y, z; (v) x, ½-y, -½+z; (vi) -x, -½+y, ½-z;
(vii) -x, -y, -z.

N(7)-Pt-N(3)' angle [175.0(2)°] at the lower end of the range. The G and C planes are 73.8° and 71.8° respectively from the Pt coordination plane. The bond lengths and angles of the cytosine and guanine ligands do not differ significantly from those for the standard (Taylor, Kennard (1982)) neutral nucleic acid base residues except for C(8)-N(9), -3.9σ; C(6)-N(1)-C(2), +3.3σ; C(5)-C(6)-N(1), -3.2σ; and N(1)'-C(2)'-N(3)', -3.2σ. Greater deviations are seen in the bond angles relative to the standard protonated (N7 for G and N3 for C) residues: C(5)-N(7)-C(8), -4.6σ; N(7)-C(8)-N(9), +4.3σ; N(1)'-C(2)'-O(2)', -3.3σ; C(2)'-N(3)'-C(4)', -5.4σ; and N(3)'-C(4)'-C(5)', +4.8σ. This difference in the effects of platination and protonation on nucleic acid base geometry has been observed previously (Faggiani, Lippert, Lock (1982)), although not for 6A. The dihedral angle between the pyrimidine and imidazole rings of the guanine ligand is 3.2°. The perchlorate geometry is normal.

An interesting feature of the trans-$[Pt(NH_3)_2(9\text{-EtG})(1\text{-MeC})]^{2+}$ ion is the weak intramolecular hydrogen-bond between N(4)' and O(6) [3.11(1)Å], shown in Figure 6.4. The two bases are almost coplanar (dihedral angle of 5.0°), and the hydrogen-bond causes the nonlinearity of the N(7)-Pt-N(3)' angle by pulling the bases together. The bases, in fact, resemble a Hoogsteen pair (Hoogsteen (1963); Guschlbauer (1976)), but with the intervening proton replaced by trans-$Pt(NH_3)_2^{2+}$ (see Figure 6.5). The problem with the Hoogsteen

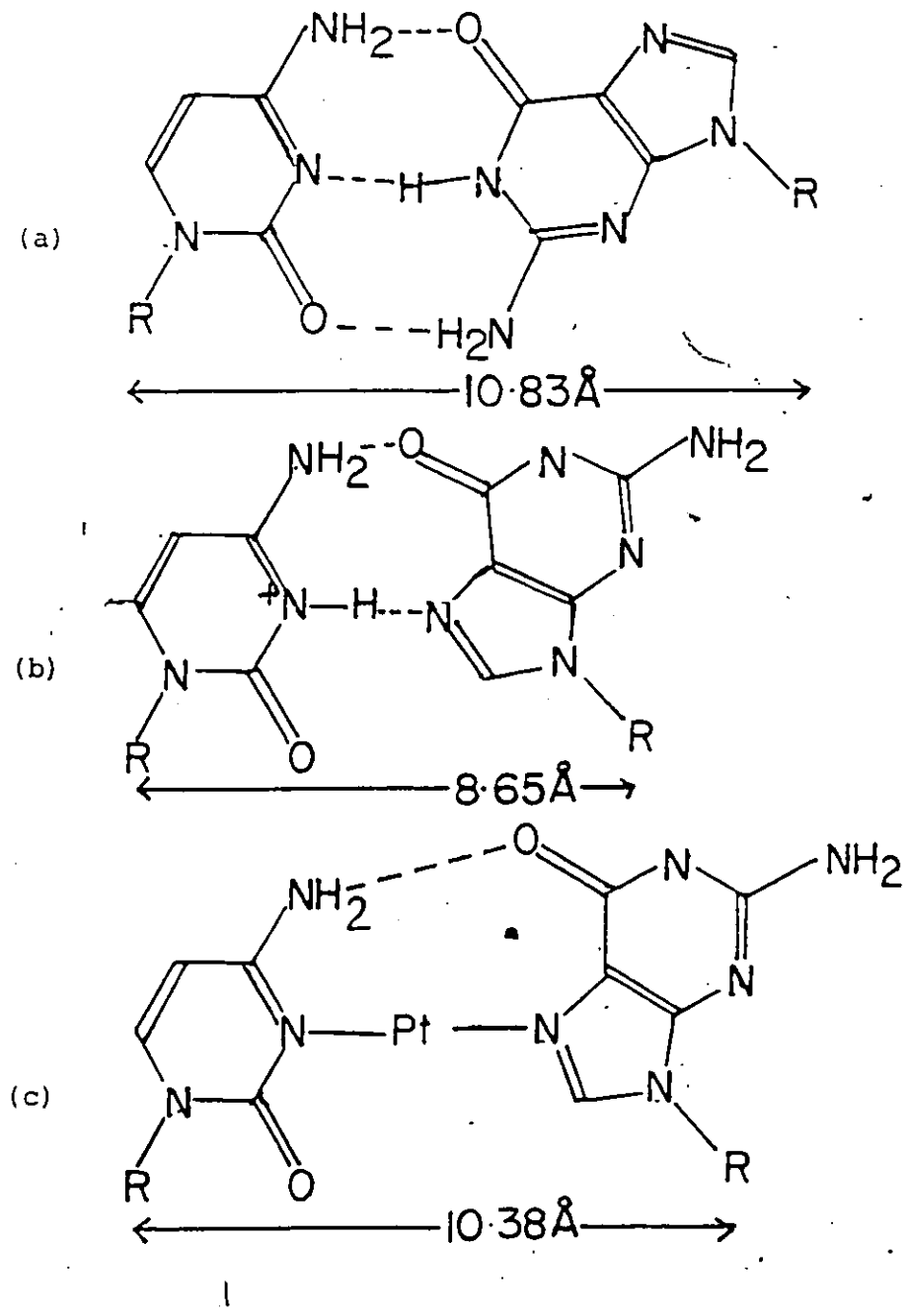

Figure 6.5. G-C base pairing

(a) Watson-Crick base pairing
(b) Hoogsteen base pairing
(c) the trans-GC complex

model is that the separation of the deoxyribose positions is only 8.80 Å, much less than the normal Watson-Crick (1953) distance of 10.85 Å (Guschlbauer (1976)). In 6B the insertion of the trans-$Pt(NH_3)_2^{2+}$ moiety separates the sugar positions by 10.34(1) Å, and this unit can easily be accommodated by the DNA double helix. This molecule, therefore, represents a model for a very stable interstrand cross-link.

Figure 6.6 illustrates the packing of 6B. The primary feature is the layers of cations and anions centered in the **bc**-face. Within the layers the cations are arranged such that the N(5)-Pt-N(6) axis is nearly parallel to the **c**-axis and an ammonia group of one molecule nearly touches the other ammonia group of the next molecule. This arrangement makes the bases nearly parallel to each other. However, there are no base-base interactions because sets of bases in adjacent cations are separated by the perchlorate ions, which in turn with the water molecules, act as links between cations by hydrogen-bonding to the ammonia groups. Separate chains of cations within the layer are linked by hydrogen-bonds from the bases to the perchlorate ions ($N(1)\ldots O(21)^{ii}$, $N(2)\ldots O(22)^{ii}$, $N(4)'\ldots O(12)^{ii}$, $N(4)\ldots O(14)^{ii}$). Interaction between the layers is by Van der Waals forces and $N(2)^{iii}\ldots N(3)$ hydrogen-bonds. This type of purine-purine bonding has been observed in several other 2-aminopurine structures (Mandel, Marsh (1975); Simundza, Sakore, Sobel (1970); O'Brien (1967); Purnell, Hodgson (1976)).

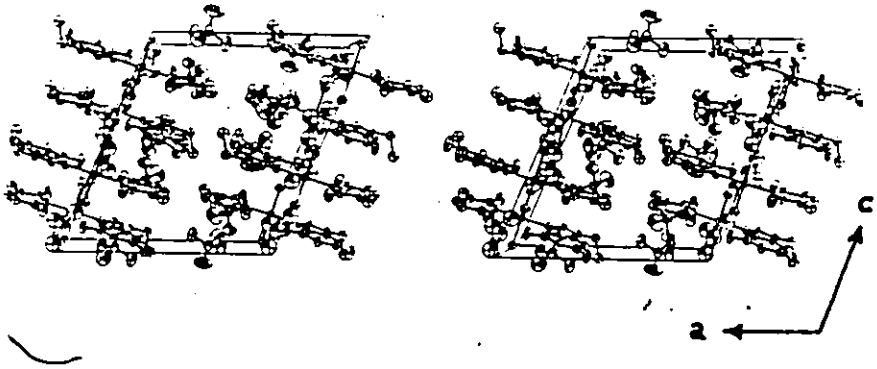

Figure 6.6. The packing in the unit cell for 6B

Within each layer there is an extended cavity which can accomodate the water molecules, and within this cavity four favourable symmetry independent sites occur twice giving eight sites in all. However, only two or three of these sites can be occupied simultaneously in any one cavity resulting in a non-stoichiometric water content. The water molecules are involved in O(2)...O(W)...ammine and O(2)... O(W)...O(perchlorate) hydrogen-bonds.

The ^{1}H NMR and acidity of 6B have been reported (Britten, Lippert, Lock (1984)).

6.4 Possible Relevance of the Cross-link Model

Mononuclear complexes of $(NH_3)_2Pt(II)$ containing two purines (adenine and/or guanine) coordinated to Pt through N7 each represent models of DNA cross-links involving two donor sites from the periphery of DNA (see Figure 6.7a). 2:1 complexes of $(NH_3)_2Pt(II)$ with 1-methylcytosine (coordination through N3) and 7,9-dimethylhypoxanthine (coordination through N1) represent models for cross-links involving donor atoms from the interior of double-stranded DNA (see Figure 6.7 d). Metal binding to these sites requires partial opening or local denaturation of DNA to permit the metal to get inside the helix. These two types of possible DNA cross-links and their effects on the DNA secondary structure have been discussed in detail by Kistenmacher, Orbell, and Marzilli (1981, 1983).

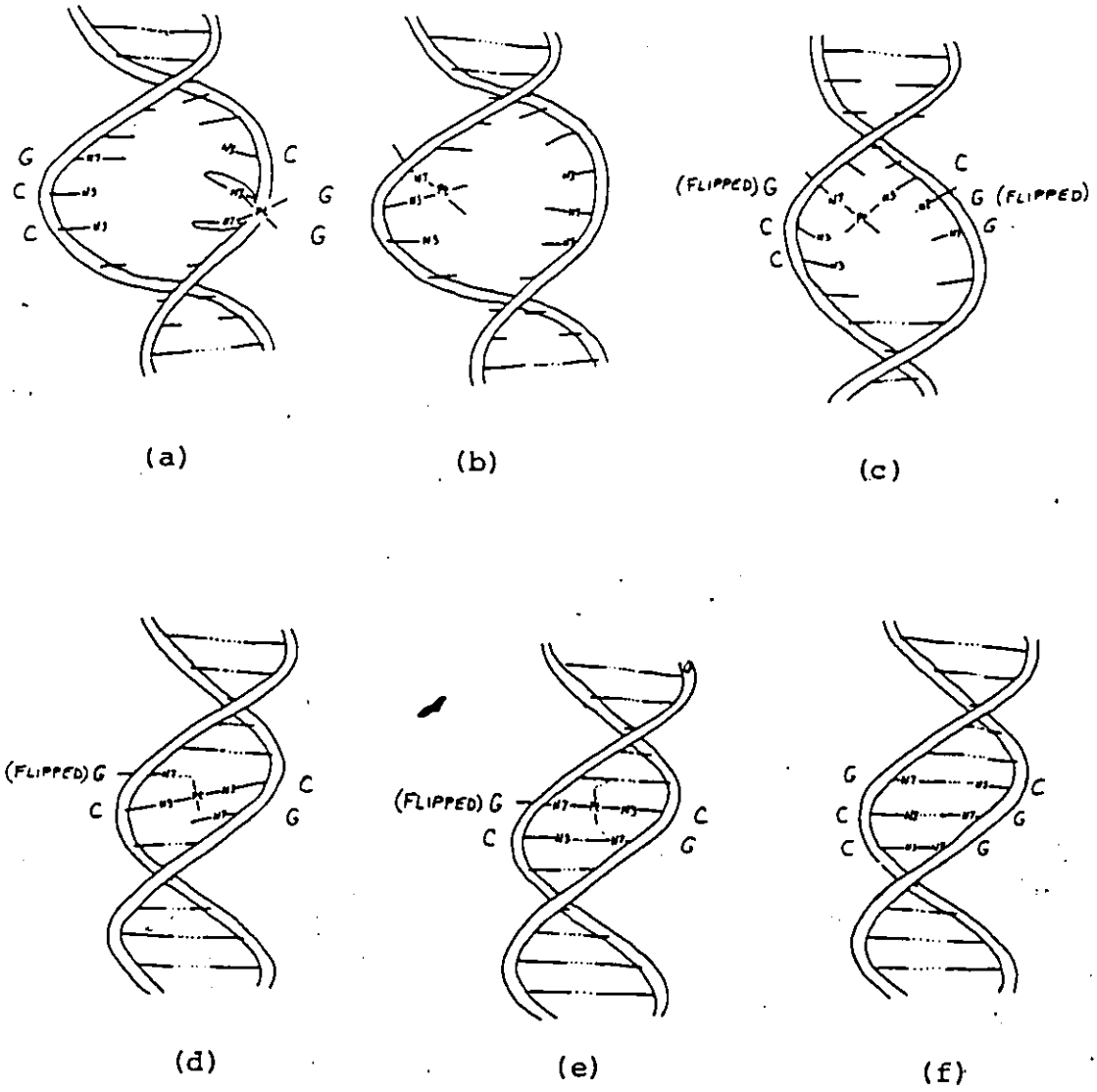

Figure 6.7. Pt-DNA lesions
(a) external intrastrand cis-G,G
(b) internal intrastrand cis-G,C
(c) interstrand cis-G,C
(d) interstrand trans-C,C
(e) interstrand trans-G(syn),C
(f) normal DNA

The mixed 1-MeC, 9-EtG complexes of cis- and trans-$Pt(NH_3)_2^{2+}$ belong to a third group of possible cross-links, involving one donor atom from the interior of DNA (N3 of C) and the second donor atom from the periphery (N7 of G). For an intra-strand cross-link, either of the two bases must rotate about the glycosidic bond from the anti to the syn conformation to bring the two donor atoms into closer proximity. Because of the lesser stereochemical restraint of purines for the syn conformation (Jordan, Pullman (1968)), rotation of guanine is more likely to occur. With the isolated dinucleotide r(GpC) the formation of a guanine-N7, cytosine-N3 cross-link through cis-$(NH_3)_2Pt(II)^{2+}$ is achieved by rotation of guanine (Chottard, Girault, Chottard, Lallemand, Mansuy (1980); Jordanov, Williams (1978)). For an interstrand crosslink, therefore, rotation of guanine to the syn conformation is required.

The syn conformation of guanine has been postulated to play a role in spontaneous base substitution mutations (Topal, Fresco (1976)) and its occurance in Z-DNA is firmly established (Dickerson (1983) and refs. therein). Platinum binding could occur either to G already in the syn conformation, or to G in the anti conformation followed by rotation of G to the syn conformation. It has been shown that $[Pt(dien)Cl]Cl$ (3C)[8] binds to poly(dG·dC)poly(dG·dC), presumably through N7, causing the rotation of the sugar to give G the syn conformation, resulting in a B⟶Z transition

(Malfoy, Hartmann, Leng (1981); Ushay, Santella, Caradonna, Gruberger, Lippard (1982)). The fact that cis- and trans-$(NH_3)_2Pt^{2+}$ prevent a similar B→Z transition may be a result of cis intra-strand GG cross-linking (non-neighbouring G's), or inter-strand cross-linking with rotation of the guanine and not its sugar.

The coplanarity of the two bases in the 6B cation, the comparable distances between the 'glycosidic bonds' in the model compound and B-DNA, and the minimal steric interference of the NH_3 groups on a hypothetical DNA sequence, suggest that a cross-link of this type should not distort DNA greatly (see Figure 6.7e). The replacement of the Watson-Crick hydrogen-bonds by the much stronger Pt-N covalent bonds further suggest that DNA might indeed be stabilized by cross-links of this type. This idea would be consistent with findings that at low Pt/base ratios, trans-$Pt(NH_3)_2^{2+}$ causes an increase in the melting temperature of DNA with no appreciable effect on base stacking (Macquet, Butour, Johnson (1983)). Furthermore, the observed prevention of intercalation of ethidium bromide by trans-$Pt(NH_3)_2Cl_2$ can be explained in terms of the trans-ammine groups blocking the space between costacked bases and, more importantly, stabilizing the costacking by hydrogen-bonding. In contrast, formation of either an intra (Figure 6.7b) or interstrand (Figure 6.7c) cross-link between G and C by cis-Pt(II) would cause serious distortions to the DNA structure because of unfavourable

dihedral angles of the bases (70-90°) and very much reduced sugar separations (7.75-8.43Å). The lowering of the DNA melting point (see Figure 6.1) and changes in the CD spectra are consistent with this. Similarly, cross-links of types cis-$[(NH_3)_2PtC_2]^{2+}$ or cis-$(NH_3)_2PtT_2$ should have such an effect. For a trans-$[(NH_3)_2PtC_2]^{2+}$ cross-link, on the other hand, a smaller distortion of DNA might be expected (Figure 6.7d). In the trans-C_2 model compound the two bases are coplanar (Lippert, Lock, Speranzini (1981b)), and the sugar-sugar distance will be a maximum of 10.7 or 9.6 Å, depending on whether the sugar positions are cis or trans with respect to the platinum. It can be argued that the former distance is comparable to the sugar-sugar distance for a Watson-Crick pair (10.85 Å) or the distance between opposite bases of adjacent pairs (assuming a 36° twist angle, 10.86 Å), but there will still be greater distortion than in the trans-$Pt(NH_3)_2GC^{2+}$ case. This is because the two cytosine molecules must come from opposite sides of adjacent base pairs, resulting in two unpaired guanine molecules and tilting of the C-Pt-C system with respect to the original base pairs (see Figure 6.7d). The trans-adenine, cytosine model, another of this type, is currently being examined by Brenda Brown in our lab.

CHAPTER 7

CONCLUSIONS

7.1 Structural Aspects of Pt-DNA Binding

A variety of chemical, physical, and biological experiments are being undertaken to clarify the mechanism of Pt-DNA interaction. Trans-$PtCl_2(NH_3)_2$ and [Pt(dien)Cl]Cl, both inactive against cancer, are often used as controls in studies of the active drug cis-$PtCl_2(NH_3)_2$. The structural aspects of the proposed DNA-binding modes of these compounds will now be outlined. The discussion is based on recent published experiments (Hacker et al. (1984)) and on the structural information outlined in this thesis.

Reaction of pure DNA or of live cells with the three chloro complexes is generally slow because of the poor solubility of the neutral complexes and the slow hydrolysis of the Pt-bound chlorides. Therefore $AgNO_3$ treatment of the Pt compounds to give soluble nitrate salts of the corresponding divalent aqua ions is often employed. The homogeneity of each of these aqueous solutions is not guaranteed, however. The cis complex (Lock (1980)) and the dien complex (Martin (1983)) form hydroxo bridged oligomers, and the same is expected with the trans complex, based on the stability of the OH^- bridge (see Chapter 3). Care must also be taken

in the preparation of the trans complex to prevent the formation of Pt(IV) and tetraammine Pt(II) complexes (Chapter 4).

Each aquaplatinum monomer can then bind to the exposed N7 position on guanine. For the cis complex this may be assisted by hydrogen-bonding of the aqua ligand to O6 of guanine (Reedijk et al. (1984)). The aquacytosine complex (3E) represents a stable aqua(base)platinum(II) intermediate. Isolation of the guanine analogue would be of interest to verify intramolecular hydrogen-bonding and to see if an O6...aqua interaction would be strong enough to help stabilize the Pt(II)-OH_2 bond. The interaction of the ammine ligand on N7-bound trans-$Pt(NH_3)_2^{2+}$ with O6 of G has been observed (Jack et al. (1977)), and would have approximately the same geometry as a cis aqua chelate. The cis, trans, and dien complexes, then, could all form hydrogen-bonds to the DNA.

The double strand helix of DNA is not a rigid structure when in solution. It undergoes a breathing (local unwinding) motion which can be enhanced by the inductive weakening of the Watson-Crick hydrogen-bonding by the N7 bound Pt (Speranzini (1980)). Thus various bifunctional modes of binding are available to the cis and trans species, but the dien complex can only bind monofunctionally. This may explain the ability of $Pt(dien)^{2+}$ to enhance B→Z transitions while the other two complexes cannot (Macquet et al. (1983)),

and why cis and trans can shorten DNA and the dien complex cannot (Macquet et al. (1983)).

It is the mode of bifunctional binding which differentiates the cis and trans complexes as far as drug activity is concerned. Only the cis-$Pt(NH_3)_2^{2+}$ moiety can form an intrastrand GG crosslink between neighbouring guanines. This is thought to be the major event in the interaction of the cis complex with DNA, and the lesion responsible for anti-tumor activity (Lippard (1984)). The resulting distortion in the local DNA helical structure must eventually result in a somewhat selective tumor cell kill by interfering with the normal (or abnormal) cell reproductive or immune process. The mechanism is still obscure.

The trans complex must form a second bond to either a protein molecule near the DNA surface or to another guanine N7 site brought nearby by a folding of the DNA. Some of the bifunctional binding is interstrand, and the trans-GC model presented in Chapter 6 describes a stable link which can easily be accomodated in the helix without extenxive disruption of the base stacking. This model nicely explains the melting point data (see Figure 6.1) when compared to the possible distortions caused by the cis isomer.

In the living cell, there are proteins and enzymes which can eventually repair the damage caused by the trans and the dien complexes, and by most of the cis lesions, when the Pt concentration is not too high. Fortunately, this

repair process is not as effective for the cis complex in the tumor cells (Rosenberg (1977)), and they can be selectively destroyed for certain cancers.

7.2 Suggestions for Further Study

The simple hydroxo and aqua complexes of cis and trans diammines which were proposed by King (1938) are currently under investigation in our lab, as are the reduction potentials of various multidentate ligand Pt(IV) complexes. Pt oligonucleotide complexes are also being synthesized and studied.

Other projects which would be of interest include the preparation of an aquaguanine complex, (mentioned above) and further studies on variation of the ligands on the Pt drug. For example, Maruta Zvagulis (1980) has examined the structure-activity relationships of various amine ligands. Certain bulky amines showed a decrease in toxicity, but were limited in activity. An examination of a list of active compounds currently under investigation (Reedijk (1984)) reveals that all have the required hydrogen atom on the bound nitrogen atom, but as yet no convincing reason for this feature is evident from the intrastrand cis-G,G crosslink model. Macquet and coworkers (1984) have suggested that the primary or secondary amine allows for rotation about the initial Pt-N7 bond to permit the proper orientation for bifunctional binding. It is curious that all of these potential drugs have a

symmetric arrangement of amine ligands. It would be interesting to prepare and test a complex with one NH_3 group and a much larger amine as the cis ligand. This complex should still have free rotation on DNA if bound trans to the bulky ligand. Would there still be a reduction in toxicity or activity?

Certainly the chemistry and biochemistry of platinum still "merits an exacter Inquiry into its Nature than hath hitherto been made."

APPENDIX 1

Hydrogen atom positional parameters ($x10^3$) and isotropic temperature factors ($Å^2$)($x10^3$). The temperature factors were fixed at approximately 1.5 times U_{eq} of the attached atom.

Table A1.1. Hydrogen atom parameters for 3C

(not refined in final cycles)

	x	y	z	U_{iso}
H(N11)	308	57	356	48
H(N12)	292	295	401	48
H(C11)	237	-124	502	56
H(C12)	154	167	484	56
H(C21)	158	-356	377	46
H(C22)	85	-234	464	46
H(N2)	56	120	349	43
H(C31)	60	-301	236	53
H(C32)	-42	-226	316	53
H(C41)	-36	210	194	52
H(C42)	-38	-74	108	52
H(N31)	114	2	92	51
H(N32)	65	366	95	51

Table A1.2. Hydrogen atom parameters for 3D

	x	y	z	U_{iso}
H(N11)	144(9)	358(13)	-22(7)	66(7)
H(C11)	311(10)	417(13)	2(8)	73(4)
H(C12)	309(11)	557(13)	-39(8)	73(4)
H(C21)	379(9)	583(12)	61(7)	60(4)
H(C22)	267(9)	645(14)	62(7)	60(4)
H(N2)	306(10)	441(11)	129(6)	51(3)
H(C31)	246(9)	640(13)	203(6)	53(3)
H(C32)	359(9)	590(12)	223(7)	53(3)
H(C41)	260(11)	419(13)	287(7)	69(4)
H(N31)	73(11)	413(13)	269(7)	69(8)

Table A1.3. Hydrogen atom parameters for 3E

	x	y	z	U_{iso}
H(31)	116(14)	464(25)	369(15)	66
H(32)	168(14)	519(25)	263(15)	66
H(51)	-40(13)	-291(23)	192(14)	60
H(52)	63(13)	-246(21)	124(13)	60
H(53)	-57(13)	-238(22)	47(14)	60
H(61)	-193(14)	-69(25)	101(14)	67
H(62)	-117(13)	159(23)	234(14)	67
H(63)	-125(13)	213(24)	117(14)	67
H(5)	445(14)	214(24)	511(14)	65
H(6)	568(13)	323(22)	370(13)	64
H(11)	460(15)	462(28)	84(17)	84
H(12)	469(15)	300(28)	90(17)	84
H(13)	586(15)	528(27)	198(15)	84
H(41)	291(15)	70(25)	576(15)	78
H(42)	123(14)	36(25)	447(15)	78
H(71)	458(15)	80(26)	814(16)	85
H(72)	315(15)	-125(28)	777(15)	85

Table A1.4. Hydrogen atom parameters for 6B

	x	y	z	U_{iso}
H(1)	228(7)	1115(7)	477(6)	54
H(8)	193(6)	609(6)	383(5)	52
H(21)	477(9)	1096(8)	517(7)	85
H(22)	398(9)	1163(9)	518(8)	85
H(91)	440(7)	724(7)	416(7)	64
H(92)	390(7)	613(8)	413(6)	64
H(93)	476(9)	728(9)	569(9)	92
H(94)	510(9)	607(9)	551(7)	92
H(95)	426(9)	620(9)	583(7)	92
H(6)	-445(9)	764(7)	267(7)	73
H(41)	-182(9)	987(9)	352(8)	79

APPENDIX 2

Anisotropic temperature factors used in the expression

$$\exp[-2\pi^2(U_{11}h^2\mathbf{a}^{*2} + U_{22}k^2\mathbf{b}^{*2} + U_{33}l^2\mathbf{c}^{*2} + 2U_{12}hk\mathbf{a}^*\cdot\mathbf{b}^* + 2U_{13}hl\mathbf{a}^*\cdot\mathbf{c}^* + 2U_{23}kl\mathbf{b}^*\cdot\mathbf{c}^*)]$$

Table A2.1. Anisotropic temperature factors ($Å^2$)($x10^4$) for 3A

	U_{11}	U_{22}	U_{33}	U_{12}	U_{13}	U_{23}
Pt	186(2)	242(2)	277(2)	0	33(1)	0
Cl(1)	333(7)	289(6)	371(7)	-20(5)	62(5)	-36(5)
Cl(2)	387(7)	314(7)	304(6)	-9(5)	11(5)	22(5)
Cl(3)	356(7)	347(7)	386(7)	-11(5)	55(6)	78(5)
Cl(4)	364(7)	439(7)	270(6)	-13(6)	43(5)	-38(5)

Table A2.2. Anisotropic temperature factors ($Å^2$)($x10^3$) for 3B

	U_{11}	U_{22}	U_{33}	U_{12}	U_{13}	U_{23}
Pt	29.4(4)	16.4(3)	15.4(3)	0.7(2)	2.1(2)	1.0(2)
Cl(1)	55(2)	30(2)	16(1)	7(2)	7(1)	1(1)
Cl(2)	43(2)	15(1)	32(2)	2(1)	3(1)	1(1)
Cl(3)	34(2)	40(2)	38(2)	4(2)	4(1)	4(1)
Cl(4)	38(2)	36(7)	29(2)	0(1)	-2(1)	0(1)

Table A2.3. Anisotropic temperature factors ($Å^2$) ($x10^3$) for 3C

	U_{11}	U_{22}	U_{33}	U_{12}	U_{13}	U_{23}
Pt	23.3(2)	24.9(2)	23.6(2)	0.1(1)	1.2(3)	-1.1(4)
Cl(1)	40(1)	44(2)	39(1)	-13(1)	5(1)	7(1)
N(1)	23(4)	35(5)	35(5)	3(4)	-9(3)	2(4)
N(2)	23(4)	35(5)	35(4)	0(4)	1(3)	2(4)
N(3)	35(5)	34(5)	30(4)	0(4)	-3(4)	1(4)
Cl(2)	36(1)	36(1)	34(1)	4(1)	-3(1)	2(1)

Table A2.4. Anisotropic temperature factors ($Å^2$)$(x10^3)$ for 3D

	U_{11}	U_{22}	U_{33}	U_{12}	U_{13}	U_{23}
Pt	32.0(2)	25.0(2)	38.9(2)	0.2(2)	-4.0(2)	2.3(2)
N(1)	61(6)	39(5)	44(5)	-6(5)	-14(4)	-10(4)
N(3)	46(5)	49(5)	47(5)	-20(5)	20(4)	-1(4)
O(1)	40(4)	37(4)	78(6)	0(3)	-10(4)	11(4)
O(2)	53(5)	35(5)	97(6)	2(4)	8(5)	16(4)
O(3)	31(4)	56(5)	106(8)	-5(4)	-3(5)	-19(5)
O(4)	51(5)	77(7)	68(5)	18(5)	-2(4)	-8(5)
O(5)	43(5)	87(7)	95(7)	13(4)	3(6)	-35(5)
O(6)	91(8)	98(8)	49(5)	3(6)	-7(5)	-6(5)

Table A2.5. Anisotropic temperature factors ($Å^2$)($x10^3$) for 3E

	U_{11}	U_{22}	U_{33}	U_{12}	U_{13}	U_{23}
Pt	28.4(2)	30.4(2)	24.7(2)	13.4(1)	5.0(1)	4.1(1)
O(3)	48(4)	38(4)	45(4)	21(3)	16(4)	3(3)
N(6)	31(4)	62(6)	40(5)	18(4)	10(4)	0(4)
O(2)	38(4)	43(4)	35(3)	21(3)	9(3)	7(3)
O(71)	53(5)	63(5)	47(5)	7(4)	14(4)	5(4)
O(72)	76(7)	81(7)	43(5)	10(5)	25(5)	5(5)
O(73)	83(8)	53(6)	93(8)	-19(5)	40(7)	-12(5)
O(81)	52(5)	49(5)	45(4)	16(4)	5(4)	2(4)
O(82)	47(5)	56(5)	60(5)	26(4)	9(4)	7(4)
O(83)	59(5)	63(5)	60(5)	19(5)	28(5)	16(4)

Table A2.6. Anisotropic temperature factors (A^2) ($x10^3$) for 4A

	U_{11}	U_{22}	U_{33}	U_{12}	U_{13}	U_{23}
Pt(1)	3.24(4)	3.13(3)	3.89(5)	0	0.30(6)	0
N(11)	5.0(6)	3.0(5)	6.2(8)	0.1(7)	2(1)	0.1(7)
N(12)	10(3)	2(1)	10(2)	0	5(2)	0
O(1)	5(1)	6(1)	10(2)	0	-2(1)	0
O(2)	13(3)	23(4)	5(1)	0	-2(2)	0
O(3)	5(2)	16(3)	14(3)	0	-2(2)	0
N(13)	10(2)	8(2)	13(3)	0	-7(2)	0
O(4)	14(2)	9(2)	13(2)	0	11(2)	0
O(5)	22(4)	23(4)	6(2)	0	-7(2)	0
O(6)	17(4)	16(3)	6(2)	0	-2(2)	0
Pt(2)	3.31(5)	3.76(3)	2.16(4)	0	0.26(5)	0
N(21)	5.6(7)	3.9(5)	4.0(6)	0.7(7)	1.0(9)	0.5(8)
N(22)	4(1)	4(1)	2(1)	0	0(1)	0
N(23)	3(1)	7(2)	7(2)	0	1(1)	0

Table A2.6. (continued)

	U_{11}	U_{22}	U_{33}	U_{12}	U_{13}	U_{23}
Rt(3)	2.68(5)	2.47(3)	2.30(4)	0	0.14(5)	0
N(31)	4(1)	6(2)	4(1)	0	0(1)	0
N(32)	3(1)	5(1)	3(1)	0	-1.6(8)	0
N(33)	4(1)	3(1)	3(1)	0	-0.1(9)	0
N(34)	3(1)	3(1)	4(1)	0	-0.5(9)	0
N(1)	6(1)	6(1)	5(1)	-2(1)	-1(1)	3(1)
O(11)	8(1)	5.2(9)	4.8(7)	2.1(8)	-2.1(8)	0.4(6)
O(12)	15(2)	10(2)	6(1)	9(2)	-1(1)	1.4(9)
O(13)	15(2)	7(1)	19(3)	-2(1)	13(2)	-7(2)
N(2)	9(2)	1.7(6)	6(1)	-2(1)	1(1)	-4(1)
O(21)	11(2)	11(2)	10(2)	-5(2)	-3(1)	0(1)
O(22)	12(2)	13(2)	16(2)	7(2)	-9(2)	-7(2)
O(23)	18(3)	14(3)	13(2)	7(2)	9(2)	5(2)

Table A2.7. Anisotropic temperature factors ($Å^2$)9x10^3) for 4B

	U_{11}	U_{22}	U_{33}	U_{12}	U_{13}	U_{23}
Pt	19.26(6)	21.80(7)	23.22(7)	6.30(4)	3.76(4)	9.56(4)
Cl	27.5(3)	43.9(4)	38.1(3)	11.6(3)	2.4(2)	22.9(3)
N(1)	31(1)	31(1)	30(1)	11.6(8)	11.4(8)	14.2(8)
N(2)	28(1)	24.3(9)	35(1)	3.7(7)	5.2(8)	10.6(8)
N(3)	32(1)	28(1)	31(1)	5.2(8)	7.3(8)	10.5(8)
O(1)	44(1)	42(1)	79(2)	16(1)	24(2)	38(2)
O(2)	42(1)	37(1)	57(2)	9(1)	0(1)	24(1)
O(3)	28(1)	45(1)	64(2)	7(1)	10(1)	9(1)

Table A2.8. Anisotropic temperature factors ($Å^2$)($x10^2$) for 5A

	U_{11}	U_{22}	U_{33}	U_{12}	U_{13}	U_{23}
Pt(1)	2.81(6)	2.81(6)	3.4(1)	0	0	0
N(1)	2(1)	7(1)	10(2)	0	0	0
Pt(2)	2.65(6)	2.65(6)	2.64(9)	0	0	0
N(2)	4(1)	5(1)	15(2)	0	0	0
Pt(3)	2.92(8)	6.7(1)	2.78(7)	0	0	0
N(3A)	6(1)	7(2)	6(1)	0	0	0
N(3C)	5(1)	11(2)	3(1)	0	0	0
Pt(4)	2.96(7)	2.96(7)	3.2(1)	0	0	0
N(4)	4(1)	2(1)	10(2)	0	0	0
Cl	7.5(6)	7.5(6)	4.6(6)	0	0	0
Cl(1)	7.2(8)	6.3(7)	3.8(5)	0	0	0
O(1)	7(1)	6.0(9)	3.9(7)	1.8(8)	-0.9(7)	0.9(7)
Cl(2)	6.8(1)	6.8(1)	5.8(2)	-0.9(3)	-0.9(2)	-0.9(2)
O(2)	23(2)	23(2)	8(1)	-1(2)	4(1)	4(1)
O(3)	59(5)	59(5)	19(2)	-53(6)	-1(1)	-1(1)
O(4)	34(3)	18(2)	41(3)	7(2)	-30(2)	-6(2)

Table A2.9. Anisotropic temperature factors ($Å^2$)($x10^3$) for 5B

	U_{11}	U_{22}	U_{33}	U_{12}	U_{13}	U_{23}
Pt	21.7(3)	23.3(3)	19.4(3)	0(1)	0.1(5)	-1.1(7)
Br(1)	51(1)	30(1)	48(1)	-10(3)	3(2)	2(2)
Br(2)	60(2)	57(2)	23(2)	24(3)	7(2)	-2(2)
Br(3)	30(2)	49(2)	21(1)	5(2)	-2(2)	5(2)
Br(4)	24(4)	25(4)	39(5)	0(3)	0	0
Br(5)	20(4)	31(4)	64(6)	-1(3)	1(3)	10(5)
N	52(11)	42(10)	24(9)	-43(17)	-3(15)	-1(14)
K	87(5)	53(4)	42(3)	-13(7)	-11(7)	-5(3)
O	46(11)	66(13)	90(16)	15(20)	-2(23)	-34(12)

Table A2.10. Anisotropic temperature factors ($Å^2$)($x10^3$) for 5C

	U_{11}	U_{22}	U_{33}	U_{12}	U_{13}	U_{23}
Pt	17.7(3)	28.3(3)	22.1(3)	-0.1(8)	-0.9(6)	-4.3(8)
Br(1)	42(1)	30.5(9)	48(1)	0(3)	-1(2)	1(2)
Br(2)	45(2)	58(2)	26(2)	13(3)	14(2)	-11(2)
Br(3)	30(2)	61(2)	24(2)	2(2)	-6(2)	1(2)
Br(4)	21(3)	18(3)	23(3)	0(2)	0	0
Br(5)	22(3)	34(4)	92(6)	0(3)	-3(4)	44(5)
N(1)	17(13)	20(6)	39(10)	0	0	0
N(2)	35(18)	104(21)	31(12)	-37(17)	-20(12)	22(13)
O	38(13)	103(17)	44(12)	41(16)	5(13)	-16(11)

Table A2.11. Anisotropic temperature factors ($Å^2$)($x10^2$) for 6A

	U_{11}	U_{22}	U_{33}	U_{12}	U_{13}	U_{23}
PtA	1.53(3)	2.22(4)	3.81(5)	0.04(3)	0.54(3)	0.22(4)
Cl(1)A	1.9(2)	6.9(4)	5.0(3)	-0.7(3)	1.0(2)	0.9(3)
N(2)A	3.1(9)	5(1)	4(1)	0.1(8)	-0.4(8)	-0.4(8)
N(1)A	1.9(8)	3.6(9)	5(1)	0.7(7)	0.8(7)	-0.6(8)
C(2)A	0.3(7)	4(1)	3(1)	-0.3(7)	0.4(7)	0.0(9)
C(5)A	1.1(8)	6(1)	3(1)	0.4(9)	-0.1(7)	0(1)
C(6)A	4(1)	3(1)	3(1)	0.5(9)	0.3(9)	-0.5(9)
C(1)A	5(1)	4(1)	5(1)	-1(1)	3(1)	0(1)
O(2)A	3.1(7)	1.7(6)	4.3(8)	0.6(5)	0.9(6)	0.8(5)
N(4)A	3.1(8)	2.6(8)	3.7(9)	0.9(7)	0.9(7)	0.0(7)
PtB	2.02(4)	2.67(4)	2.94(4)	0.04(3)	0.59(3)	0.06(4)
Cl(1)B	2.0(2)	5.1(3)	5.6(3)	-0.4(2)	1.4(2)	-0.3(3)
N(2)B	2.8(8)	2.6(8)	7(1)	-1.0(7)	2.3(8)	0.1(8)
N(5)B	3.0(8)	1.0(7)	5(1)	-0.5(6)	1.5(7)	-0.6(6)
N(1)B	3.3(9)	2.7(8)	4(1)	-0.8(7)	1.4(8)	0.9(8)
C(2)B	6(1)	1.7(9)	3(1)	0.7(9)	2(1)	0.4(8)
N(3)B	2.1(7)	1.1(7)	5(1)	-0.9(6)	0.8(7)	-1.8(7)
C(4)B	1.3(9)	5(1)	5(1)	-0.3(9)	-0.1(9)	-2(1)
C(5)B	4(1)	3(1)	8(2)	0(1)	2(1)	0(1)
C(6)B	2(1)	4(1)	5(1)	-0.7(9)	1.3(9)	0(1)
C(1)B	4(1)	5(1)	4(1)	0(1)	0(1)	1(1)
O(2)B	3.4(7)	2.6(7)	4.1(8)	0.3(6)	-0.1(6)	1.6(6)
N(4)B	7(1)	4(1)	3(1)	-1(1)	1(1)	0.7(8)
Cl(2)	4.2(3)	4.8(3)	6.4(4)	1.3(3)	1.8(3)	1.7(3)
Cl(3)	2.6(3)	6.1(3)	5.5(4)	0.2(3)	1.4(2)	0.7(3)
O(W1)	4.8(9)	3.1(7)	8(1)	-0.9(7)	1.5(9)	-1.2(8)
O(W2)	8(1)	9(1)	6(1)	0(1)	2.6(9)	0(1)
O(W3)	11(2)	5(1)	11(2)	2(1)	5(1)	-1(1)

Table A2.12. Anisotropic temperature factors ($Å^2$)($x10^3$) for 6B

	U_{11}	U_{22}	U_{33}	U_{12}	U_{13}	U_{23}
Pt	24.2(1)	37.8(2)	37.6(2)	-4.2(1)	10.6(1)	-3.1(1)
N(5)	44(4)	77(5)	37(3)	-7(4)	12(3)	-7(4)
N(6)	36(3)	84(5)	37(4)	-1(4)	16(3)	3(4)
N(1)'	34(4)	60(4)	49(4)	-7(3)	8(3)	-3(3)
N(3)'	22(3)	49(4)	45(3)	-1(3)	9(2)	-2(3)
O(2)'	49(4)	50(3)	96(5)	-14(3)	32(4)	-20(3)
N(4)'	55(5)	39(4)	86(7)	5(3)	22(5)	-9(4)
N(1)	29(3)	30(3)	65(5)	-1(3)	21(3)	-6(3)
N(3)	25(3)	46(3)	45(4)	-1(3)	16(3)	-7(3)
N(7)	25(3)	47(4)	42(3)	3(3)	14(2)	-1(3)
N(9)	25(3)	36(3)	44(3)	-4(2)	14(3)	-5(3)
N(2)	31(4)	43(4)	118(8)	-6(3)	27(5)	-22(5)
O(6)	26(3)	51(3)	94(5)	4(2)	23(3)	-8(3)
Cl(1)	58(1)	59(1)	45(1)	11(1)	21.1(9)	0(1)
O(11)	88(6)	105(6)	68(5)	-10(5)	28(5)	-23(5)
O(12)	95(6)	134(7)	107(7)	34(6)	69(6)	12(6)
O(13)	89(7)	109(6)	78(6)	36(5)	41(5)	6(5)
O(14)	150(9)	61(5)	149(8)	-19(5)	96(7)	-10(5)
Cl(2)	45(1)	45(1)	64(1)	-2.6(9)	21(1)	-1(1)
O(21)	56(4)	53(4)	121(7)	-7(3)	39(4)	3(4)
O(22)	47(4)	94(6)	119(7)	-4(4)	28(5)	-6(5)
O(23)	104(7)	72(5)	135(8)	23(5)	38(6)	-25(5)
O(24)	190(12)	173(10)	70(6)	-35(9)	53(7)	14(7)

REFERENCES

	Page Cited
Allen, D., Lock, C.J.L., Turner, G., Powell, J. (1975), Can. J. Chem., 53, 2707.	105
Appleton, T.G., Bowie, C.A., Hall, J.R., Ralph, S.J. (1984), "Platinum Coordination Complexes in Cancer Chemotherapy", Nijhoff: Boston, (poster abstract), 54	4
Authier-Martin, M., Beauchamp, A.L. (1977) Can. J. Chem., 55, 1213	101
Basolo, F., Gray, H.B., Pearson, R.G. (1960), J. Am. Chem. Soc., 82, 4200.	53
Beauchamp, A.L., Layek, D., Theophanides, T. (1982a), Acta Cryst., B38, 1901.	148,162
Beauchamp, A.L., Layek, D., Theophanides, T. (1982b), Acta Cryst., B38, 1158.	167
Bjorling, C.O. (1941), Arkiv. Kemi. Min. Geol., B15, No. 2.	126
Bond, W.L. (1974), "International Tables for X-ray Crystallography", Vol. II, Kynoch Press: Birmingham, 291.	24
Bragg, W.L. (1913), Proc. Cambridge Phil. Soc., 17, 43.	17

	Page Cited
Britten, J.F. (1984), McMaster University Thesis Tables #1, Available from Thode Library, McMaster Univ., Hamilton, Canada.	49,52
Britten, J.F., Faggiani, R., Gayowski, T., Harvey, D.A., Lock, C.J.L., Montgomery, C., Beauchamp, A.L., Layek, D., Theophanides, T. (1984), Acta Cryst. C, in press.	154
Britten, J.F., Lippert, B., Lock, C.J.L. (1984), Inorg. Chem., in press.	191
Britten, J.F., Lippert, B., Lock, C.J.L., Pilon, P. (1982), Inorg. Chem., 21, 1936.	55,100,102
Britten, J.F., Lippert, B., Lock, C.J.L., Speranzini, R.A. (to be submitted to Acta Cryst.)	101,174
Britten, J.F., Lock, C.J.L., Pratt, W.M.C. (1982), Acta Cryst., B38, 2148.	55,79
Brown, D.B., ed. (1980), "Mixed-Valence Compounds", NATO ASI Series C, 58, D. Reidel Pub. Co.: Dordrecht, Holland.	165
Brown, I.D. (1981), Structure and Bonding in Crystals, Vol. II, 1.	55,94,97, 99,130
Brown, I.D. (1982), personal communication.	132
Brown, I.D., Shannon, R.D. (1973), Acta Cryst., A29, 266.	94

	Page Cited
Buerger, M.J. (1942), "X-ray Crystallography", John Wiley and Sons, Inc.: New York.	12
Buerger, M.J. (1964), "The Precession Method", Wiley: New York.	37
Bushnell, G.W. (1978), Can. J. Chem., 56, 1773.	111
Calabrese, J.C., Burnett, R.M. (1980), TAPER, locally modified for CDC Cyber by Z. Tun, with permission of Nicolet XRD Corp.	47
Chottard, J.C., Girault, J.P., Chottard, G., Lallemand, J.Y., Mansuy, D. (1980), J. Am. Chem. Soc., 102, 5566.	193
Clark, R.J.H. (1980), "Mixed-Valence Compounds", Dordrecht: Reidel, 271.	163
Cleare, M.J. (1974), Coord. Chem. Rev., 12, 349.	2,53
Cleare, M.J. (1977), J. Clin. Hematol. Oncol., 7, 1.	53
Cleare, M.J., Hoeschele, J.D. (1973), Bioinorg. Chem., 2, 2.	2
Corey, E.J., Bailar, J.C., Jr. (1959), J. Am. Chem. Soc., 81, 2620.	75,77
Cotton, F.A., Elder, R.C. (1964), Inorg. Chem., 3, 397.	76
Cotton, F.A., Richardson, D.C. (1966), Inorg. Chem., 5, 1851.	76

	Page Cited
Cotton, F.A., Wilkinson, G. (1980), "Advanced Inorganic Chemistry", John Wiley and Sons, Inc.: New York.	57
Cotton, F.A., Wing, R.M. (1965), Inorg. Chem., 4, 314.	76
Craven, B.M., Hall, D. (1961), Acta Cryst., 14, 475.	126,162
Cromer, D.J. (1974), "International Tables for X-ray Crystallography", Vol. IV, Birmingham: Kynoch Press, Table 2.3.1, 149.	21,23
Cromer, D.J., Waber, J.T. (1974), "International Tables for X-ray Crystallography", Vol. IV, Birmingham: Kynoch Press, Table 2.2.B, 99.	13
Cruickshank, D.W.J. (1970), "Crystallographic Computing", Munksgaard, 187.	50
Dickerson, R.E. (1983), Scientific American, 249, no. 6, 94.	7,193
Elleman, J.S., Rishus, J.W., Martin, D.S., Jr. (1958), J. Am. Chem. Soc., 80, 536.	145
Endres, H., Keller, H.J., Martin, R., Notzel, S. (1980), Z. Naturforsch., 35b, 1274.	167
Endres, H., Keller, H.J., Martin, R., Traeger, U., Novotny, M. (1980), Acta Cryst. B36, 35.	162,166
Faggiani, R., Howard-Lock, H.E., Lock, C.J.L., Lippert, B., Rosenberg, B. (1982), Can. J. Chem., 60, 529.	126

	Page Cited
Faggiani, R., Lippert, B., Lock, C.J.L. (1982), Inorg. Chem., 21, 3210.	172,187
Faggiani, R., Lippert, B., Lock, C.J.L., Rosenberg, B. (1977), J. Am. Chem. Soc., 99, 777.	101
Faggiani, R., Lippert, B., Lock, C.J.L., Rosenberg, B. (1977), Inorg. Chem., 16, 1192.	101
Faggiani, R., Lippert, B., Lock, C.J.L., Speranzini, R.A. (1981), J. Am. Chem. Soc., 103, 1111.	183
Faggiani, R., Lippert, B., Lock, C.J.L., Speranzini, R.A. (1982), Inorg. Chem. 21, 3216.	172,183
Faggiani, R., Lock, C.J.L., Pollock, R.J., Rosenberg, B., Turner, G. (1981), Inorg. Chem., 20, 804.	183
Fanwick, P.E., Martin, D.S., Jr. (1973), Inorg. Chem., 12, 24.	145
Filipski, J., Kohn, K.W., Bonner, W.M. (1980), Chem.-Biol. Interaction, 32, 321.	171
Flack, H.D. (1974), Acta Cryst., A30, 569.	23
Fowlie, A.D., House, D.A., Robinson, W.T., Rumball, S.S. (1970), J. Chem. Soc. (A), 803.	76
Gagnon, C., Beauchamp, A.L., Tranqui, D. (1979), Can. J. Chem., 57, 1372.	101

	Page Cited
Gainsford, A.R., House, D.A., Robinson, W.T. (1971), Inorg. Chem. Acta, 5, 595.	76
Gellert, R.W., Bau, R. (1979), Met. Ions Biol. Syst., 8, 1.	101
Greenhough, T.J., Ladd, M.F.C. (1977), Acta Cryst., B33, 1266.	61
Guschlbauer, W. (1976), "Nucleic Acid Structure", Springer-Verlag: New York, p. 35.	187,189
Hacker, M.P., Douple, E.B., Krakoff, I.H. (1984), "Platinum Coordination Complexes in Cancer Chemotherapy", Nijhoff: Boston.	1,196
Hamilton, W.C. (1965), Acta Cryst., 18, 502.	81,102
Hitchcock, A.P., Lock, C.J.L., Pratt, W.M.C., Lippert, B. (1983), A.C.S. Symp. Ser. 209; 209.	172
Hoogsteen, K. (1963), Acta Cryst., 16, 907.	187
Hughes, R.P., Krishnamachari, N., Lock, C.J.L., Powell, J., Turner, G. (1977), Inorg. Chem. 16, 314.	105
"International Tables for X-ray Crystallography", Birmingham: Kynoch Press. (Four volumes).	38
IUPAC (1970), "Nomenclature of Inorganic Chemistry", Butterworths: London.	77
Jack, A., Ladner, J.E., Brown, R.S., Klug, A. (1977), J. Mol. Biol., 111, 315.	171,197

	Page Cited
Jensen, K.A. (1939), Anorg. Allg. Chem., 242, 87.	2,123,134
Johnson, C.K. (1976), ORTEPII. Report ORNL-5138. Oak Ridge Nat. Lab., Tennessee, U.S.A..	52
Johnson, N.P., Hoeschele, J.D., Rahn, R.O., O'Neill, J.P., Hsie, A.W. (1980), Cancer Res. 40, 1463.	8
Johnston, J.H., Freeman, A.G. (1975), J. Chem. Soc. Dalton Trans., 2153.	76
Jordan, F., Pullman, L.B., (1968), Theor. Chim. Acta, 9, 242.	193
Jordanov, J., Williams, R.J.P. (1978), Bioinorg. Chem., 8, 77.	193
Karle, J., Hauptman, H. (1956), Acta Cryst., 9, 635.	27
Kauffman, G.B., Cowen, D.O. (1963), Inorg. Syn., 7, 239.	112,133
Kauffman, G.B., Teter, L.A. (1963), Inorg. Syn., 7, 232.	58,112
Keene, F.R., Searle, G.H. (1972), Inorg. Chem. 11, 148.	75
Keene, F.R., Searle, G.H. (1974), Inorg. Chem. 13, 2173.	75
Keller, H.J., Keppler, B., Ledezma-Sanchez, G., Steiger, W. (1981), Acta Cryst., B37, 674.	162

	Page Cited
King, H.J.S. (1938), J. Chem. Soc., 1338.	4,199
Kistenmacher, T.J., Orbell, J.D., Marzilli, L. G. (1983), A.C.S. Symp. Ser. 209, 191.	172,179,191
Kistenmacher, T.J., Rossi, M., Marzilli, L. G. (1979), Inorg. Chem., 18, 240.	101
Kistenmacher, T.J., Wilkowski, K., deCastro, B., Chiang, C.C., Marzilli, L.G. (1979), Biochem. Biophys. Res. Commun., 91, 1521.	172
Kobayashi, M., Marumo, F., Saito, Y. (1972), Acta Cryst., B28, 470.	76
Konno, M., Marumo, F., Saito, Y. (1973), Acta Cryst., B29, 739.	76,77
Larson, A.C. (1967), Acta Cryst. 23, 664.	22,50
von Laue, M. (1912), Sitzber. Math. Physik. Kl. Bayer. Akad. Wiss., 303.	18
Layek, D. (1981), Ph.D. Thesis, Athens, Greece.	145
Levine, L. (1969), "Biology of the Gene", C. V. Mosby Co.: St. Louis.	6
Lim, M.C., Martin, R.B. (1976), J. Inorg. Nucl. Chem., 38, 1911.	4
Lippard, S.J., ed. (1983), "Platinum, Gold, and Other Metal Chemotherapeutic Agents", A.C.S. Symp. Ser., 209, Am. Chem. Soc.: Washington, D.C..	1

	Page Cited
Lippard, S.J. (1984), "Platinum Coordination Complexes in Cancer Chemotherapy", Nijhoff: Boston, 11.	7,198
Lippert, B. (1983), A.C.S. Symp. Ser., 209, 147.	54
Lippert, B., Lock, C.J.L., Rosenberg, B., Zvagulis, M. (1977), Inorg. Chem., 16, 1525.	53,87,94, 111
Lippert, B., Lock, C.J.L., Speranzini, R.A. (1981a), Inorg. Chem., 20, 335.	105,179, 181,183
Lippert, B., Lock, C.J.L., Speranzini, R.A. (1981b), Inorg. Chem., 20, 808.	105,172, 179,183,195
Liu, C.F., Ibers, J.A. (1970), Inorg. Chem. 9, 773.	126
Lock, C.J.L. (1980), A.C.S. Symp. Ser., 140, 209.	2,53,55, 100,111,196
Lock, C.J.L., Bradford, J., Faggiani, R., Speranzini, R.A., Turner, G., Zvagulis, M. (1977), J. Clin. Hematol. Oncol., 7, 63.	53
Lock, C.J.L., Speranzini, R.A., Zvagulis, M. (1980), Acta Cryst., B36, 1789.	67,109,183
Luger, P. (1980), "Modern X-ray Analysis on Single Crystals", Walter de Gruyter: Berlin.	12,27,30, 39
Macquet, J.-P., Butour, J.-L. (1978), Biochimie, 60, 901.	7
Macquet, J.-P., Butour, J.-L., Johnson, L.P. (1983), A.C.S. Symp.Ser., 209, 75.	7,8,170, 194,197,198

	Page Cited
Macquet, J.-P., Butour, J.-L., Johnson, N.P., Razaka, H., Salles, B., Vieussens, C., Wright, M. (1984), "Platinum Coordination Complexes in Cancer Chemotherapy", Nijhoff: Boston, 27.	8,9,199
Malfoy, B., Hartmann, B., Leng, M. (1981) Nucleic Acid Res., 9, 5659.	194
Mandel, G.S., Marsh, R.E. (1975), Acta Cryst., B31, 2862.	189
Martell, A.E., ed. (1980), "Inorganic Chemistry in Biology and Medicine", A.C.S. Symp. Ser., 140, Am. Chem. Soc.: Washington, D.C..	1
Martin, R.B. (1983), A.C.S. Symp. Ser. 209, 231.	196
Martin, R.B., Mariam, Y.H. (1979), Met. Ions Biol. Syst., 8, 57.	101
Marzilli, L.G., Kistenmacher, T.J., Eichorn, G. L. (1980), "Nucleic Acid-Metal Ion Interactions", Wiley: New York, 179.	101
Marzilli, L.G., Wilkowski, K., Chiang, C.C., Kistenmacher, T.J. (1979), J. Am. Chem. Soc., 101, 7504.	101
Matsumoto, N., Yamashita, M., Ueda, I., Kida, S. (1978), Memoirs of the Faculty of Science, Kyushu U., Ser. C, 11, 209.	162,163,167
Melanson, R., Rochon, F.D. (1978), Acta Cryst., B34, 3594.	88

	Page Cited
Melanson, R., Rochon, F.D. (1979), Can. J. Chem., 57, 57.	88
Melanson, R., Rochon, F.D., Hubert, J. (1975), Can. J. Chem., 53, 1139.	80,88
Melanson, R., Rochon, F.D., Hubert, J. (1979), Acta Cryst., B35, 736.	88
Milburn, G.H.W., Truter, M.R. (1966), J. Chem. Soc., A, 1609.	3
Moller, M.R., Bruck, M.A., O'Connor, T., Armatis, F.J., Knolinski, E.A., Kottmair, N., Tobias, R.S. (1980), J. Am. Chem. Soc., 102, 4589.	171
O'Brien, E.J. (1967), Acta Cryst., 23, 92.	189
Orbell, J.D., Marzilli, L.G., Kistenmacher, T.J. (1981), J. Am. Chem. Soc., 103, 5126.	172,191
Orbell, J.D., Wilkowski, K., Marzilli, L.G., Kistenmacher, T.J. (1982), Inorg. Chem., 21, 3478.	172,181
Papavassilion, G.C., Layek, D., Theophanides, T. (1980), J. Raman Spec., 9, 69.	163
Patterson, A.L. (1935), Z. Krist., A90, 517.	29
Pauling, L. (1960), "The Nature of the Chemical Bond", 3rd. ed., Ithaca; Cornell Univ. Press.	87,94,160
Pilon, P. (1984), Ph.D. Thesis, McMaster University, Hamilton, Canada.	55,100,101, 105,111

	Page Cited
Pippy, M.E., Ahmed, F.R. (1968), Mean Plane and Torsion Angles, Report NRC-22, National Research Council of Canada, Ottawa.	35,50
Popa, E.V., Ablov, A.V., Mazus, M.D., Biyushkin, V.N., Malinovskii, T.I. (1977), Dokl. Akad, Nauk SSSR Ser. Khim., 6, 556. Translated from Dokl. Akad. Nauk SSSR, 236, 630.	76
Poulet, H., Delorme, P., Mathieu, J.P. (1964), Spectrochimica Acta, 20, 1855.	123
Purnell, R.G., Hodgson, D.J. (1976), J. Am. Chem. Soc. 98, 4759.	61,189
Reedijk, J. (1984), "Platinum Coordination Complexes in Cancer Chemotherapy", Nijhoff: Boston, 3.	199
Reedijk, J., den Hartog, J.H.J., Fichtinger-Schepman, A.M.J., Marcelis, A.T.M. (1984), "Platinum Coordination Complexes in Cancer Chemotherapy", Nijhoff: Boston, 39.	9,197
Reishus, J.W., Martin, D.S. Jr. (1961), J. Am. Chem. Soc., 83, 2457.	53
Roberts, J.J. (1981), "Metal Inos in Genetic Information Transfer", Elsevier, North Holland: New York, 273.	172
Robin, M.B., Day, P. (1967), Adv. Inorg. Chem. Radiochem., 10, 247.	160

	Page Cited
Rosenberg, B. (1971), Plat. Met. Rev., 15, 42.	1
Rosenberg, B. (1977), J. Clin. Hem. Onc., 7, 817.	199
Rosenberg, B. (1978), Biochimie, 60, 831.	111
Rosenberg, B. (1980), "Nucleic Acid-Metal Ion Interactions", Wiley: New York, 1.	169
Rutherford, J. (1965), SYMFOU. McMaster University, Hamilton, Canada.	49
Sayre, D. (1952), Acta Cryst., 5, 60.	27
Sayre, D., ed. (1982), "Computational Crystallography", Oxford University Press Inc.: New York.	27
Schmidtke, H.-H., Garthoff, D. (1968), Inorg. Chim. Acta, 2, 357.	54,72,74, 75,77,89
Scovell, W.M., Kroos, L.R., Capponi, V.J. (1983) A.C.S. Symp. Ser., 209, 101.	8
Sheldrick, G.M. (1976), SHELX. Univ. of Cambridge, Cambridge, England.	22,32,49, 50
Shustorovich, E.M., Porai-Koshits, M.A., Buslaev, Yu.A. (1975), Coord. Chem. Rev., 17, 1.	126
Simundza, G., Sakore, T.D., Sobel, H.M. (1970), J. Molec. Biol., 48, 263.	189
Sparks, R.A. (1982), "Computational Crystallography", Oxford Univ. Press: Oxford, 1.	44

	Page Cited
Speranzini, R.A. (1980), Ph.D. Thesis, McMaster University, Hamilton, Canada.	197
Stephens, J. (1973), CUDLS. McMaster University, Hamilton, Canada.	49
Stewart, J.M. (1976), XRAY76. Tech. Rep. TR-446. Computer Science Center, Univ. of Maryland, College Park, Maryland, U.S.A..	47
Stout, G.H., Jensen, L.H. (1968), "X-ray Structure Determination", The Macmillan Company: Toronto.	12,19,28, 35
Taylor. R., Kennard, O. (1982), J. Am. Chem. Soc., 104, 3209.	174,187
Thomson, A.J. (1974), "Platinum Coordination Complexes in Chemotherapy", Springer-Verlag: New York, 38:	53
Topal, M.D., Fresco, J.R. (1976), Nature, 263, 285.	193
Ushay, H.M., Santella, R.M., Caradonna, J.P., Grunberger, D., Lippard, S.J. (1982), Nucleic Acids Res., 10, 3573.	8,194
Watt, G.W., Cude, W.A. (1968), Inorg. Chem., 7, 335.	54,56,72, 78
Watson, J.D., Crick, J.H.C. (1953), Nature, 171, 737.	5,189
Werner, A. (1896), Z. Anorg. Chem., 12, 46.	145

	Page Cited
Werner, A., Miolati, R. (1893), Z. Physikal. Chem., 12, 49.	2
Wilson, A.J.C. (1942), Nature, 150, 151.	25
Woolfson, M.M. (1970), "An Introduction to X-ray Crystallography", Cambridge Univ. Press: Cambridge.	12,16
Zachariasen, W.H. (1963), Acta Cryst., 16, 1139.	22
Zvagulis, M. (1980), Ph.D. Thesis, McMaster University, Hamilton, Canada.	183,199
Zwelling, L.A. (1983), A.C.S. Symp. Ser., 209, 27.	8